

NEURAL ENSEMBLE INTERACTIONS UNDERLYING MEMORY CONSOLIDATION

C. DANIELA SCHWINDEL

Dipl.Biol., Otto-von-Guericke University of Magdeburg, 2008

A Thesis

Submitted to the Graduate Council
of the University of Lethbridge
In Partial Fulfilment of the
Requirements of the Degree

DOCTOR OF PHILOSOPHY

Department of Neuroscience
University of Lethbridge
LETHBRIDGE, ALBERTA, CANADA

© C. Daniela Schwindel, 2014

PREPARATION OF THESIS

C. DANIELA SCHWINDEL

Date of Defense: December 3, 2014

Dr. Bruce L. McNaughton Supervisor	Professor	Ph.D.
---------------------------------------	-----------	-------

Dr. Robert Sutherland Thesis Examination Committee Member	Professor	Ph.D.
--	-----------	-------

Dr. Masami Tatsuno Thesis Examination Committee Member	Associate Professor	Ph.D.
---	---------------------	-------

Dr. David Euston Thesis Examination Committee Member	Assistant Professor	Ph.D.
---	---------------------	-------

Dr. Artur Luczak Internal External Examiner	Associate Professor	Ph.D.
--	---------------------	-------

Dr. Francesco Battaglia External Examiner Radboud Universiteit, Nijmegen, The Netherlands	Associate Professor	Ph.D.
--	---------------------	-------

Dr. Sergio Pellis Chair, Thesis Examination Committee	Professor	Ph.D.
--	-----------	-------

Abstract

Episodic memory formation and spatial navigation are core functions of the hippocampus. Embedded in a path integration based navigational system, the hippocampus generates orthogonal codes for different environments. To separate events within the same spatial map, the magnitude of individual place cell firing is modulated by external sensory information. The rate differences are also expressed to separate different running directions within an environment. Previous work suggested that the maps can be perturbed by external cues, but that the rate perturbations are not associatively stored. The present result shows that the rate code is reinstated offline and thus likely associatively stored, which fits well with the theory that describes the hippocampus as generating an index code for episodic memories to assist in retrieval of distributed information stored in the cortex. Lastly, this thesis addresses the methodological challenges of current electrophysiological techniques in detecting excitatory local connectivity on the example of the prefrontal cortex.

Acknowledgements

A PhD is a long and windy road, on which many people have travelled alongside me. I am grateful to their time, efforts and company.

First and foremost I would like to thank my advisor, Dr. Bruce McNaughton, who has inspired me in many ways. Not only is he a great mind in the field to which he has contributed influential theories, but he is also a great mentor. His confidence in me and my abilities has encouraged me and helped me grow as a scientist. I am grateful for the generous opportunities he has provided me with, especially the opportunity to accompany him on his sabbatical to NERF at IMEC/KU Leuven for one year and work very closely with him on pioneering large-scale single unit recordings with silicon probes. This was an extremely valuable learning and networking experience and the highlight of my PhD.

I owe thanks to my PhD thesis supervisory committee, Dr. Robert Sutherland, Dr. David Euston, and Dr. Masami Tatsuno, who have been supportive. In addition, I would like to thank the members of my Thesis Examination Committee, Dr. Francesco Battaglia, Dr. Artur Luczak and Dr. Sergio Pellis. In particular, I would like to thank Dr. Masami Tatsuno who has taught me a great deal about analytical tools for neurophysiological data and statistical analysis with extraordinary patience. He was brave enough to share his expertise despite my initial lack of knowledge in Matlab programming and has been extremely supportive throughout my training in graduate school.

I am grateful to Karim Ali who readily provided technical assistance in Matlab programming and data analysis. I enjoyed my collaborations with Masami and Karim on

the cross correlation project as well as on the reactivation of rate remapping project very much and value the knowledge they shared with me.

Amanda Mauthe-Kaddoura has become indispensable to a smooth running of the everyday life in the laboratory and I would like to thank her for all the support she provided in administrative matters in Lethbridge and Leuven.

During my stay in Leuven, I appreciated the open research atmosphere at NERF that Dr. Staf Borghs encouraged and am happy that I had the chance to be part of it. I especially enjoyed the collaborations with the Kloosterman lab and Arno Aarts from ATLAS Neuroengineering and am grateful to them for sharing technical knowledge and scientific discussion. I enjoyed my stay in Leuven in- and outside of NERF thanks to my fellow PhD colleague Davide Ciliberti. His, Ine Michel's and Raluca Radu's friendship truly enriched my life in Leuven.

It took me a while to get used to the life in the prairies, but I was lucky to have fellow students like Zaneta Navratilova and Jeanne Xie and to meet Luke Booker, Tom Rutherford and Jonathan Sheppard who formed a crucial social support network and shared a common passion: rock climbing. We had many outdoor adventures together that helped me build both physical and mental strength.

I thank my neighbors Tom and Luke for their sympathy and understanding during stressful and hard times, especially towards the end, and Erin Zelinski for sharing her house with me, when I needed a place to move last minute.

I especially thank Zaneta for being a mentor as a senior graduate student during my early years in graduate school and for sharing authorship with me on her directionality paper that she provided very generously for my thesis.

I deeply appreciate the friendship of Corinne Montes and Charlotte Alme that carried me through some tough times that are inevitable during a PhD, especially when so far from home. Life in Lethbridge would have not been as much fun without the Latin influence from Andrea Gomez and Edgar Bermudez, who know how important laughs and drinks in good company, and dance is in life.

I am grateful to the love that Adam Saunders has shown me. He never failed to make me appreciate the beauty of my surroundings, especially B.C. He understood the sacrifice of time I had to make and helped me relax in stressful times, especially in the final stages. We share a lot of beautiful memories of adventurous times.

I would have not had the endurance, discipline and strength to complete my PhD without the continuous strong support and inspiration of my family, my mother Monika Götz, and brothers, Thomas and Michael Schwindel with his wife Sabine and children Judith, Gabriel and Elias, who provided encouragement when I needed it. I am grateful to my friends Stefan Fenn, Marina Mayer, Alexandra Karch, Stefanie Eberl and Jana Kuchenbaur, to just name a few, for being close despite the geographical distance.

There are many more who deserve to be acknowledged here. Thanks to all that have contributed to my success in graduate school.

Lastly, I would like to thank AI-HS for financial support for 5 years.

Table of Contents

ABSTRACT	III
ACKNOWLEDGEMENTS	IV
LIST OF FIGURES	IX
LIST OF TABLES	XI
<u>CHAPTER 1 GENERAL INTRODUCTION</u>	1
DIFFERENT TYPES OF MEMORY	2
MEMORY CONSOLIDATION	3
THE HIPPOCAMPAL FORMATION	3
CIRCUITRY	8
SPATIAL NAVIGATION AND ATTRACTOR DYNAMICS IN THE HIPPOCAMPAL FORMATION	10
REMAPPING IN THE HIPPOCAMPUS	13
OSCILLATORY PATTERNS IN THE HIPPOCAMPUS	16
HIPPOCAMPAL SEQUENCE PATTERNS	18
THESIS OUTLINE	19
<u>CHAPTER 2 HIPPOCAMPAL-CORTICAL INTERACTIONS AND THE DYNAMICS OF MEMORY TRACE REACTIVATION</u>	22
ABSTRACT	22
CORTICAL MODULAR ORGANIZATION AND MEMORY INDEXING	23
SPARSE VS. DISTRIBUTED CODING TO MAXIMIZE STORAGE CAPACITY	28
BASIC DATA STRUCTURE AND ANALYSIS OF ENSEMBLE RECORDINGS	30
USING PLACE CELLS TO STUDY MEMORY	33
COHERENT REACTIVATION OF MEMORY TRACES IN HIPPOCAMPUS AND NEOCORTEX	37
MEMORY TRACE REACTIVATION DYNAMICS DURING SLOW WAVE SLEEP	41
<u>CHAPTER 3 EXPERIENCE-DEPENDENT FIRING RATE REMAPPING GENERATES DIRECTIONAL SELECTIVITY IN HIPPOCAMPAL PLACE CELLS</u>	48
ABSTRACT	48
INTRODUCTION	50
METHODS	53
RESULTS	61
DISCUSSION	77
<u>CHAPTER 4 REACTIVATION OF RATE REMAPPING IN CA3</u>	87
ABSTRACT	87
INTRODUCTION	88
METHODS	91
RESULTS	98
FIRING RATES ENCODE RUNNING DIRECTION WITHIN A STABLE SPATIAL CODE	99
REACTIVATION IN CA3 INCLUDES CONTEXTUAL MODULATION OF FIRING RATES	104
DISCUSSION	109

CONCLUSION	110
<u>CHAPTER 5 LONG-TERM RECORDINGS IMPROVE THE DETECTION OF WEAK EXCITATORY-EXCITATORY CONNECTIONS IN RAT PREFRONTAL CORTEX</u>	112
ABSTRACT	112
INTRODUCTION	113
MATERIALS AND METHODS	115
RESULTS	129
CHANGES OF DETECTION PROBABILITY OVER VARIOUS LENGTHS OF RECORDINGS	131
CURVE FITTING AND EXTRAPOLATION OF THE RELATIONSHIP BETWEEN STATISTICAL POWER AND SAMPLE SIZE	138
FALSE-POSITIVES AND THE DISTRIBUTION OF EFFECT SIZE	144
HYPERRECIPROCITY IN MPFC	147
EXCITATORY CONNECTIVITY IN MPFC IS PREDOMINANTLY LOCAL	148
VARIOUS TYPES OF EXCITATORY CONNECTIONS ARE THE MOST ABUNDANT IN MPFC AND THEIR DETECTION PROBABILITY INCREASES WITH SAMPLE SIZE.	150
DISCUSSION	152
<u>CHAPTER 6 GENERAL DISCUSSION</u>	159
SUMMARY	159
DISCUSSION	160
UNDERSTANDING RATE REMAPPING IN THE CONTEXT OF ATTRACTOR DYNAMICS	160
IS THERE SIMULTANEOUS REACTIVATION OF MULTIPLE EPISODIC EVENTS ENCODED THROUGH RATE REMAPPING?	165
CONCLUSION	167
<u>REFERENCES</u>	168
<u>APPENDIX</u>	189

List of Figures

Figure 1.1 Orientation of the hippocampus in a 3-dimensional drawing of the rat brain	7
Figure 1.2 The hippocampal formation	9
Figure 2.1 Hierarchical organization of cortex and hippocampus and the indexing encoding principle	25
Figure 2.2 Data analysis of multi-unit recordings	31
Figure 2.3 Place cells in the hippocampus	35
Figure 2.4 Connectivity matrix and pairwise correlations between hippocampal neurons during pre-task sleep, behavior and post-task sleep	36
Figure 2.5 Hippocampal EEG and concurrent spike activity during REM and slow wave sleep	38
Figure 2.6 The relationship between K-complexes and memory reactivation	43
Figure 2.7 Cross correlations between neuron pairs in medial prefrontal cortex during task and sleep	44
Figure 2.8 Relationship between neocortical neural activity and hippocampal sharp waves	45
Figure 3.1 Assigning boundaries around fields	62
Figure 3.2 Development of directionality on a circular track	65
Figure 3.3 Examples of firing rate changes in individual cells on day 1	66
Figure 3.4 Control analyses	69
Figure 3.5 Remapping in individual fields	72
Figure 3.6 Local cues and the development of directionality	73
Figure 3.7 Directionality in an open field	75
Figure 4.1 Rate remapping in different running directions on a circular track	101
Figure 4.2 Similarity between spatial maps, directionality index, lognormal firing rate distributions and reactivation of rate remapping	103
Figure 4.3 Asymmetry of place fields and its effect on their overlap	107
Figure 4.4 Relationship between CA3 unit activity and ripple events	108
Figure 5.1 Neuron classification	121
Figure 5.2 Examples of cross correlograms for detected excitatory connections, firing rate distribution and the distribution of the jitter corrected effect size	130
Figure 5.3 The experimentally derived detection probability	135
Figure 5.4 The relationship between the significance level α and the fitting parameter α_{param}	140
Figure 5.5 The distribution of effect sizes for short-range and long-range connections	141
Figure 5.6 The distribution of effect sizes for unidirectional connections (EE1) and for reciprocal connections (EE2) within and between tetrodes	143
Figure 5.7 Counts of unconnected and excitatory connected neuron pairs relative to the random-connection null hypothesis	146
Figure 5.8 Number of excitatory connections per tetrode versus the total number of excitatory connections	149

Figure 5.9 Detection probabilities over different hour segments for different categories of connection types	151
Figure 5.10 The cross correlogram matrix for all simultaneously recorded neurons	153
Figure 5.11 Summary of local and long-range connections per dataset	155

List of Tables

Table 3.1 Statistics of each session analyzed	63
Table 5.1 The number of neuron pairs, significant excitatory connections and the experimentally derived detection probability of excitatory connection pairs	132
Table 5.2 Optimization results for fitting the statistical power function to the experimental data	136

Chapter 1 General Introduction

Memory is the ability to encode, store and recall information and to use this information to construct a model of the world that facilitates adaptive behavior. Memories have often been viewed as information stored in associated patterns of connections between neurons that give rise to a neural representation of this memory. Hebb (1949) proposed a mechanism that enables a change of the strength of the connection among neurons that could explain how memory representations can be formed. He introduced the concept of synaptic plasticity based on correlated activity: "whenever an axon of cell A is near enough to excite a cell B and repeatedly or persistently takes part in firing it, some growth process or metabolic change takes place in one or both cells such that A's efficiency as one of the cells firing B is increased". About 20 years after this hypothetical proposal, Bliss and Lømo and (1973) Bliss and Gardner-Medwin (1973) described a durable increase in efficiency of transmission after repeated stimulation at the perforant path-granule cell synapse in the rabbit hippocampus, a phenomenon currently referred to as long-term potentiation (LTP). This finding was not linked to Hebb's idea until a few years later, when McNaughton et al. (1978) demonstrated that synaptic enhancement is a cooperative process and requires the concurrent activity of many perforant path fibers. The hippocampus has long been used as an example system to model how memories can be stored through autoassociative, symmetric connections between

coactive neurons that Hebb called 'cell assemblies' (1949) in the recurrent network of CA3 (McNaughton and Morris, 1987).

DIFFERENT TYPES OF MEMORY

According to Squire (2004), various types of memory are supported by different systems (in the anatomical and functional sense) (Tulving, 1985; Sherry and Schacter, 1987; Squire, 2004). Generally memory is divided into declarative and nondeclarative memory. Declarative memory can be verbally reported and provides an internal representation of the world with informational contents that can be compared and contrasted. It depends on temporal lobe and diencephalic structures. Declarative memory is further subdivided into episodic (i.e., autobiographic) and semantic (memory of facts) memory (Tulving, 1972). In contrast, non-declarative memory is dependent on the system it was acquired with, cannot be verbally reported and its retrieval becomes apparent through performance rather than through recollection. Examples of non-declarative memories are procedural memory (skills and habits) dependent on the striatum, priming and perceptual learning (dependent on the neocortex), simple classical conditioning (emotional responses are dependent on the amygdala and the skeletal responses are dependent on the cerebellum), and finally nonassociative learning (dependent on reflex pathways)(Squire, 2004).

MEMORY CONSOLIDATION

Following observations of patients that suffered amnesia after trauma, the early French psychologist Theodule-Armand Ribot described that recent memories around and leading up to the event are more affected than much more remote memories (Ribot, 1882). German experimental psychologists, Müller and Pilzecker (1900), investigated how new learning interferes with the retrieval of a memory acquired just before the new learning occurred. These observations led Müller and Pilzecker to the conclusion that memory initially exists in a fragile state and becomes strengthened ('consolidated') over time (Lechner et al., 1999). The seminal case study on one of the most famous and extensively studied patients in history, patient H.M., of Scoville and Milner (1957) linked the ideas and early experimental results on learning and memory research to a neurobiological substrate: the hippocampal formation. Henry Molaison (H.M.) suffered from severe epilepsy that was cured with bilateral dissection of the hippocampus and related temporal lobe structures. However, the procedure had dramatic consequences regarding his memory functions. H.M now suffered from anterograde and graded retrograde amnesia, i.e., the inability to form new episodic memories and to retrieve recently acquired ones (Scoville and Milner, 1957).

THE HIPPOCAMPAL FORMATION

The hippocampal formation can be described along two main axes that are oriented perpendicular to each other: the longitudinal axis, extending from the septal pole

(rostr dorsally, close to the septal nuclei) to the temporal pole (caudoventrally in the incipient temporal lobe) and the transverse or proximo-distal axis, extending from the dentate gyrus (proximal) to the entorhinal cortex (distal) (Figure 1.1).

The hippocampus is a C-shaped structure buried in the medial temporal lobe. It consists of a 3-layer archi-cortex comprised of the subfields Dentate Gyrus (DG) and cornu ammonis (CA) 1,2 and 3. Beginning with the DG, the most superficial layer and closest to the hippocampal fissure, is the almost cell free molecular layer. Underneath it is the granule cell layer that contains densely packed granule cells, which are the principal cells of the DG and innervate CA3. The deepest layer is a polymorph layer and contains afferents, efferents and interneurons. The most known cell type in the polymorph layer is probably the mossy cell, which is glutamatergic, like the granule cells. The mossy cells send axons to the dendrites of the granule cells in the ipsilateral and contralateral inner third of the molecular layer via the associational and commissural projections. The DG receives its main input from the entorhinal cortex, predominantly layer II, via the perforant pathway. This input can be divided into a lateral pathway that arises from the lateral entorhinal cortex and terminates in the most superficial third of the molecular layer, and into a medial pathway, arising from the medial entorhinal cortex and terminating in the middle third of the molecular layer. The projections from both parts of the entorhinal cortex target the entire transverse extent of the molecular layer. Apart from the entorhinal input, there are also minor projections from the pre- and parasubiculum entering the molecular layer of the DG. The granule cells innervate

CA3 through unmyelinated mossy fibers, which are mainly located in the stratum lucidum (just above the CA3 pyramidal layer). In proximal CA3, mossy fibers are also located below and within the pyramidal layer. CA2 does not receive mossy fiber input, which marks a clear border between the two CA subfields. Each granule cell targets about 15 CA3 pyramidal cells, distributed across the entire transverse extent (Acsady et al., 1998). As granule cells outnumber the CA3 pyramidal cells by a factor of 12:1 at the septal pole (the ratio drops to 2:3 at the temporal pole as the packing density of CA3 pyramidal cells and DG granule cells follows inverse gradients), it has been estimated that each pyramidal cell receives input from about 50-72 granule cells (Henze et al., 2000). Because the synapses of mossy fibers are relatively big (up to 3-5 microns in diameter) and have a number of synaptic release sites (30-40)(Henze et al., 2000), a spike train from a single granule cell can activate a CA3 pyramidal cell (Henze et al., 2002). The deepest layer of the CA regions is the stratum oriens, a relatively cell-free layer just below the pyramidal layer containing some of the CA3 to CA3 associational connections and CA3 to CA1 Schaffer collateral connections. In this layer, the basal dendrites of the pyramidal neurons and several classes of interneurons are located. Deeper to this runs the thin fiber containing alveus. The suprapyramidal layer (directly above CA1 and CA2 and above stratum lucidum in CA3) is the stratum radiatum, which contains the CA3 to CA3 associational connections and the CA3 to CA1 Schaffer collaterals. The most superficial layer in CA1 and CA2 is the stratum lacunosum moleculare, in which the entorhinal and thalamic nucleus reunions inputs terminate. The

hippocampus proper is surrounded by the parahippocampal region (PHR) that is bordering the subiculum. The PHR is comprised of the presubiculum, the parasubiculum, the entorhinal cortex, which is further divided into a medial and lateral area, the perirhinal cortex and postrhinal cortex. The PHR is generally described as 6-layer cortex (Amaral and Lavenex, 2007).

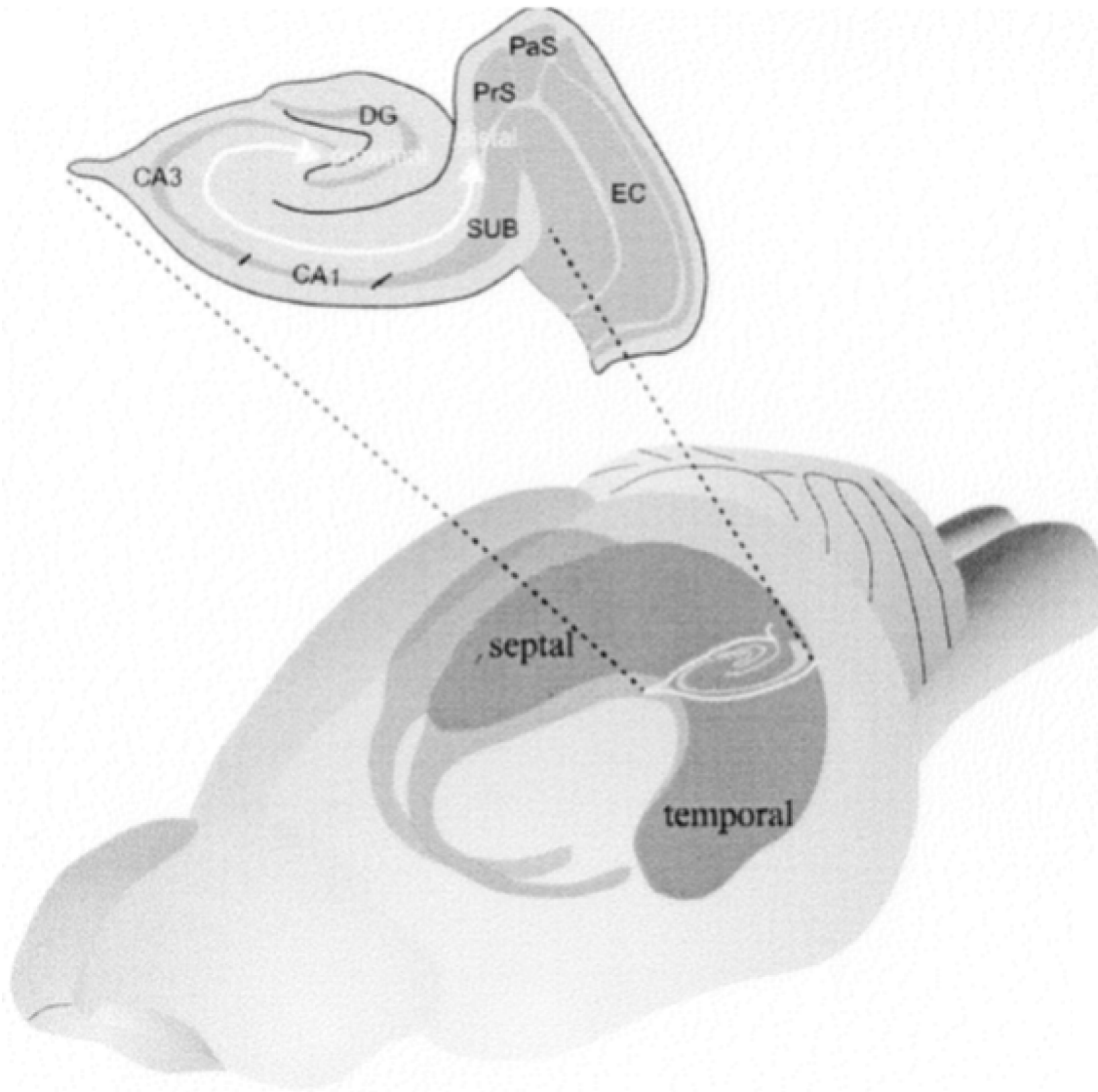


Figure 1.1 Orientation of the hippocampus in a 3-dimensional drawing of the rat brain
 Lateral view on the rat brain with the C-shaped hippocampus located in it. The septal and temporal pole are marked. A section is magnified with the subfields of the hippocampal formation indicated as well as the transverse axis running from proximal (close to the DG) to distal (close to the EC) (Witter et al., 2000).

CIRCUITRY

The original description of the trisynaptic pathway (Andersen et al., 1971) in the hippocampal formation is a simplified version of the today's accepted 'classical pathway' (van Strien et al., 2009)(Figure 1.2). The entorhinal cortex provides the main input to the hippocampus proper. Layer II projects to the area CA3 and collaterals of the same cells also reach the DG. The mossy fibers project from the DG to CA3 pyramidal neurons, which in turn send the Schaffer collaterals to area CA1. Entorhinal cortex layer III cells send direct projections to CA1, with proximal CA1 receiving input from medial entorhinal cortex and distal CA1 receiving input from lateral entorhinal cortex, as well as to the subiculum.

Area CA1 projects to the subiculum and both project back to the deep layers (V and VI) of the entorhinal cortex and other cortical areas (Witter et al., 2000). The return projections from pyramidal neurons in CA1 to the entorhinal cortex are roughly to the same areas from which they receive their input. The subiculum targets the lateral septal nuclei, the nucleus accumbens and the mammillary nuclei. The Pre- and Parasubiculum have reciprocal connections with the subiculum and project to the superficial layers of the entorhinal cortex. Projections from layer V to layer II and III of entorhinal cortex close the loop (not in figure) (Amaral and Lavenex, 2007).

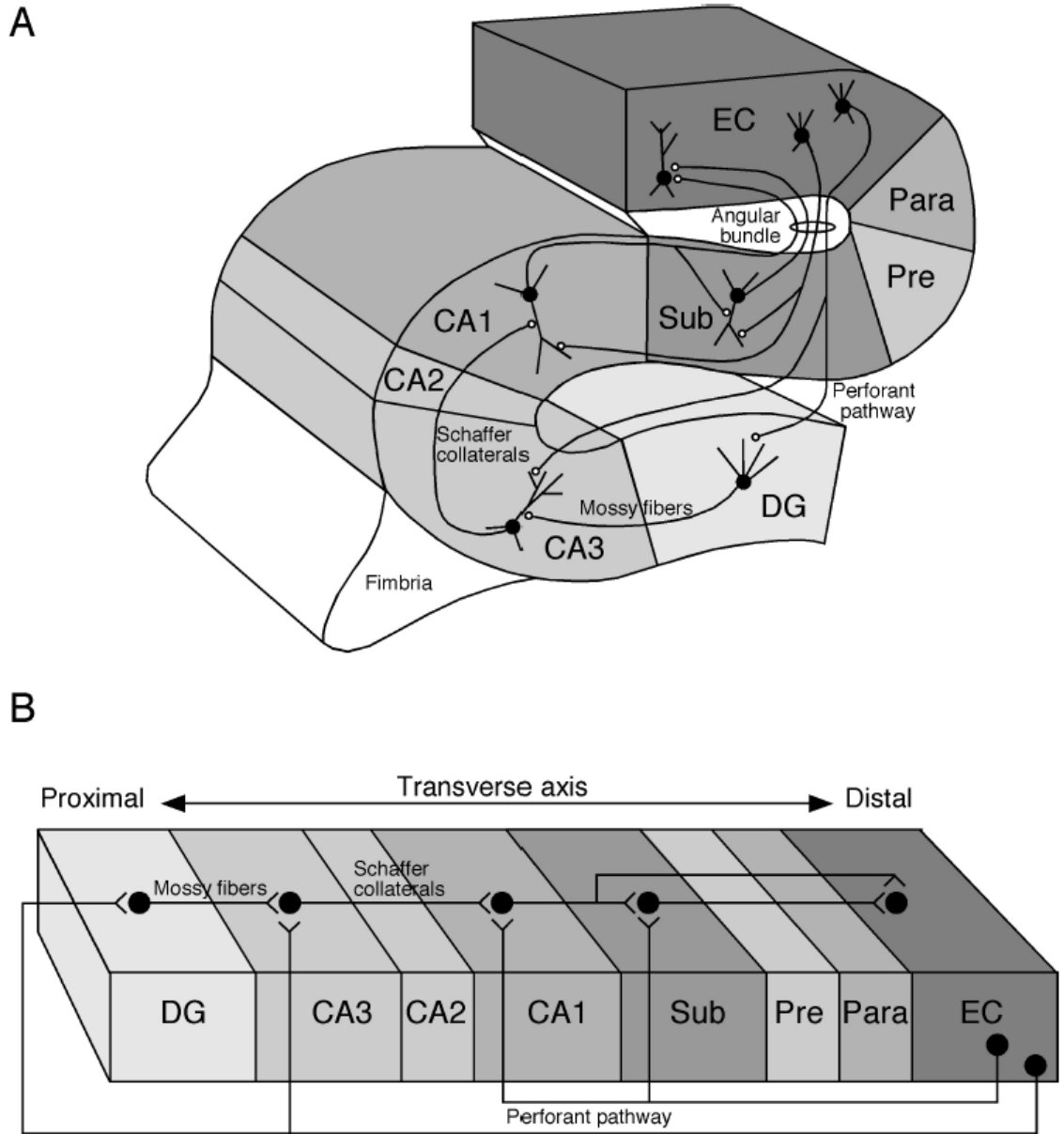


Figure 1.2 The hippocampal formation

A) Output from entorhinal cortex layer II targets the DG and CA3 via the perforant pathway. Entorhinal cortex layer III neurons project to CA1 and the subiculum. The granule cells in the DG send the mossy fibers to CA3. The pyramidal cells in CA3 project to CA1 via the Schaffer collaterals. Pyramidal cells in CA1 project to the subiculum and both CA1 and subiculum project back to the deep layers of the entorhinal cortex. B) Projections of the hippocampal formation along the transverse axis (Amaral and Lavenex, 2007).

This thesis is mainly concerned with dynamics in the CA3 region, which differs from other subareas in terms of its recursive organization. The recurrent connections run mainly in strata oriens and radiatum (Sik et al., 1993; Wittner et al., 2007) and involve only a few synaptic release sites. They are generally weaker than the synapses from the mossy fibers. The synapses onto interneurons, however, are more effective (Le Duigou et al., 2014). Because of its recurrent nature, CA3 has been described as an autoassociative network, which associates the input to its principal cells with their output. This enables it to complete a stored representation when only presented with a fragmented version of the original (McNaughton and Morris, 1987) and even reverberate activity so that sequential patterns (what Hebb called “phase sequences”) can be associated with each other and recalled in order (McNaughton and Morris, 1987).

SPATIAL NAVIGATION AND ATTRACTOR DYNAMICS IN THE HIPPOCAMPAL FORMATION

The discovery of spatial selective cells, so called ‘place cells’ in the hippocampus by O’Keefe and Dostrovsky (1971) led to the proposal that the hippocampus is the neural substrate of a ‘cognitive map’ forming a mental representation of the environment and the animal within it. The current location of an animal is encoded in the ensemble activity of place cells (Wilson and McNaughton, 1993). However, ensemble activity in different environments is typically unrelated and therefore does not allow predictions of the animal’s position in other but the already explored environments (Muller and Kubie, 1987; Leutgeb et al., 2004; Leutgeb et al., 2005b; Colgin et al., 2008; Colgin et al., 2010).

A computational study implemented a map-based path integration system (Samsonovich and McNaughton, 1997), but since the 2-dimensional spatial maps or charts are limited, the question of what happens when the animal goes beyond the represented space, arises. Samsonovich and McNaughton (1997) proposed periodic boundaries, which implies that cells activate repeatedly. This has not been reported for place cells, although they can express multiple fields in large environments (Maurer et al., 2006a; Kjelstrup et al., 2008; Park et al., 2011). However, such a cell type exists upstream of the hippocampus in the medial entorhinal cortex and is called 'grid cells' (Fyhn et al., 2004; Hafting et al., 2005). Grid cells show spatially periodic firing fields in a hexagonal pattern that spans the entire environment. Neighboring grid cells show similar spacing and field size. Their phases are offset to each other, but their relative firing relationships are maintained across environments (Hafting et al., 2005). The size of grid fields scales along the dorso-ventral axis in discretized steps (Stensola et al., 2012) and suggests a modular organization. The converging input from grid cells of different scales can lead to non-periodic place fields, which are also scaling field size along the septo-temporal axis (Jung et al., 1994; Maurer et al., 2005; Maurer et al., 2006a; Solstad et al., 2006; Kjelstrup et al., 2008).

Path integration is based on updating positional information by keeping track of distance travelled using internal cues, such as proprioceptive and vestibular information as well as visual flow and motor efference copy. It is a continuous rather than discrete process. Because of the regular geometrical firing pattern, grid cells have been proposed

to form a continuous attractor network for path integration, along which activity moves as the animal moves in space (McNaughton et al., 2006). In a continuous attractor, stable activity can be formed and maintained and, different from discrete attractors, moved continuously along the attractor network (Amit, 1989; Tsodyks, 1999; Trappenberg, 2010). The grid cells' activity across environments and persistence against manipulations of landmark features (Hafting et al., 2005; Fyhn et al., 2007) is in consensus with this role. Locally generated activity can be pushed along a continuum of attractor states through head direction information (McNaughton et al., 2006). Cells sensitive to head direction are found in the presubiculum (Taube et al., 1990) and in the medial entorhinal cortex, intermingled with cells that show conjunctive head direction and grid firing (McNaughton et al., 1991; Sargolini et al., 2006; Giocomo et al., 2014). Landmarks can be bound onto the spatial metric system and reinstate the activity at the appropriate location (McNaughton et al., 2006; Fyhn et al., 2007; Derdikman et al., 2009; Jezek et al., 2011) to prevent accumulation of error. Independent alignment of entorhinal modules could lead to unique representations in the hippocampus for different environments (Monaco and Abbott, 2011) and the hippocampal ensemble activity could therefore be understood as the result of continuous attractor dynamics in the MEC (McNaughton et al., 2006).

REMAPPING IN THE HIPPOCAMPUS

It appears to be at the core of hippocampal function to contribute to the formation of episodic and semantic memory, and thus it is of utmost importance that even similar events are stored in a way to enable unambiguous retrieval. Two forms of pattern separation exist and can be observed in different experimental conditions. The decorrelation of events in different places is referred to as global remapping and manifests in orthogonal (statistically independent) spatial maps for different environments. Global remapping is observed when animals move between different locations (Leutgeb et al., 2005b; Leutgeb et al., 2007; Colgin et al., 2010) or when a single environment is substantially altered (Jeffery et al., 2003). The second form of remapping is referred to as rate remapping and corresponds to a change in the rate distribution within an otherwise stable spatial map (Leutgeb et al., 2005b). This form of pattern separation can be observed when a subset of cues such as geometrical shape, wall colors or task demands are changed within an environment (Muller and Kubie, 1987; Anderson and Jeffery, 2003; Leutgeb et al., 2005a; Leutgeb et al., 2005b; Leutgeb et al., 2007; Colgin et al., 2010; Allen et al., 2012). The key determinant of whether global remapping is used appears to be whether there are differences in the spatial input as provided by the medial entorhinal cortex (Leutgeb et al., 2007). The rate modulation in rate remapping is likely due to lateral entorhinal cortex input (Lu et al., 2013), which itself shows little spatial modulation and is thought to provide the

hippocampus with the external sensory content and processing of local cues (Hargreaves et al., 2005; Neunuebel et al., 2013; Knierim et al., 2014).

The observation of abrupt transitions between stored representations, as in global remapping, and the persistence of hippocampal ensemble activity against minor changes, resemble discrete attractor dynamics. Spatial and contextual information have been proposed to be stored associatively in the recurrent network of CA3 (Hopfield, 1982; McNaughton and Morris, 1987; Amit and Treves, 1989). In a recent study, however, in which one familiar shape was morphed into another, CA3 ensemble and single unit activity showed hysteresis (i.e., lag in the change of representation) and abrupt transitioning coherently at the midpoint of the morph series from one place field configuration into another, but only when the animal was familiarized with the shapes in different spatial locations during training. When both shapes were experienced at the same location, morphing between them resulted in a gradual transition between the two different firing rate distributions in CA3 associated with the two familiar shapes with almost no change in the location of cell firing (Leutgeb et al., 2005a; Colgin et al., 2010). The attractor-like dynamics observed in the hippocampus during global remapping might therefore be a result of the continuous attractor dynamics upstream in the medial entorhinal cortex, rather than the result of discrete attractor dynamics within the hippocampus, as context alone was insufficient to elicit an abrupt shift in the neural representation. The current understanding of spatial processing suggests that internal information about position that is based on speed and head direction information

moves activity along a continuum of grid cells in the medial entorhinal cortex, which activate different subsets of CA3 place cells in different parts of the environment, resulting in global remapping. The gradual transitioning between the rate distributions, observed when both shapes were experienced at the same location originally, was a result of averaging across a population of cells that showed a mix of gradual and abrupt transitions at different points in the morph sequence (Colgin et al., 2010). Computational studies have addressed this observation by proposing local attractor dynamics for rate remapping (contextual information) embedded in a continuous attractor for spatial position (Solstad et al., 2014). In this study, lateral entorhinal cortex (LEC) input to CA3 was set up to be spatially homogenous, but different for different contexts, whilst medial entorhinal cortex (MEC) input to CA3 had a unimodal spatial profile that was identical for all contexts. CA3 was modelled as a recurrent network in which memories were stored using a Hebbian learning rule, in which the synaptic weights between CA3 units depended on the Euclidean distance between their field peak positions and peak firing rates in each of the two memories that were stored. In this model, combined inputs from LEC and MEC result in CA3 activity that represents the rat's position in an environment, determined by the identity of active CA3 units, with a given context, specified in the pattern of firing rates stored at that location. The hypothesis was that if discrete memories were stored in the network as attractor states, the feedback connections should affect the output of the network when LEC input is linearly changed from memory A to memory B. Indeed, the network responses

resembled the ones that were observed experimentally in terms that the average population response showed a smooth transition from representation A to B, but individual responses were heterogeneous. Some units transitioned gradually and some showed abrupt transitions at different points along the morph series. In chapter 4, the question, whether the rate distributions, that are modelled in Solstad et al., (2014) to be stored in the recurrent network of CA3, are reactivated during sleep after behavior and thus amenable to retrieval, is addressed.

OSCILLATORY PATTERNS IN THE HIPPOCAMPUS

The dense layers in the hippocampus generate high amplitude electroencephalographic (EEG) patterns, because the fields generated by individual cells summate due to the parallel alignment of the dendritic arbors. One prominent pattern, which is observed during (voluntary) motor behaviors, such as walking, rearing, postural adjustment (Vanderwolf, 1969), and during REM sleep (Jouvet, 1969; Vanderwolf, 1969), is the hippocampal theta rhythm, a large (exceeding 1mV) sinusoidal pattern with a frequency of 6-10 Hz in the rat that depends on septal input (Petsche et al., 1962; Mizumori et al., 1990; Brandon et al., 2011; Koenig et al., 2011). Theta has also been recorded in other mammals, such as bats, monkeys and humans (Ekstrom et al., 2003; Hori et al., 2003; Ulanovsky and Moss, 2007). The largest amplitude theta signal is recorded near the hippocampal fissure, which separates the molecular layer of CA1 from molecular layer in the DG. The phase of the hippocampal principal neurons' firing correlates with the

animal's location in the place field. As the animal advances through the field, hippocampal units fire at a progressively earlier phase of each successive theta cycle until they advanced about one full theta cycle (O'Keefe and Recce, 1993; Skaggs et al., 1996; Huxter et al., 2003; Dragoi, 2013). CA3 spike times advance only about half a theta cycle (Mizuseki et al., 2012). This so-called phase precession implies that the pyramidal neurons' intrinsic firing frequency (~10 Hz) is slightly greater than the local field potential theta (~8 Hz)(Maurer et al., 2006a).

Another prominent pattern that characterizes hippocampal activity during slow wave sleep and quiet wakefulness are the sharp wave ripple (SPWR) complexes (Buzsaki, 1986). Sharp waves are field potentials of about 50-150 ms duration and arise from excitation build up in the recurrent network of CA3. They occur stochastically at a frequency of 0.02-3 Hz (Ylinen et al., 1995). Sharp waves co-occur with a high-frequency oscillation (150-200 Hz), the so-called 'ripples'. The excitatory input from the Schaffer collaterals to the apical dendrites of CA1 causes strong depolarization, which can lead to voltage-dependent sodium channel activation and rhythmic discharge (Ylinen et al., 1995; Csicsvari et al., 2000). Parvalbumin-positive basket cells may be involved in the control of spike timing (Ylinen et al., 1995) as these inhibitory neurons phase-lock their firing through recurrent connections and feed forward the phase-locked inhibition to CA1 (Ylinen et al., 1995; Schlingloff et al., 2014). Sharp wave ripple complexes have been associated with memory reactivation (Wilson and McNaughton, 1994; Kudrimoti et al., 1999; Diekelmann and Born, 2010) and interruption of these events impairs learning of

spatial memory tasks (Girardeau et al., 2009; Nakashiba et al., 2009; Ego-Stengel and Wilson, 2010).

HIPPOCAMPAL SEQUENCE PATTERNS

Hippocampal neurons appear to fire in spatiotemporal patterns. The order of place cell firing within one theta cycle reflects the order of place fields in a given trajectory in a compressed manner, sometimes referred to as sequence compression (Skaggs et al., 1996; Dragoi and Buzsaki, 2006; Dragoi, 2013). The temporal sequence within a theta cycle is compressed about 8-16 times compared to the distance of the fields (Skaggs et al., 1996; Dragoi and Buzsaki, 2006; Dragoi, 2013). The activity of a neuron is best predicted by the activity of its peers within a window of 10-30 ms (Harris et al., 2003). Through sequence compression, the cofiring of pyramidal neurons is brought within this window, which also corresponds to the membrane time constant of pyramidal neurons (Spruston and Johnston, 1992), the window for spike time dependent plasticity (Magee and Johnston, 1997) and the period of the gamma oscillation (Csicsvari et al., 2003b). Thus, sequence compression might be a suitable mechanism to use LTP for storing the temporal pattern of the animal's experience (Skaggs et al., 1996).

Interestingly, a similar compression of place cell sequences can be observed during sharp-wave ripple complexes, which correspond extremely well to the ones in behaviour (Skaggs and McNaughton, 1996; Kudrimoti et al., 1999; Nadasdy et al., 1999; Lee and Wilson, 2002; Dragoi, 2013). The duration of ripples (60-120 ms) corresponds

roughly to the length of a theta cycle. Evidence for sequence replay from sleep episodes following a behavioral epoch supports the notion that place cell sequences that have been activated during behavior are replayed offline during sleep so as to strengthen the connections among their neocortical targets (Wilson and McNaughton, 1994; Kudrimoti et al., 1999; Nadasdy et al., 1999; Lee and Wilson, 2002).

THESIS OUTLINE

The formation of memory and the extraction of knowledge from it, is the basis of intelligence and adaptive behavior. Distributed neural ensembles are able to process and store information of different sensory domains into a coherent representation by means of coordinated activity during behavior and subsequent sleep. The hippocampal formation is anatomically and functionally in a suitable position to coordinate the storage and retrieval of episodic information efficiently by means of an index code that is based on spatial information. *Chapter 2* explains the need of a hierarchical cortical organization due to the limited number of cortical intercolumnar connections and introduces the indexing theory as a possible solution to this computational problem. The hippocampus, as top of the hierarchy, is thought to form an index code that is broadcasted to the cortex during sleep to coordinate recall and allow synaptic reorganization.

The hippocampus is part of the navigational system of the brain. Its principal cells fire selectively in space and, as ensembles, establish spatial maps onto which contextual

information can be bound. Different episodes occurring in the same space can be separated by means of different firing rate distributions. This feature of hippocampal coding is called rate remapping. In *chapter 3* it is demonstrated that different running directions are a possible paradigm to induce rate remapping, which is a plastic phenomenon and learned within the first day.

It is well established that the hippocampal place code is reactivated during sleep following behavior, and hypothesized to serve as index code into the cortical columns to allow correct retrieval of contextual information associated with the spatial index. However, if the spatial code is retrieved without the associated firing rate distribution for a specific event, then the index code is ambiguous and would likely lead to mixed and erroneous recall. It seems obvious therefore, that during replay the hippocampus would also need to reactivate the correct firing rate distribution, i.e. rate remapping. However, a recent neurophysiological study indicates that only differences in spatial location are able to induce associative recall, whereas the feature (i.e., 'episodic') information is not. This presents a major problem for the central theory, and the main experiment in this thesis was designed to test whether both spatial and episodic components can be reactivated during sleep. *Chapter 4* deals with this question by taking advantage of the directionality paradigm established in *chapter 3* and comparing the firing rate distributions in sleep during sharp wave ripple episodes with the firing rate distributions associated with the two running directions during behavior.

All memory theory is based on Hebb's fundamental notion of neurons that "fire together, wire together" and information storage in the neocortex is assumed to be based on the (plastic) connectivity between pyramidal neurons, the most abundant cell type. To test whether extracellular large-scale single unit recordings are able to capture the abundance of presumably mainly weak connections between excitatory neurons, 25 hour long spike trains recorded in rat medial prefrontal cortex were analyzed using cross correlations (*chapter 5*). The approach developed in this work provides a possible method to assess changes in synaptic connectivity that might take place during "cell assembly formation" and memory consolidation in neocortex.

The results of this thesis and their implications for future research are discussed in *chapter 6*.

Chapter 2 Hippocampal-cortical Interactions and the Dynamics of Memory Trace

Reactivation

C. Daniela Schwindel and Bruce L. McNaughton

Canadian Centre for Behavioural Neuroscience, Department of Neuroscience, The University of Lethbridge, Lethbridge, Alberta, Canada

Published in: E. J. W. Van Someren et al. (Eds.) (2011), Progress in Brain Research 193: 163-175.

ABSTRACT

The formation of memory and extraction of knowledge from it is the basis of intelligence. It is believed that, during slow wave sleep, the brain reorganizes its connectivity matrix so as to store new information optimally. As the probability of direct synaptic connection between arbitrarily chosen neurons in the cortex is extremely low (on the order of 10^{-6}), a combination of modular and hierarchical organization appears to be necessary to enable rapid association of arbitrary items. During waking, an 'index' of the neural pattern in lower order cortical modules may be created and stored in the highest order association cortex, the hippocampus, and broadcast back to the relevant

cortical modules, where it is stored with the local data. In this manner, the pattern can be spontaneously reactivated and reinstated in all modules to enable the establishment of crossmodular connections. Such replay of patterns of neural activity or 'phase sequences' has been observed in hippocampus and neocortex. In prefrontal cortex, the playback of 'phase sequences' is associated with periods of intense up down state transitions, and can be accelerated 5-8 fold relative to the waking state. The playback speed declines over time as does the strength of the replay, which is consistent with a simple decay of an asymmetric component of the synaptic weight matrix induced during the experience itself. Since the hippocampal events associated with memory reactivation (sharp-wave-ripple events) tend to be correlated with up transitions in the neocortex, hippocampus may coordinate reactivation in neocortex, at least under some conditions.

CORTICAL MODULAR ORGANIZATION AND MEMORY INDEXING

The ability to remember facts and episodes is a critical component of thought and intelligence. Hebb (1949) proposed that memory is based on the formation of assemblies of cells that are mutually connected with strengthened synapses. The problem with this general idea is that the average connectivity of the cortex is extremely sparse (less than about 10^{-6}), and, therefore, the cortex cannot support the acquisition of new, arbitrary associations by modifying pre-existing connections alone; however, activity in two neurons that are not themselves directly connected can, nevertheless, be

associated by virtue of their common reciprocal connections with a third, higher order neuron. Thus, by organizing the cortex into functional modules that are reciprocally connected and arranged in a hierarchical structure, sparsely distributed connections may be sufficient to organize the acquisition and storage of information effectively. Within this conceptual framework, the lowest level modules are represented by primary cortices, the level above by association cortices and at the top resides the hippocampal formation, which has been recognized as the highest order association cortex (Swanson, 1983)(Figure 2.1 left). This organizational principle links neurons that are receiving and processing similar information to form modules that subserve a common function. Connectivity within modules is presumably high, enabling local (within module) associations, whereas connectivity between modules is very sparse. Therefore, slow growth and rearrangement of connections would be required to connect cells of different modules that together represent an experienced episode. The pattern of 'vertical' information flow, from primary to higher order association cortices, would ultimately give rise to a unique pattern that is stored in the hippocampus. In addition, the hippocampal output pattern at the time of the experience would also be stored in the lower level modules as part of their 'current input'. In this manner, each module would store module-specific information plus a small component of common information that it receives from the hippocampus. The common information could thus serve as an index pattern that could be used to coordinate retrieval and memory trace reactivation. Recreating the index pattern would evoke the corresponding patterns in

the lower level modules, thus completing the retrieval of the whole memory (Figure 2.1 right). The trace reactivation theory of memory consolidation holds that reactivation of cortical modules that were involved during the original encoding of the pattern provides a training trial through which the modules can become appropriately connected through growth and rearrangement of horizontal, intermodular connections. In this manner, a cortical representation could be established which is independent of the hippocampus. Presumably this representation would differ in some ways from the original form.

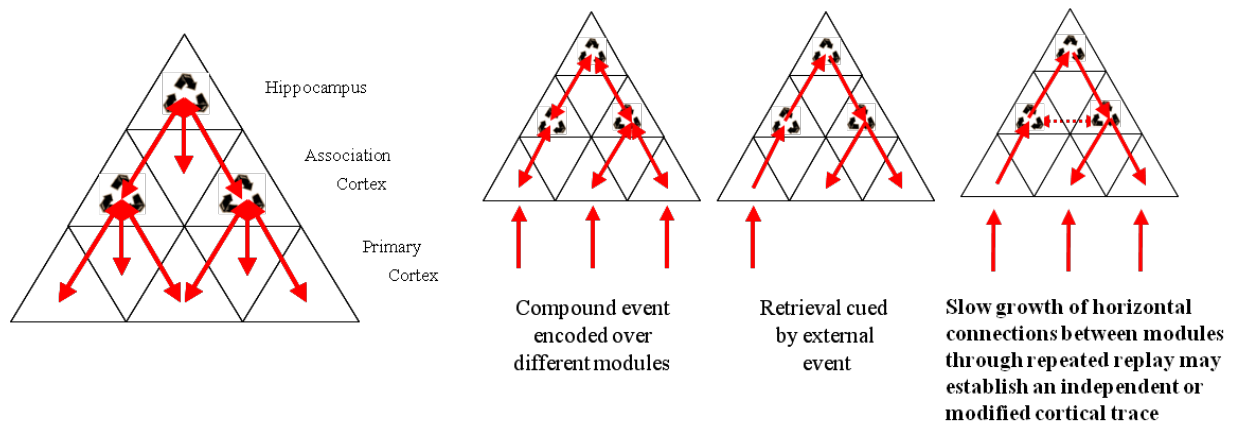


Figure 2.1 Hierarchical organization of cortex and hippocampus and the indexing encoding principle

In the foregoing theoretical framework, rapid plasticity (LTP) in different encoding stages supports the indirect association of modules via an 'index' pattern generated in the hippocampus. The ascending input from sensory areas to association cortices and hippocampus, mainly entering the hippocampus through entorhinal cortex layers II and III, and also the descending outputs from the hippocampus (Swanson and Kohler, 1986), should undergo rapid plasticity (Insausti et al., 1997). The hippocampal output is

predominantly directed back to the NMDA-receptor rich (Monaghan and Cotman, 1985), superficial layers of almost the entire neocortical mantle either directly through the deep layers of the entorhinal cortex or indirectly via the perirhinal cortex (Insausti et al., 1997). Within-hippocampus and within-module plasticity processes would also be essential to enable the formation of local cell assemblies that can be retrieved autoassociatively. Through lengthy and slow plasticity processes, involving the rearrangement of intermodular connections, the modules would become directly linked. In patients with anterograde amnesia, the ability to form new memories and to incorporate information from these into the existing semantic knowledge base is dramatically impaired. Such patients almost always have severe damage to the hippocampus and are therefore missing the module that, according to theory, enables indirect association among lower cortical modules. After hippocampal damage, however, some remote memories, cognitive functionality and categorized knowledge are left intact. According to the Standard Consolidation Theory, the hippocampus supports memory storage and recall only for a limited amount of time, after which the memory or the links are thought to be transferred to neocortical sites and protected from hippocampal damage through a process of systems consolidation. Accumulating evidence calls this theory into question (Sutherland et al., 2010) because, in many studies with hippocampal lesions or temporary inactivations, the memory deficits are not graded, meaning that memories that have been acquired further back in time are impaired as much as recent ones (Martin et al., 2005; Sutherland et al., 2008). This

phenomenon seems to be independent of the extent of hippocampal damage and the memory task used. Only a small number of studies make an exception to this observation (Clark et al., 2002; Tse et al., 2007). Although episodic memory recall seems to depend on the hippocampus at all time intervals measured, it is unlikely that the memory persists in its original form throughout life. More likely, information may be extracted from these memory traces and incorporated into what is generally called 'semantic memory' or knowledge (McClelland et al., 1995). Thus, whereas the hippocampal code represents direct associations of details that compose the experienced event, the cortical code represents the knowledge and general information that can be deduced from it. 'Consolidated' information is no longer necessarily linked to specific space and time information, but probably incorporated into the pre-existing semantic knowledge about the world through a classification process (Marr, 1970, 1971).

It is now generally believed that the process of extracting knowledge from memory occurs mainly during sleep, when the brain is not occupied with processing current sensory information, and is essentially functionally disconnected from the environment (Marr, 1971). A way to accomplish the post learning re-sorting of information would be to 'replay' the episodic information interleaved with knowledge representations from past experience (McCloskey and Cohen, 1989; McClelland et al., 1995). Indeed, there is abundant evidence in rats that behavioral activity patterns are re-expressed during post behavioral sleep episodes (Wilson and McNaughton, 1994;

Kudrimoti et al., 1999; Euston et al., 2007; Lansink et al., 2008; O'Neill et al., 2008; Karlsson and Frank, 2009; Lansink et al., 2009; Dupret et al., 2010). Such synchronous reactivation of various subcomponents of the memory that may be stored in different cortical modules may enable the rearrangement and strengthening of selective connections at this time. After the gradual formation and/or reorganization of the horizontal connections, the memory might be sustainable through the new associations (possibly in 'semanticized' form) without the top-down linkage from the hippocampus. However, multiple reinstatements of the experience that trigger replay episodes are likely a requirement to establish a hippocampus-independent memory trace. If the amount of replaying episodes does not suffice to establish a strong enough extra-hippocampal representation, the memory will likely not be spared after inactivation of the hippocampus.

Most of the experimental data, which gives clues about memory consolidation in the mammalian cortex is derived from electrophysiological ensemble recordings, mainly from the rat brain. In this chapter we discuss how these data are acquired, organized and analyzed, as well as what is our current knowledge about memory trace reactivation in the hippocampo-neocortical circuit during slow wave sleep.

SPARSE VS. DISTRIBUTED CODING TO MAXIMIZE STORAGE CAPACITY

The degree of sparsity in coding appears to differ systematically as one ascends in the hierarchy of cortical modules and peaks in the hippocampus. In a sparse code, the

proportion of units used to store a memory (α) is minimized to maximize the number of distinct patterns that can be stored. In low-level modules, such as primary sensory or motor cortex, where high resolution and smooth generalization is emphasized rather than rapid information storage, coding is not sparse but rather fully distributed ($\alpha = 0.5$). In some areas of the hippocampus, coding appears to be optimized to store a maximal number of patterns rapidly in the network, thus α must be minimal. Electrophysiological recordings and immediate early gene (IEG) studies together confirm that the proportion of hippocampal neurons active at any given location is, in general, extremely small, and that sparsity is greatest in DG, and becomes progressively less in CA3, CA1, subiculum and deep entorhinal cortex (Alme et al.; Barnes et al., 1990; Guzowski et al., 1999; Leutgeb et al., 2004; Vazdarjanova and Guzowski, 2004; Alme et al., 2010).

Although sparse coding maximizes the number of items that can be stored, it does so at a cost of reduced information transmission per neuron. Thus, where only transmission and not storage is required, it is more economical to use a more distributed code so that the same amount of information can be sent over fewer channels. It appears that the hippocampal formation exploits this possibility by compressing the CA3 and CA1 output to a less sparse code prior to transmission back to the neocortex via the subiculum and deep layers of the entorhinal cortex (Barnes et al., 1990).

The main outputs of the hippocampal formation target the superficial layers of the neocortex. Recent evidence based on activity-dependent immediate-early gene activation indicates that, whereas the deep layers of the neocortical modules express

purely domain-specific information (e.g., touch, taste, vision, movement, etc.), neurons in the superficial layers express the conjunction of spatial context and the domain-specific information (Burke et al., 2005). Although further study is needed, these observations are consistent with the ‘indexing’ theory (Teyler and DiScenna, 1986; Teyler and Rudy, 2007), which postulates that the pattern transmitted from the hippocampus back to the neocortex is stored in the superficial layers of neocortex along with information about the current experience or motor output, thus serving as a means of top-down associative retrieval. Also consistent is the fact that the superficial layers possess the highest density of NMDA-receptors (Monaghan and Cotman, 1985) and thus may be more susceptible to rapid plasticity.

BASIC DATA STRUCTURE AND ANALYSIS OF ENSEMBLE RECORDINGS

In order to present the neurophysiological evidence for memory trace reactivation, it is useful first to discuss some general ways that neural ensemble recording data can be conceptualized and analyzed. In single-unit extracellular recordings (and, more recently, in optical imaging studies), spike trains (i.e., lists of action potentials over an arbitrary time interval) of a sample of a few hundred cells can be obtained with today’s available technology. These lists comprise a matrix (i.e., $N \times T$ spike rate matrix Q , where N is the number of cells and T is the number of time intervals) that contains information about the animal’s brain state at various time points (Figure 2.2A). Each row corresponds to one cell’s activity across the recorded time intervals (rate vector, reflecting the firing

rate of one neuron) and each column corresponds to the ensemble activity of all neurons at a certain moment (state vector, reflecting the brain state by the ensemble activity at a given time). Summation along the first dimension would result in a vector containing the mean firing rates of all neurons. Summation along the second dimension would result in a time series of the mean population activity, which is sometimes considered to be reflected in the filtered local field potential trace. The simple correlation between any two rate vectors (temporal correlation) represents the correlation of firing between two neurons over a certain time interval, while the correlation between any two state vectors (state correlation) estimates the similarity of the global states of the system at the corresponding times.

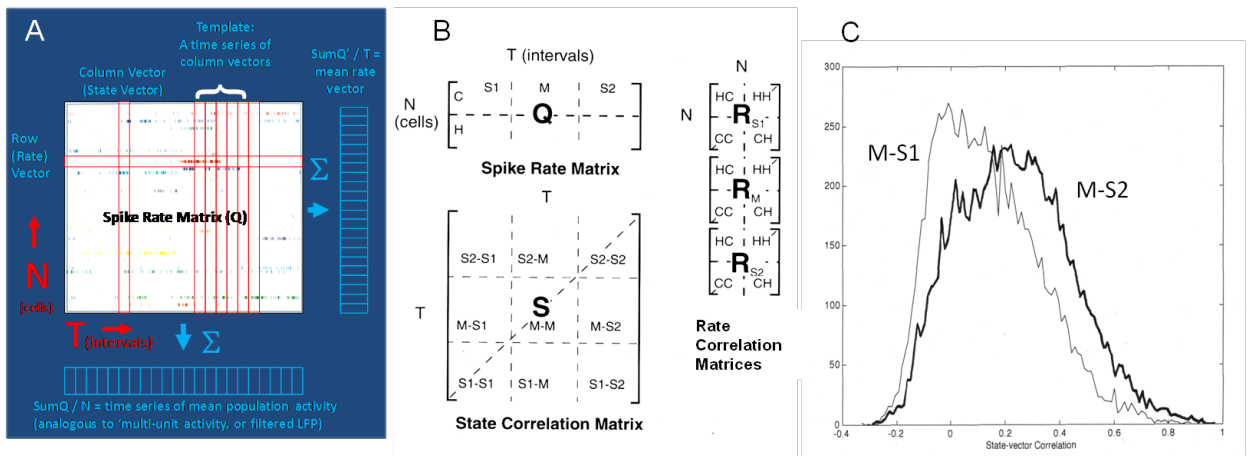


Figure 2.2 Data analysis of multi-unit recordings

(A) Modern neurophysiologic methods allow the simultaneous recordings of about a few hundred neurons. In this plot, the spike activity (colored vertical ticks) of about 50 neurons is plotted for about 10 seconds. This constitutes the $N \times T$ spike rate matrix (Q), where each row represents the spike activity of an individual neuron and the columns can be considered as time, binned into regular intervals of arbitrary size. Column-wise correlation measures similarity of brain states, while row-wise correlation detects co-firing between neuron pairs. (B) Data analyses of multi-unit recordings. The column-wise correlation of the Q -matrix yields the $T \times T$ state correlation matrix (S -matrix). The S -matrix can be divided into subdivisions corresponding to the different epochs correlated with each other. Along the diagonal, within-epoch

correlations will be high on average if the behaviour is repetitive. The subdivisions S1-M and M-S2 are of main interest in terms of reactivated patterns in sleep. The row-wise correlation of the Q-matrix results in separate R-matrices (rate correlation matrices) for each epoch. (C) Distribution of state-vector correlation values. Correlation values between post-task sleep and behaviour are higher than correlation values between pre-task sleep and behaviour, which peak around 0. The shift toward higher values of the state-vector correlation distribution of M-S2 indicates that behavioural firing patterns are re-expressed in sleep after behaviour (McNaughton, 1998).

An established method to quantify memory reactivation is to express the Pearson correlation coefficients of the temporal correlations (rate vector correlations) between neuron pairs for each epoch (pre-task sleep, task, post-task sleep) and assemble them into single matrices. Memory trace reactivation is measured by computing how much of the variance in the firing rate correlation matrix in post-task sleep can be accounted for by the variance in the correlation matrix of the firing patterns established during the task, when controlling for all effects that were already present in the active cell population in pre-task sleep (Kudrimoti et al., 1999; Tatsuno et al., 2006).

Another way to assess memory reactivation is to compare state vectors between epochs to identify patterns that emerge during behavior and are re-expressed during post-task sleep. If there is increased probability of a state vector to reappear in sleep after its appearance in a behavioral episode, either because of the formation of new cell assemblies through associative synaptic modifications or because they were already defined in the synaptic matrix before the behavioral epoch, it suggests that there is some form of memory being reactivated. By constructing a ($T \times T$) correlation matrix S of all state vector correlations, which will consist of different submatrices (Figure 2.2B), of

which S1-M and M-S2 are of main interest, one can compare the means of the correlation distribution for the S1-M and M-S2 matrix. If activity states of the preceding behavior are being re-expressed in S2 then we expect the average of the elements of the M-S2 matrix to be significantly larger than of S1-M. Consequently, the distribution of state-vector correlations for M-S2 is shifted towards higher values than the distribution of M-S1 (Figure 2.2C).

A more sophisticated and elegant approach to determine state vector similarities among task and sleep epochs is to define a series of state vectors during behavior as a template and shift it across a target period (pre-task and post-task sleep, respectively) to identify matching episodes (Louie and Wilson, 2001)(Louie and Wilson, 2001). Unlike the previously described analytic methods, the template matching procedure is sensitive to the temporal sequence of state vectors and also to possible temporal compression of the template pattern (Tatsuno et al., 2006).

USING PLACE CELLS TO STUDY MEMORY

The dominant characteristic of neuronal activity in the rodent hippocampus is selectivity for spatial location, a discovery, which led to the term 'place cells' (Figure 2.3)(O'Keefe and Dostrovsky, 1971). This feature makes them particularly suitable to study memory because it is generally the case that simply being in different locations leads to distinct patterns of neuronal activity, which can subsequently be identified during potential retrieval periods such as sleep. How could we tell if memory traces were being

reactivated during sleep after a behavioral episode? Cells that fired together during the task should also fire together during subsequent sleep (Wilson and McNaughton, 1994), whereas cells that did not fire together during the task should not do so afterwards (Figure 2.4). By recording a large ensemble of cells in the hippocampus during task and sleep, a multiple regression analysis of pairwise firing rate correlations can be used to quantify memory trace reactivation (Kudrimoti et al., 1999)(Figure 2.4B). The spike rate correlation structure has been observed to persist during rest for up to 30-60 minutes following an episode of behavior, such as track running. This phenomenon is dependent on NMDA-receptor activation, as the correlation persistence disappears when NMDA-receptors are blocked (Stanis et al., 2004) during the behavioral epoch. Reactivation can also be observed using the state vector approach. In a typical maze running task, a rat runs laps repetitively, so the same states in the hippocampus repeat periodically at a rate that is dependent on the animal's speed. This repetitive pattern is reflected in high correlation values along the diagonal of a state vector correlation matrix for the behavioral episode. If one compares the similarity of each state vector in sleep to each state vector during behavior (Figure 2.2), then it is observed that there is generally a higher similarity of S2 vectors to the behavior than there is for S1, which is what one would expect if memories were retrieved during S2.

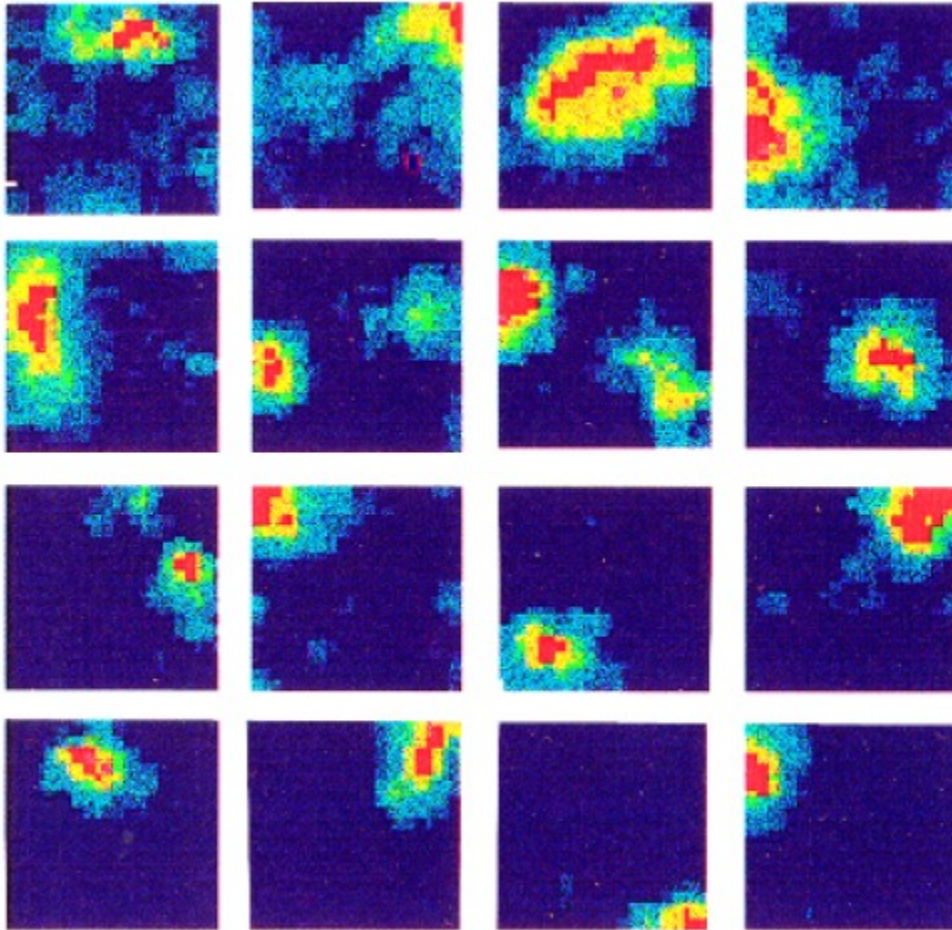


Figure 2.3 Place cells in the hippocampus

Sixteen firing rate maps from representative dorsal hippocampal neurons (CA1) which had 'place fields' in a 70 x 70 cm enclosure while the rats foraged for randomly scattered food pellets are depicted (Jung et al., 1994).

Experiences and memories for them are not typically discrete events but rather play out as temporal sequences. The neural basis for this temporal evolution was first proposed by D.O. Hebb (1949), who proposed the concept of “phase sequences”, which he envisioned as sequences of cell assemblies which become directionally (i.e., asymmetrically) linked by strengthening connections from cells active earlier in the sequence onto cells active later. One prediction of this concept is that, due to the rapid

forward spread of neural activation, subsequent activation of cells earlier in the

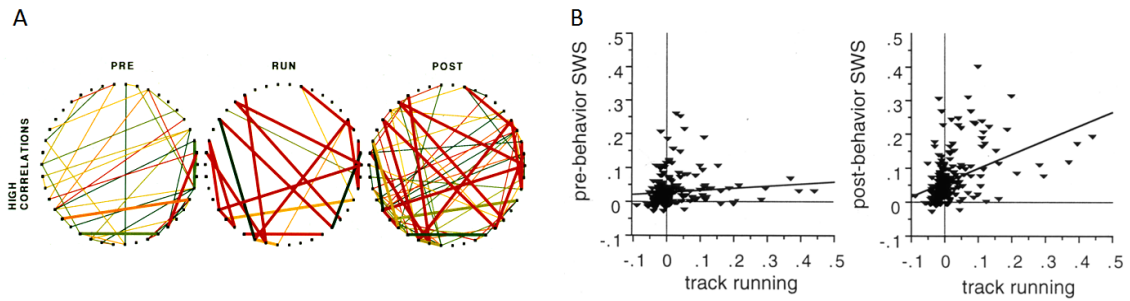


Figure 2.4 Connectivity matrix and pairwise correlations between hippocampal neurons during pre-task sleep, behavior and post-task sleep

(A) Diagram of synaptic connections among simultaneously recorded hippocampal neurons during pre-task sleep, behaviour and post-task sleep. Lines indicate positive correlations between neuron pairs with the magnitude of the correlations coded in false colours (red: max, blue: min). Bold lines indicate pairs that were correlated during RUN and also correlated during either PRE or POST. Cell pairs that are strongly correlated during RUN are mostly also correlated during POST but generally absent in the pre-task sleep (Wilson and McNaughton, 1994). (B) Scatterplots to illustrate the relationships of hippocampal pairwise correlations between track running and pre-task sleep and between track running and post-task sleep, respectively. A simple linear regression line can be fit to the correlation data between run and post-task sleep (Kudrimoti et al., 1999).

sequence would lead to activity in the cells at later points, before those points were actually reached. This phenomenon has been observed in hippocampal place cells, which expand their fields with experience in the direction opposite to the rat's movement (Mehta et al., 1997). If cells have become sequentially linked during behavior, one might expect to see evidence of this linkage during off-line retrieval. A simple test would be to compute the temporal cross-correlograms of cells during sleep and compare their symmetry characteristics to the preceding behavior. For example, if cell A leads cell B in its firing during behavior, it should also tend to lead cell B during sleep after behavior. This was indeed observed by Skaggs and McNaughton (1996) and the reactivation of sequence data during sleep has now been documented using several

different analytical approaches and in several different brain regions (Kudrimoti et al., 1999; Louie and Wilson, 2001; Hoffman and McNaughton, 2002; Tatsuno et al., 2006; Euston et al., 2007; O'Neill et al., 2008; Karlsson and Frank, 2009; Lansink et al., 2009; Dupret et al., 2010). Explained variance has proven to be a fairly robust measure of memory reactivation. The reason for this is that the measurement is based on pair-wise correlations of binned spike trains of neurons within the time window of interest without taking into account complex fine time-scale sequences expressed by the ensemble of neurons. Therefore shuffling the 'population vectors' (i.e., columns in the Q-matrix), which equals segmented or incomplete replay of sequences, would not affect the correlation values. Sequences replayed at speeds different from the original encoding do not compromise the strength of the multiple correlations, but they do affect results obtained from template matching. Template matching, a powerful method to identify matching sequences of population vectors in two recording epochs, would need to employ an exhaustive and computationally expensive search to identify compression factors.

COHERENT REACTIVATION OF MEMORY TRACES IN HIPPOCAMPUS AND NEOCORTEX

The trace reactivation theory of memory consolidation requires that the reactivation of subcomponents of an experience is coherent across all the modules in which these subcomponents are stored. Such coherence is necessary to ensure that the correct

features are associated with one another. Here we summarize the evidence supporting this requirement and review the current knowledge about the dynamics of the process. Whereas, during behavior and REM sleep, the hippocampal EEG is dominated by 8-12 Hz oscillations (theta), during slow wave sleep, the hippocampal EEG is characterized by 'sharp waves' and 'ripples'. Sharp waves reflect strong depolarizations of the CA1 dendrites due to synchronous activation of many Schaffer collaterals of CA3 pyramidal cells, which make excitatory synapses there. These sharp waves often have high frequency oscillations called ripples (synchronous population discharge of CA1 pyramidal cells at ~150 Hz) superimposed on them. It is predominantly, if not exclusively during these synchronized population events, that memory traces are reactivated in the hippocampus (Kudrimoti et al., 1999)(Figure 2.5). The temporal relationships of the reactivating ensemble in sleep after behavior are preserved (Skaggs and McNaughton, 1996). If the hippocampus orchestrates the reinstatement of experience-specific

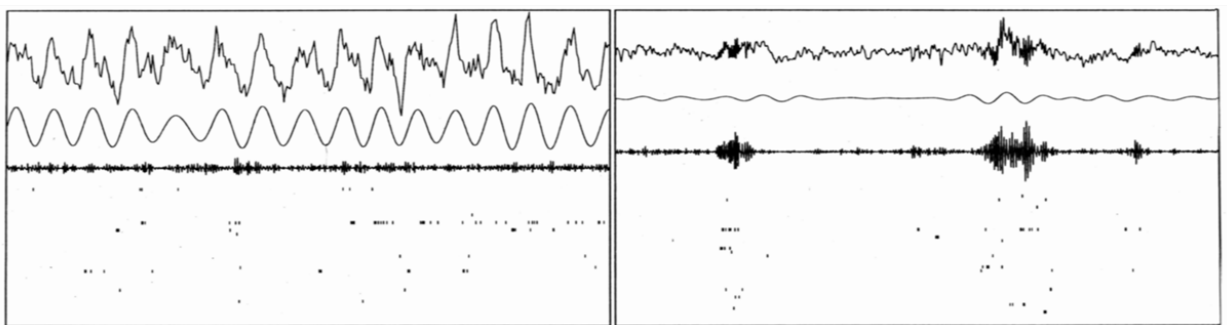


Figure 2.5 Hippocampal EEG and concurrent spike activity during REM and slow wave sleep
Hippocampal EEG and concurrent spike activity during a REM (left) and slow wave sleep (right) episode. The size of the windows is 2 s. The top trace in both panels is the raw EEG trace (sampling rate 200 Hz), the two traces below are the EEG band pass filtered between 6 and 10 Hz (second trace) and between 100 and 300 Hz (third trace). Below, each row represents the spiking activity of a hippocampal pyramidal neuron. Each tick mark represents a spike. (left) Theta activity is prominent in the EEG during REM sleep, but is absent in slow wave sleep (right,

missing 7-8 Hz component in filtered hippocampal trace). The third EEG trace shows 100-300 Hz components (ripples) in slow wave sleep, which entail increased spiking activity of pyramidal neurons that are essentially silent in the absence of ripples. Adapted from (Kudrimoti et al., 1999).

patterns in the neocortex, as suggested by consolidation theories, then coordinated firing between hippocampal and neocortical units should emerge. Evidence supporting this hypothesis was obtained by recording from hippocampus and parietal cortex simultaneously (Qin et al., 1997). Simple correlation analyses of spike trains within and between areas showed that co-firing during behavior has effects on co-firing during subsequent sleep when taking into account pre-existing correlations during pre-behavioral sleep. The indexing theory postulates that hippocampal memory retrieval would coordinate reactivation of the relevant information in lower level modules to establish the necessary connections for pattern completion to occur without the indirect hippocampal associations. Consistent with this prediction, coherent reactivation among widespread neocortical modules has been observed following a simple reaching task in monkey (Hoffman and McNaughton, 2002). Activity patterns in motor, somatosensory, and parietal cortex were significantly reactivated. Contrary to at least the simple version of the theory, however, Ji and Wilson (2007) observed that during spontaneous retrieval in primary visual cortex and hippocampus, short sequences in the cortex may precede sequences in the hippocampus by about 50 ms after running on a highly familiar figure-8-shaped maze. Similarly, preliminary data suggests that in sleep after performing a highly familiar sequence task, medial prefrontal unit activity tends to lead hippocampal

unit activity (Euston et al., 2008). However, direct pairwise correlations between hippocampal and prefrontal neurons during sleep after various spatial tasks reveal a consistent lead of hippocampal neurons during sharp wave events (Wierzynski et al., 2009). Although it is unclear how familiar the tasks are in the latter study, these data may suggest that the direction of interaction in initiating replay events in sleep after behavior might depend on the degree of 'consolidation' of the memory. Reactivation of recent memory may be led by the hippocampus, while reactivation of already established memory traces may be coordinated by the medial prefrontal cortex, at least in certain cases. One possible scenario could be the integration of new information into an already existing, 'consolidated' memory trace. In this case, the pattern would be reinstated in the cortical modules first and hippocampal activity would follow, which would allow the addition of the new episodic information to be incorporated into the cortical pattern. These observations remain to be studied and analyzed in more detail to allow for further interpretations. Since the actual memories are thought to be stored over multiple neocortical modules, it is also possible that reactivation of even a novel memory may be initiated within one of the relevant modules, which would trigger the reactivation of the hippocampal index code and lead to the synchronous reactivation of the entire memory.

Spontaneous memory trace reactivation has also been observed in subcortical structures, such as the ventral striatum (Pennartz et al., 2004). Neurons in that area also engage in memory trace reactivation, but only those neurons whose activity is

modulated by sharp waves in the hippocampus, suggesting a close coordination between structures (Pennartz et al., 2004). This is consistent with the idea that the hippocampus acts as the coordinating module during spontaneous reactivation episodes in its projection areas. Furthermore, only neurons coding for motivationally relevant information (such as reward) in the ventral striatum exhibited reactivation with hippocampal place units in a forward direction (Lansink et al., 2008; Lansink et al., 2009). Despite the accumulating data on reactivation in different brain regions, there is still no compelling evidence that memory trace reactivation is beneficial or critical for correct memory retrieval. Individual differences in reactivation scores in rats explain significant variance of performance in the water maze spatial task and therefore provide a piece of evidence suggesting that there is a direct relationship between reactivation and memory performance (Gerrard et al., 2008). This idea is further supported by the observation of impaired performance of a spatial reference task after selective interruption by electrical stimulation of hippocampal ripples in sleep after behavior (Girardeau et al., 2009; Ego-Stengel and Wilson, 2010). Nevertheless, the more direct evidence for this hypothesis remains a major challenge in the field.

MEMORY TRACE REACTIVATION DYNAMICS DURING SLOW WAVE SLEEP

Slow wave sleep is characterized by a bimodal distribution of spike activity after the onset of slow oscillations and K-complexes (Johnson et al., 2010) and has become more strongly associated with memory reactivation than other sleep stages (Louie and Wilson,

2001; Euston et al., 2007; Johnson et al., 2010). Memory reactivation in the prefrontal cortex during slow wave sleep is dynamically modulated by various patterns in the cortical EEG. One prominent pattern associated with reactivation is the K-complex. K-Complexes are rapid voltage transitions that typically appear when the down to up state transition is extremely synchronized among a number of pyramidal neurons and are typically followed by a low voltage spindle (LVS, 6-20 Hz in rat)(Figure 2.6A). Periods of frequent K-complexes, LVS and the down to up state transitions are correlated with strong cortical memory reactivation as measured with EV and template matching (Figure 2.6B)(Johnson et al., 2010). During high voltage spindles (HVS, 6-8 Hz in rat), however, reactivation appears to be fairly weak (Johnson et al., 2010). In the prefrontal cortex, replay of activity patterns of a highly stereotyped behavior is compressed by a factor of six to seven (Euston et al., 2007), which can be inferred from similarly shaped cross correlations of neuron pairs of the task and the post-task sleep epoch, with the only difference being the temporal scale (Figure 2.7). This observation is consistent with the notion that memory replay speed is not constrained to real-time parameters during encoding, but rather proceeds at speeds determined by network parameters such as synaptic strength and connection asymmetry, dendritic integration times, and conduction speeds. The compression factor declines during a prolonged sleep session concomitant with a reduction of reaction strength (Tatsuno et al., 2006). This is consistent with the hypothesis of a gradual decline of the synaptic potentiation underlying the memory.

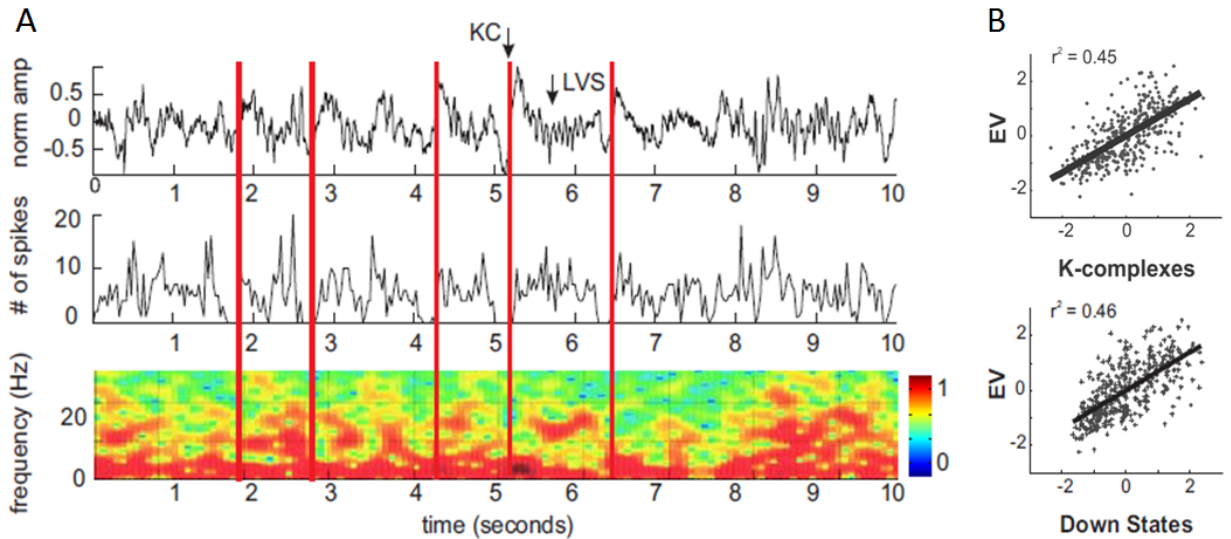


Figure 2.6 The relationship between K-complexes and memory reactivation

(A, top) K-complex/LVS epochs occur during periods of low-frequency, high-amplitude activity in the local field potential (LFP) (first panel). These periods correspond to periods of up state/down state fluctuations in the total spike activity (124 cells, 30 ms bins, second panel). A clear example LVS preceded by a K-complex is marked by the arrow in the top panel. Each K-complex in the LFP is matched by a network down state in the total spike activity (red bars). In the spectrogram of the LFP (third panel), the K-complexes correspond to high power in the 2–6 Hz range, while LVSs correspond to a peak in the 10–20 Hz range. (B) Linear regression plot showing the relationship between memory reactivation, measured with explained variance, and the number of down states and K-complexes, respectively. The data points for sleep and behavioural epochs are compiled. Memory reactivation strength is positively correlated with the number of K-complexes (top) and down to up transitions (bottom) in a given epoch. Adapted from (Johnson et al., 2010).

Memory replay in the prefrontal cortex and hippocampus are most likely not isolated events, but may influence each other. This assumption is based on the observation that hippocampal sharp waves are most likely to occur at down to up state transitions in the cortex during slow wave sleep (Battaglia et al., 2004b; Mölle et al., 2006) (Figure 1.8). It is

possible to detect frequently reactivated patterns in the prefrontal cortex with a high

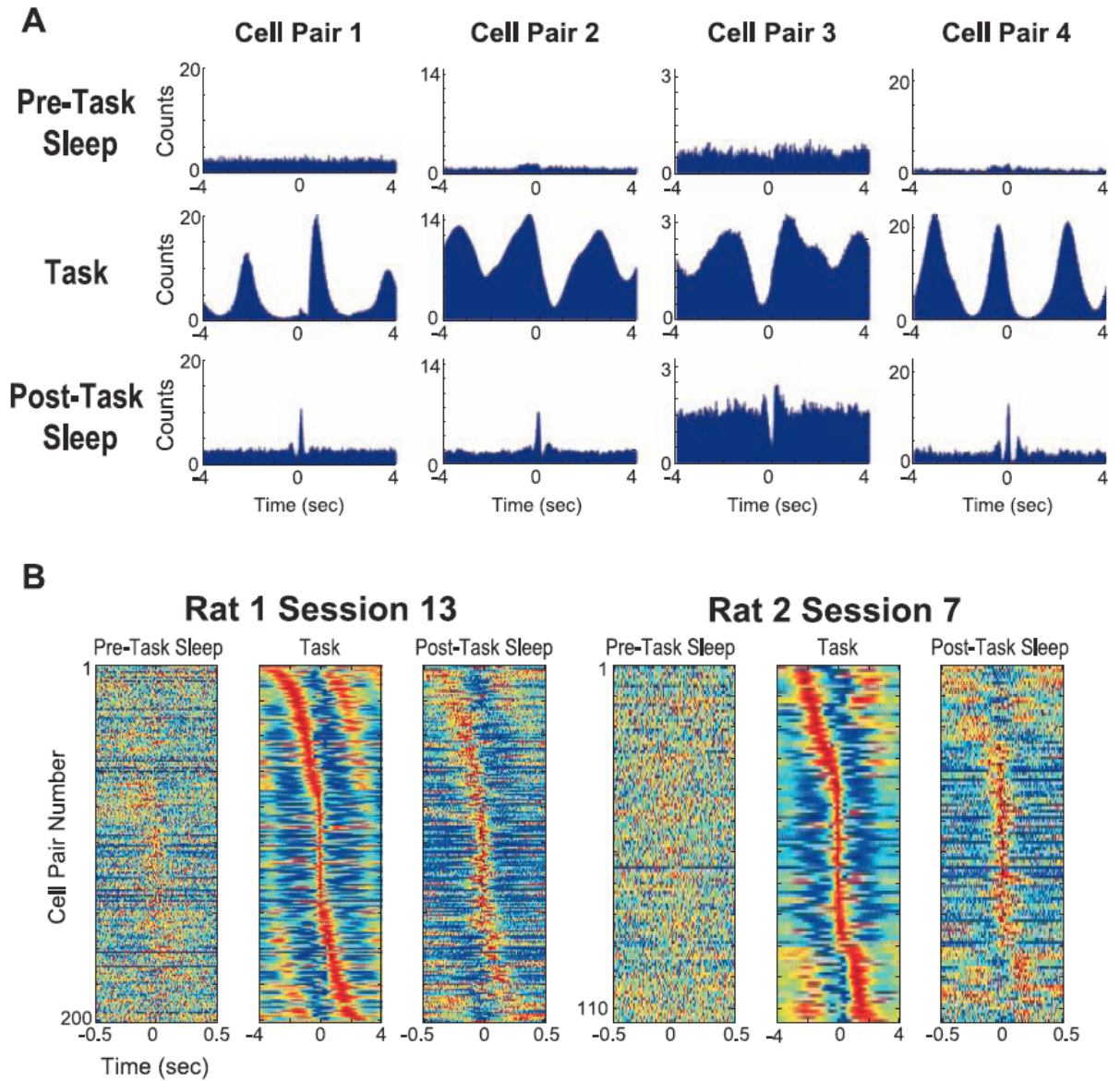


Figure 2.7 Cross correlations between neuron pairs in medial prefrontal cortex during task and sleep

(A) Cross correlations of neuron pairs in the rat medial prefrontal cortex. Each row corresponds to a different behavioural epoch (pre-task sleep, task and post-task sleep). Each column corresponds to a different cell pair. Note that the peaks of the correlogram of the task epoch are re-expressed in post-task sleep in a compressed fashion, but are not identifiable in pre-task sleep. This suggests that cells that have been active together during the behavioural epoch reactivate together during sleep after behaviour. (B) In each panel cross correlations are sorted according to the peak in their correlogram for the task epoch. For two rats, the cell pairs are

depicted for pre-task sleep, task and post-task sleep. Note that the patterns of the peaks in the correlograms are similar in task and post-task sleep but the temporal scale varies. Activity seems to be sped up by a factor of 6 to 7 in post-task sleep compared to behavior (Euston et al., 2007).

temporal precision and relate their times of occurrence to hippocampal sharp-wave ripple events (Peyrache et al., 2009). This is achieved by applying principal component analysis, a statistical tool to identify the structure of the data by converting a number of correlated variables into a smaller number of uncorrelated values. In fact, principal components representing sequences of replayed firing patterns from the behavioral episode of a highly familiar task are reinstated as often in pre-task sleep as in post-task sleep. However, during post-task sleep the principal components have a stronger correlation with the appearance of sharp waves in the hippocampus. This suggests the conclusion that, after consolidation, the reactivation of familiar events has become relatively independent of the hippocampus, but when the memory is reinstated, new bouts of reactivation episodes are triggered in the hippocampus.

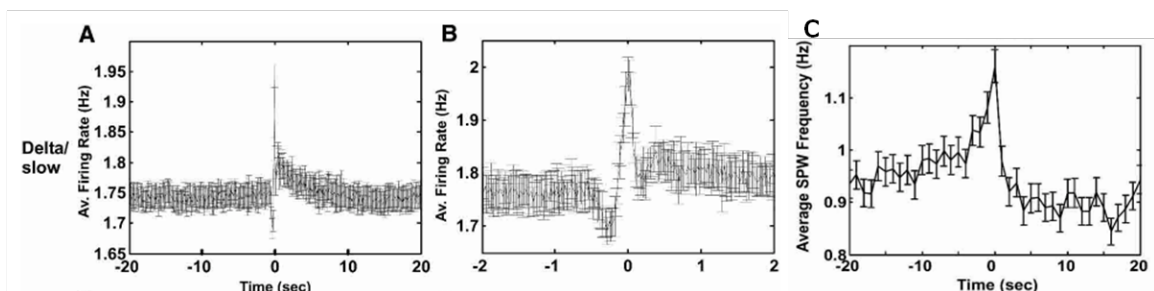


Figure 2.8 Relationship between neocortical neural activity and hippocampal sharp waves

(A) Peri-event time histogram (PETH) of cortical neural population activity during identified delta/slow wave oscillations centered on hippocampal sharp wave events. At the time of sharp waves, there is a transient increase of cortical activity and a subsequent increase in firing rates as compared to before the sharp waves. The sharp peak in the cortical activity is preceded by a

dip (200-400 ms) as can be seen in the same PETH with a finer timescale (B). This transient decreased activity could be entailed by delta oscillations that are occurring in phase. (C) PETH of hippocampal sharp wave events centered on the transitions from cortical down to up states.

Sharp wave occurrence was maximal at down to up state transitions of cortical population activity. Baseline activity is higher during down (left of 0) than during up states, indicating that sharp waves are more likely to occur during down than during up states. Adapted from (Battaglia et al., 2004b).

Memory trace reactivation is a process with complex dynamics that are not yet fully understood. The power of the analysis methods that are currently in use to assess reactivation processes increases with the number of units recorded, and substantial increases in this number can be expected to result from ongoing technical developments in many laboratories, including the application of optical recording methods. With the existing evidence, we can already attempt to make some speculations about how the cortex and hippocampus interact to replay memories. During sharp-wave ripple events in the hippocampus, events experienced in the immediate past are either spontaneously retrieved or their retrieval may be triggered by partial recall of the event in a cortical module. The hippocampal outflow during sharp waves coordinates reactivation of the relevant information distributed over multiple neocortical modules. Sharp waves tend to coincide with the down to up fluctuations in the cortical slow rhythm, but tend to be of shorter duration than the up states. Thus, hippocampal reactivation may simply initiate the retrieval of neocortical sequences which play back during the remainder of the up state. During the up state, reactivated cortical neurons may strengthen or rearrange their synaptic connections with other neurons that were engaged in the sequence that is

being replayed. This could be a mechanism through which knowledge is extracted from acquired memory and established in horizontal intermodular cortical connections.

Acknowledgements: This work was supported by an Alberta Heritage Foundation for Medical Research Polaris Award and an Alberta Innovates Health Solutions studentship.

Chapter 3 Experience-Dependent Firing Rate Remapping Generates Directional Selectivity in Hippocampal Place Cells

Zaneta Navratilova^{1,2}, Lan T. Hoang³, C. Daniela Schwindel¹, Masami Tatsuno¹ and Bruce L. McNaughton^{1*}

¹ Canadian Centre for Behavioural Neuroscience, University of Lethbridge, Lethbridge, AB, Canada ² Graduate Interdisciplinary Program in Neuroscience, University of Arizona, Tucson, AZ, USA ³ Evelyn F. McKnight Brain Institute, University of Arizona, Tucson, AZ, USA

Published in: Navratilova et al. (2012), Front Neural Circuits 6:1-12.

ABSTRACT

When rodents engage in irregular foraging in an open field environment, hippocampal principal cells exhibit place-specific firing that is statistically independent of the direction of traverse through the place field. When the path is restricted to a track, however, in-field rates differ substantially in opposite directions. Frequently, the representations of the track in the two directions are essentially orthogonal. We show that this directionally selective firing is not hard-wired, but develops through

experience-dependent plasticity. During the rats' first pass in each direction, place fields were highly directionally symmetric, whereas over subsequent laps, the firing rates in the two directions gradually but substantially diverged. We conclude that, even on a restricted track, place cell firing is initially determined by allocentric position, and only later, the within-field firing rates change in response to differential sensory information or behavioral cues in the two directions. In agreement with previous data, place fields near local cues, such as textures on the track, developed less directionality than place fields on a uniform part of the track, possibly because the local cues reduced the net difference in sensory input at a given point. Directionality also developed in an open environment without physical restriction of the animal's path, when rats learned to run along a specified path. In this case, directionality developed later than on the running track, only after the rats began to run in a stereotyped manner. Although the average population firing rates exhibited little if any change over laps in either direction, the direction-specific firing rates in a given place field were up- or down-regulated with about equal probability and magnitude, which was independent in the two directions, suggesting some form of competitive mechanism (e.g., LTP/LTD) acting coherently on the set of synapses conveying external information to each cell.

INTRODUCTION

Principle neurons in the hippocampus proper exhibit activity correlated with the location in which an animal is located (O'Keefe and Dostrovsky, 1971). In an open environment, when an animal is moving around in a random path, such as while foraging for food, the majority of place cells fire at rates that are independent of the direction in which the animal is passing through the cell's 'place field' (Muller et al., 1987). These findings are consistent with the predominant view of the hippocampus encoding an allocentric representation of space (O'Keefe and Nadel, 1978). It is clear that the hippocampus is necessary for spatial memory (e.g. Morris et al., 1982); however, the degree to which this structure encodes changes in sensory cues or behavioral contingencies occurring in a single spatial environment is still debated (e.g. Eichenbaum et al., 1999).

One view is that the selection of which hippocampal cells fire at a given location is initially determined by path integration mechanisms (McNaughton et al., 1996), whereas sensory information that may vary at that location may become associatively linked to the selected cells, thus enabling future correction of path integrator errors. Such associative linking would typically not involve changing the membership of the active population (which would be considered 'global remapping'), but could affect their relative firing rates ('rate remapping'; Leutgeb et al., 2005b). Global remapping is typically induced when a rat is transferred between separate, distinct, recording rooms

(Leutgeb et al., 2004), when the rat locomotes between two boxes (Skaggs and McNaughton, 1998; Colgin et al., 2010), or when a large mismatch is introduced between its path-integrated heading direction and familiar visual landmarks (Knierim et al., 1998; Fuhs et al., 2005). In addition to local sensory information, internal information such as working memory, current goals, behavioral set, and possibly even circadian rhythms may also affect firing rates without significantly changing the locations at which the hippocampal cells fire (O'Keefe and Conway, 1978; Hetherington and Shapiro, 1997; Wood et al., 2000; Leutgeb et al., 2005b; Leutgeb et al., 2006; Sparks et al., 2010).

A long unresolved problem with the mainly allocentric view of hippocampal place cells has been that whereas, in an open environment, a large majority of place cells exhibit firing that is not direction specific (Muller et al., 1994; Markus et al., 1995), on a track that is repeatedly traversed along a specific path, the activity of place cells in each direction differs substantially (McNaughton et al., 1983a; Muller et al., 1994). In addition to the configuration of the traversable portion of the environment, the task the animal is performing also affects directionality of place cells: if the animal is repeatedly running a path between specified goal locations even in an open environment, the place cells show distinct directional firing (Markus et al., 1995). Interestingly, the presence of many local cues on the track reduces the difference in firing between the two running directions (Battaglia et al., 2004a), but the complexity of distal room cues appears not to affect directionality (Markus et al., 1995).

Recent findings suggest that the firing of 'grid cells' in the medial entorhinal cortex is generated by path integration and is the primary source of relative position information to the hippocampus (Hafting et al., 2005; Fyhn et al., 2007). Also notably, under conditions that induce rate remapping in hippocampal cells, grid cells do not exhibit changes in firing location or relative firing rate; however, conditions that induce global remapping in hippocampal cells also induce global remapping in grid cells (Fyhn et al., 2007). Overall, current data suggest that path integration occurs in the medial entorhinal cortex (McNaughton et al., 2006), and this information is then passed on to the hippocampus, which can combine it with other information, such as landmarks or other spatial cues, and task demands or other internal state variables, to form a conjunctive code for locations and the events that occur there (Leutgeb et al., 2005b). Path integration by the medial entorhinal cortex does not, however, explain why the place cell activity in two running directions on a track is so different, while the activity in an open environment is essentially independent of direction of travel. In the current study, we recorded from hippocampal cells while a rat traversed a circular track in both directions, beginning with the very first time that the rat had experienced the track in a given spatial context. We observed that, while the track was novel to the animal, the two running directions were in fact highly correlated. During repeated traversals of the track, the firing rates of place cells changed in both running directions, becoming highly dissimilar by the end of the session, as previous studies had shown. We present evidence that, unlike the expression of place fields per se, directional selectivity is an

experience-dependent phenomenon driven by gradual changes in the response of a cell to external sensory cues and/or internal variables such as goals or recent trajectories which occurs when the traversal of a path becomes stereotyped.

METHODS

Subjects. Five male rats (four Brown Norway-Fisher hybrids and one Brown Norway) were used for this study. The rats were housed individually and kept on a 12-hr dark / 12-hr light schedule. Training and experiments and occurred during the dark phase. During pre-training, and then again during recording, they were kept at ~85% of their free-feeding body weight, in order to be motivated to run for food rewards. All animal protocols complied with National Institutes of Health guidelines and Canadian Council for Animal Care (CCAC) regulations under the guidance of the University of Arizona Institutional Animal Care and Use Committee (IACUC) or the institutional animal care committee at the University of Lethbridge.

'Hyperdrive' assembly and implant. Rats were implanted with a 'hyperdrive' consisting of 14 individually movable tetrodes. Each tetrode consisted of four strands of insulated 13 μm nichrome wire twisted together, and was inserted in silica tubing and secured with cyanoacrylate glue to a drive cannula. The drive cannula was coupled by a plastic nut to a drive screw, so that rotation of the nut allowed vertical movement of the tetrodes through another (30 gauge) guide cannula. The 14 guide cannulae were placed within the inverted conical core of the hyperdrive, evenly spaced and angled at 30° from the

vertical axis at the top, and bundled together and vertical to the brain surface at the bottom of the hyperdrive, where they would be contacting the brain. For rats 1-3, the guide cannulae were bundled into a 2x7 linear array, to be placed along the proximal-distal axis of dorsal CA1. The remaining 2 animals (rats 4&5) were implanted with hyperdrives with a bundle forming a circle, and lowered to dorsal proximal-mid CA3. A more detailed explanation of the hyperdrive, implantation and recording techniques is published in Gothard et al. (1996a).

Surgery was performed under Isoflurane anesthesia. A 3mm in diameter craniotomy was opened above the right dorsal hippocampus (coordinates of the center of the craniotomy differed slightly between rats, between 3.3-3.8mm posterior and 2.0-3.0 mm lateral). The Dura was removed, the hyperdrive bundle was centered above the craniotomy, with guide tubes just touching the surface of the brain, and the craniotomy was sealed with Kwik-Sil and then cemented in place with dental acrylic anchored by dental screws spread over the rest of the dorsal surface of the skull. After surgery rats were administered 26mg of acetaminophen orally for pain relief, and given Ampicillin in their food for 10 days or given subcutaneous injections of Metacam and Tribissen to prevent infection. All tetrodes were lowered into the brain immediately following surgery by turning the screws three full turns (954 μ m).

Recording procedures. Twelve tetrodes were lowered over the course of 2-4 weeks to CA1 (rats 1-3) or CA3 (rats 4&5). The remaining 2 tetrodes were lowered to the corpus callosum, to serve as a reference, and the hippocampal fissure as an EEG recording

probe. For recording, the hyperdrive was connected to a unity-gain headstage (Neuralynx, Bozeman, MT), which allowed low noise transmission of signals from each of the four channels of each tetrode, via a multi wire cable and a commutator mounted on the ceiling, to digitally programmable amplifiers and then to the Neuralynx Cheetah system. Local field potential activity was continuously sampled from one channel of each tetrode at 2.4 kHz, amplified 500-1000 times, filtered between 1 and 300 Hz, and recorded. For this analysis, only the LFP signal from the tetrode with the largest number of cells on each day (the one most likely to be in the cell body layer) was used (filtered off-line at 6-10 Hz to determine the theta signal). Spike signals from each channel of the 12 hippocampal tetrodes were referenced against the corpus callosum electrode signal, amplified 1000-5000 times and filtered between 600-6000 Hz. Signals were digitized at 32 kHz, and a 1ms sample was recorded when the signal reached a pre-determined threshold. The thresholds were adjusted manually for each channel, depending on the noise level and spike amplitude on that channel. The headstage also contained a circular array of LEDs that were detected by an overhead camera and recorded by the Cheetah system along with the neural signals to allow tracking of the position of the rat on the maze. Video spatial resolution was approximately 3 pixels/cm.

After the completion of recordings, the location of the tetrodes was ascertained by creating a small electrolytic lesion at the tip of each tetrode (by passing 5 μ A current for 10 s). Histological sections were Nissl stained to localize the lesions. Based on coronal sections from the 3 CA1 rats, it was determined that the recordings of rats 1 and 2 came

from a wide range of proximal-distal coordinates in CA1, and rat 3 was found to have most tetrodes in proximal CA1, one tetrode in CA2, and 2 tetrodes in distal CA3. Thus the day 1 recordings included 183 CA3 cells, 22 CA2 cells, and 83 CA1 cells (51 from the proximal half).

Pre-training and behavioral tasks. All rats were pre-trained prior to hyperdrive surgery to run laps back and forth between food dishes on a circular track, as well as to forage for randomly sprinkled food rewards in an open field environment. All pre-training sessions occurred in a different room than the room in which recording took place. The track used during recording was usually different from the one used during pre-training, or when the same track was used, a different surface was placed on the track.

The first behavioral task involved the rats running on a circular track. Two rats ran on a track 120 cm in diameter, one rat on a 115 cm track and one on a 152 cm diameter track. A barrier was placed at one end of the track, with food dishes on either side of it, so the rat would have to turn around and run back to get the next food reward. Small objects and textures were placed on half of the track ('cue-rich'), and the other half had a uniform surface with no nearby objects ('cue poor'). Each running session lasted 25-30 min, and was preceded and followed by 30 min-1hr of rest in a small pot near the track. Because the rats were pre-trained to perform this task, three of the rats showed good enough behavior during their very first exposure to the track to allow us to analyze individual laps. Rat 3, however, did not run on the track during his very first exposure, and ran too slowly and too few laps (6) during his second exposure for that data to be

analyzed. Thus, the data analyzed as rat 3's "session 1" is actually his third day being placed on the track. Nevertheless, this data showed very similar results to the actual first exposure of the other 3 animals, and so was included in this study. The second task involved the rats running on a circular open platform. One rat ran on a platform 115 cm in diameter, and the other rat on a 142 cm platform. A three-walled box was placed at the edge of the platform, and the rat was acclimated to this environment for 5 minutes prior to each running session, by being confined to the box with a barrier placed along the opening. Once the barrier was removed, the rat was expected to run to the food dish on the opposite edge of the platform, pick up a food reward, and return to the box to eat the reward. The task was designed to be able to manipulate the speed of the rat as he returned with food rewards of different sizes. That aspect of the task, however, was not important to this study. Each running session lasted 30 minutes. The rats also foraged for randomly distributed food rewards in the same environment every day for 30 minutes (prior to the shuttle task, with a 30 min rest between tasks). It took the rats 2-4 days to learn the shuttle task, but once they learned it, they were running over 20 laps per session, most of them directly between the box and the food dish. Only the spikes occurring along a direct path were analyzed, and laps in which the rat diverged from a direct path to the food dish for more than 20% of the run in either direction were excluded from the analysis.

Spike sorting. Spikes recorded during the entire recording session (2-3 rest periods and 1-2 running epochs) were sorted based on energies and first 2 principle components of

the waveforms recorded on each electrode of a tetrode, using a semi-automated procedure. An automated algorithm (KlustaKwik, K.D. Harris, <http://klustakwik.sourceforge.net/>) was used to find clusters, which were then merged and adjusted manually using a modified version of MClust 3.1 (A.D. Redish, <http://redishlab.neuroscience.umn.edu/MClust/MClust.html>).

4.6. Position Tracking. The position during the running epochs was extracted at each video frame by fitting a circle to the ring of LEDs on the headstage. The position determined during previous frames was used to eliminate active pixels at a distance of greater than 20 pixels, which could not have been from the headstage, but were a result of other spurious light sources. This 2D position was then deconstructed into a 1D representation along the track. For the circular track task, a circle was fit to the position data, and the coordinate along the diameter of the track was determined for each frame (with the barrier assigned a position of 0). For the shuttling task, principal component analysis on the XY coordinates was used to find the axis of the 'track' and the coordinates along that axis were used (with the outer edge of the home box assigned a position of 0). Periods when the rat was stopped on the track were removed, by finding any periods when the rat was moving at less than 2cm/s. Velocity was calculated by smoothing XY position with a 1-second hamming window, and then calculating the distance moved between subsequent frames. For the shuttling task, periods when the rat diverged from the track (the coordinates along the axis orthogonal to the 'track' crossed a threshold value in either direction) were also removed from the analysis. If the

rat diverged from the 'track' for more than 20% of the distance in either direction, the whole lap (both directions) was removed from the analysis. Laps were identified by finding the turn-around points at the ends of the track.

Field analysis. Individual fields were delineated by smoothing (with a hanning window of 5 bins) the firing rate in (2cm) position bins and automatically finding the peaks and troughs on either side of those peaks. Peaks at a minimum of 0.8 Hz were considered fields, and the first trough away from the peak that had a firing rate of less than 0.05 of the peak rate was considered the field boundary. Fields that had two peaks that were separated by a trough of at least 0.6 of the smaller peak rate were split in two. Fields were outlined individually in each running direction, and then combined if the majority of the field overlapped with the field in the opposite direction. This way all the spikes from fields that had shifted in the forward running direction would be considered. If a field was not found in the opposite direction, the spikes occurring in the same position bins were considered as the opposite direction field. All field boundaries were checked manually on a phase precession plot (figure 3.1), and overlapping fields, fields that did not show phase precession in at least one running direction, or overlapped with food dish locations were excluded. Approximately 30% of the fields found by the automated algorithm were deleted in the manual step, most of these because they included few spikes and did not show phase precession, or they overlapped with a food dish location. The phase precession criterion was not applied very stringently, instead it was used in conjunction with the other criteria, for example to differentiate low firing rate fields

from spurious spikes, or to determine if overlapping fields could be successfully separated with a single boundary or should not be used. The boundaries of approximately 30% of the remaining fields were adjusted manually, because the automated algorithm did not identify the full phase precession of a field (especially low firing rate fields), or it included some noise spikes from outside of a field. Spikes occurring within the boundaries thus set were then considered for the lap-by-lap analysis of each field. See table 3.1 for the number of cells and fields analyzed from each animal.

Directionality index. The directionality of cells was determined by counting the number of spikes fired in each direction within each field, because this measures rate remapping better than a correlation. Spatial correlations are also influenced by the fact that fields are often offset in the two running directions (Battaglia et al., 2004). Thus, we calculated a 'directionality index,' which was the difference in number of spikes fired in each running direction divided by the total spikes in both directions on each lap, based on the rate remapping difference ratio in Leutgeb et al. (2005). The difference between the higher firing rate direction (on average over the whole session) and the lower firing rate direction was used instead of the absolute value of the difference, because this way the same direction is being subtracted for all laps. Negative directionality index values resulted when the running direction in which more spikes occur switched between laps. When a cell spiked only in one running direction, the directionality index was 1.

RESULTS

To study whether and how the directionality of place cells changes during initial experience on a track, we compared firing rates during passes through place fields in either direction across laps during the animal's first session on the track. For each cell, each place field was delineated (see figure 3.1 and methods), and all spikes that occurred within the field boundaries on each lap were counted. The 'directionality index' of each field was calculated for each lap. The 'higher firing rate direction' is defined as the direction in which, over the whole session, the number of spikes fired is greater. The directionality index (DI) is the number of spikes fired in the higher firing rate direction minus the lower firing rate direction, divided by the total number of spikes in both directions, and is the same as the rate remapping difference ratio used by Leutgeb et al. (2005). The average directionality index increased from a very low value (cells show almost identical firing in both directions) to a high value in about 5 laps of experience on the track (figure 3.2), even though the average firing rates of the population stayed the same (figure 3.4A). During the second and third sessions of experience on the track, the directionality index was already high on the first lap, but still increased slightly during the next few laps (figure 3.2). There was a significant difference between the directionality index on the first lap compared to the last lap on all three days (paired t-tests, day 1: $p < 0.0001$, day 2: $p < 0.05$, day 3: $p < 0.01$). This was true for both the CA1 and CA3 cells in our analysis, although, consistent with the more robust rate remapping in CA3 reported by Leutgeb et al., (2005), the CA3 cells showed higher directionality at the

end of the session (CA1 DI during last lap: 0.42, +/- SEM 0.056, CA3 DI during last lap: 0.66 +/- SEM 0.074, t-test: $p < 0.05$). We cannot, however, rule out individual differences between rats in this case, because the CA3 and CA1 samples came largely from different animals. While the average pattern clearly shows that the directionality of place cells increases from the first few laps to the end of the first session, individual cells showed different patterns of firing rate changes within different fields (discussed below). Some examples of firing rate changes in individual fields are shown in figure 3.3.

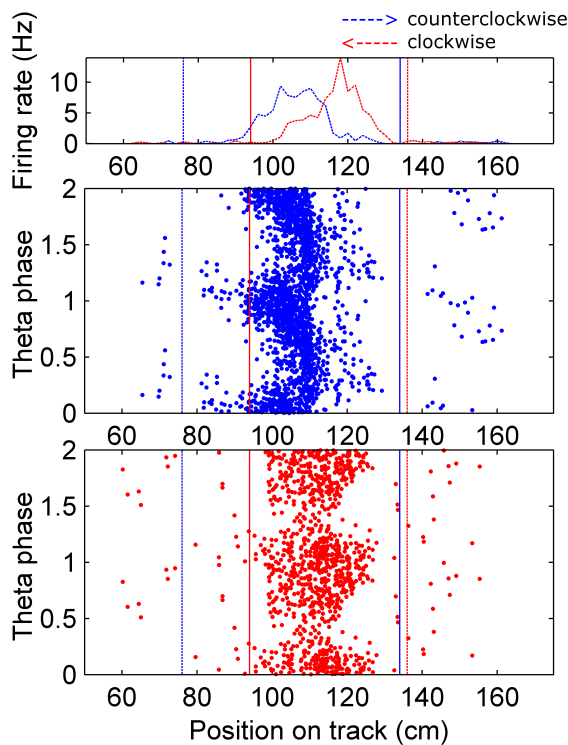


Figure 3.1 Assigning boundaries around fields

Top: Occupancy normalized firing rate for an example cell is plotted on the coordinates of the circular track (the barrier was at 0 cm, which wraps around to 361.3 cm, and the food dishes were near that, at ~10 cm and 351 cm). The firing rate in the clockwise direction (right to left on this plot) is colored red, and the counter-clockwise direction is in blue. Fields were identified by an automated algorithm, which found peaks (in each direction separately) in the smoothed version of this plot, and set boundaries at the troughs around those peaks. If the majority of the field found in one direction overlapped with a field in the opposite direction the two fields were

combined, and the spikes within the boundaries outlined in each direction were considered for further analysis. The boundaries were set separately for each direction to account for the shifting of fields in the backwards running direction. If a field did not overlap with one in the opposite direction, any spikes occurring in the same position bins were considered as the opposite direction field. Dotted vertical lines indicate the beginning and solid lines the end of the field. Bottom: All fields identified were visualized on a theta phase plot, to ensure they exhibited phase precession. Fields that did not show complete phase precession in at least one direction, overlapped with another field, or showed truncated phase precession because of overlap with a food dish location were eliminated from the analysis.

Table 3.1 Statistics of each session analyzed

Two tasks were performed by 5 rats. Each rat ran a task for at least 3 days, and the first 3 sessions were analyzed. (Rat 1 ran on the circular track twice a day, so the afternoon session of day 1 was considered session 2 and analyzed with the other rats' day 2, and the morning session of day 2 was session 3.) The numbers of laps completed by the rat, cells recorded, and fields analyzed are displayed for each rat and session. The smallest number of laps traversed by any of the rats during a given session was analyzed.

Rat #	Session #	# full, direct laps run	# cells	# fields in analysis
Cue-rich cue-poor circular track				
1	1	24	50	63
	2	12	72	80
	3	15	74	82
2	1	14	13	20
	2	7	43	39
	3	11	26	33
3	1	25	69	79
	2	7	65	28
	3	20	69	45
5	1	34	156	32
	2	20	175	22
	3	19	137	42
Shuttling Task				
4	1	13	47	9
	2	53	48	13

	3	77	39	18
5	1	20	94	15
	2	21	69	10
	3	29	81	14

The average running speed of the rats tended to increase throughout the session, as the rats explored the track relatively slowly during the first few laps and later ran faster, now purely to receive their rewards (from 14.2 cm/s, SEM = 0.25 on lap 1 to 26.7 cm/s, SEM = 0.78 on lap 10). It is known that the firing rate of place cells increases with running speed (McNaughton et al., 1983a); however, as the rat runs faster, he passes through each field more quickly, which compensates for the higher firing rate, and the total number of spikes fired during the pass through the field is approximately the same (Ekstrom et al., 2001). In our results, the number of spikes fired during each pass through a field actually decreased slightly with running speed (analysis of variance of the effect of velocity rank on number of spikes: $F = 7.3$, $p < 0.01$; figure 3.4B). A decrease in the number of spikes in both directions would not, however, affect the directionality index, because this measure compensates for the total number of spikes. The number of spikes did, in fact, decrease with velocity similarly in both running directions (interaction between running direction and velocity rank: $F = 0.2$, $p > 0.1$; figure 3.4B), but changed in opposite directions with chronological lap number (interaction between running direction and chronological lap number, $F = 9.53$, $p < 0.01$; figure 3.4A). Thus, the observed change in firing rates over the first few laps cannot be accounted for by the effects of different running speeds seen during those laps.

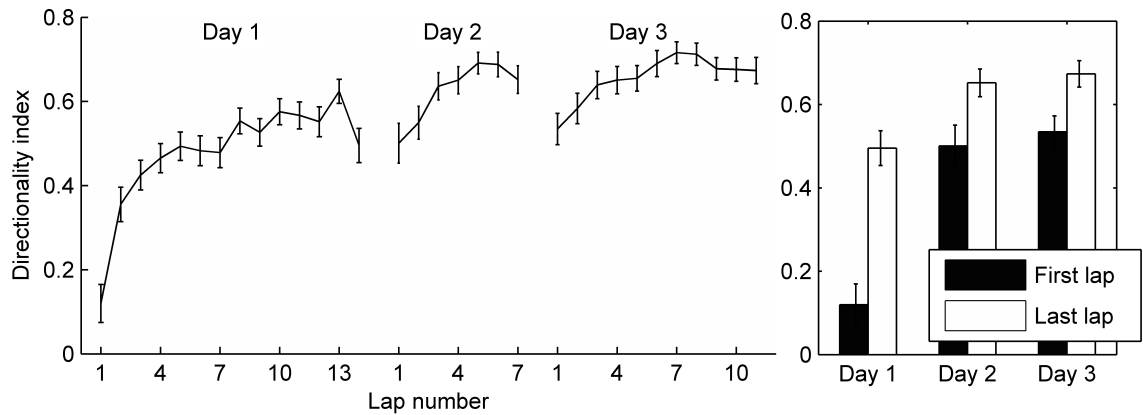


Figure 3.2 Development of directionality on a circular track

The number of spikes occurring within the field boundaries in each running direction was analyzed. The directionality index was calculated for each field on each lap as the difference in number of spikes fired in the preferred and non-preferred running directions divided by the total spikes in both directions (see methods). The mean directionality index for all fields is plotted for each lap and each session. Error bars represent standard error of the mean. Laps are cut off at the least number of laps run by the four rats in a given session. Right: Comparing the directionality index during the first lap and the last lap in each session shows a significant increase from beginning to the end of each session.

Even though the track was narrow (~10 cm), it is possible the rats were following slightly different paths in the clockwise vs. counter-clockwise directions. To study whether a possible difference in paths could have affected place cell firing rates and contributed to the directionality index, we analyzed the effect of the difference in paths taken through a field on the directionality index. The difference in position along the width of the track of paths taken on two subsequent passes through a single field was on average 1.67 cm, and varied with a standard deviation of 1.86 cm. We found that the difference between position along the width of the track during passes in either direction accounted for only 0.2% of the variability in directionality indexes ($R^2=0.0023$, $p=0.015$) on day 1. During subsequent days, when the directionality index was greater, the effect of difference in position between passes on directionality index was not

significant (day 2: $R^2=0.00017$, $p=0.1$; day 3: $R^2=0.00036$, $p=0.1$). Thus, the differences in firing rates in the two running directions are barely, if at all, affected by differences in paths traversed.

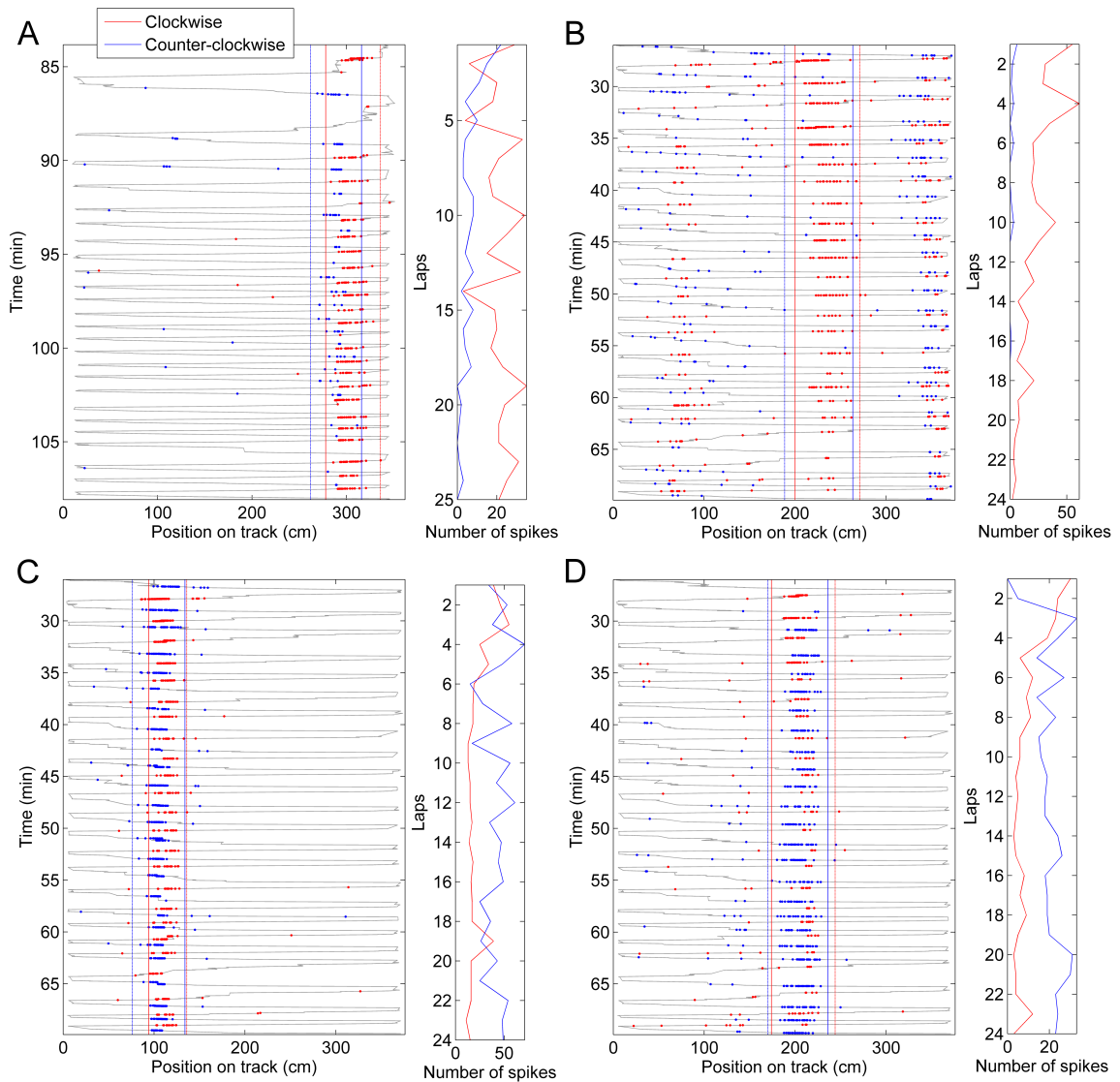


Figure 3.3 Examples of firing rate changes in individual cells on day 1

A. A proximal CA1 cell from rat 3 expressing a field on the cue rich side of the track showed a typical pattern of directionality increase. Many cells (those falling in the category shown in figure 3.5B) showed a directionality increase such as this. **B.** Some cells expressed fields that started with significant directionality in the first few laps, such as the highlighted field of the intermediate CA1 cell shown here. Like this example, many cells in the category shown in figure

3.5C increased their directionality even more after the first few laps. **C.** An intermediate CA1 cell from rat 1 expressing a field on the cue-rich part of the track showed a small directionality increase. Many cells remained bi-directional throughout the session. **D.** A few cells started directional and became less so, or reversed their preferred direction of firing (cells in the categories in figure 3.5E&F). This intermediate CA1 cell from rat 1 didn't start firing until the return (clockwise) direction on the first lap, and then, over the next 2 laps, increased its firing rate in the counter-clockwise direction, eventually firing more spikes in that direction.

The change in relative firing rate within place fields in the two running directions has the characteristics of rate remapping, because changes in rate occurred without overall changes in firing location. To confirm this assessment, we analyzed several parameters that would indicate global remapping. First, global remapping would predict that many fields would appear in a novel location, which did not show firing during the first few laps. During the first 3 laps, no spikes were fired only in 10 fields (5.2 percent), and 6 or fewer spikes were fired in 26 (13 percent) fields in those first 3 laps. When these fields were removed from the analysis, the average directionality index did not change noticeably (DI on lap 1 including all fields: $0.12 \pm \text{SEM } 0.045$, including only fields that exhibited more than 6 spikes in the first 3 laps: $0.14 \pm \text{SEM } 0.045$). Second, global remapping would predict that many cells stopped firing completely in one running direction; however, even during rate remapping the changes in rate can be sufficient to cause a few cells to have firing probabilities that approach zero in a given location in one or other condition (Leutgeb et al., 2005). Forty-eight fields (25 percent) ended with no spikes in at least one running direction. Removing these fields from the analysis reduced the directionality index both at the beginning and end of the session, but the change in directionality was still significant, both for the fields that ended with spikes in both

directions, and for the fields that ended with no spikes in one direction (paired t-test between DI on first and last lap, $p < 0.001$ in both cases). Additionally, the size of each place field was measured on each lap, as the distance between the first and last spike (within the field boundaries) during that lap. The average field sizes did not change very much (about 35% - figure 3.4C, compared to a 50% change in firing rates - figure 3.3A, and only 20% when fields with no spikes are not included). To check for stability in the locations of place fields, we analyzed the center of mass of each field on each lap. The average center of mass (COM) of the fields shifted in the direction opposite to the direction of running, as has been observed previously (Mehta et al., 1997), but no other shifting of individual fields was observed (average COM shift from first to last lap was 4.6 ± 12.6 cm, SEM=0.83; figure 3.4D). Interestingly, the experience-dependent backwards center of mass shift was observed both in the direction in which the field was becoming stronger, as well as in the direction in which the field was becoming weaker. The center of mass shift was observed for both CA3 and CA1 cells on day 1, and also observed on days 2 and 3 in the preferred firing direction of CA1 cells, but not CA3 cells (similar to previous data of Lee et al., 2004).

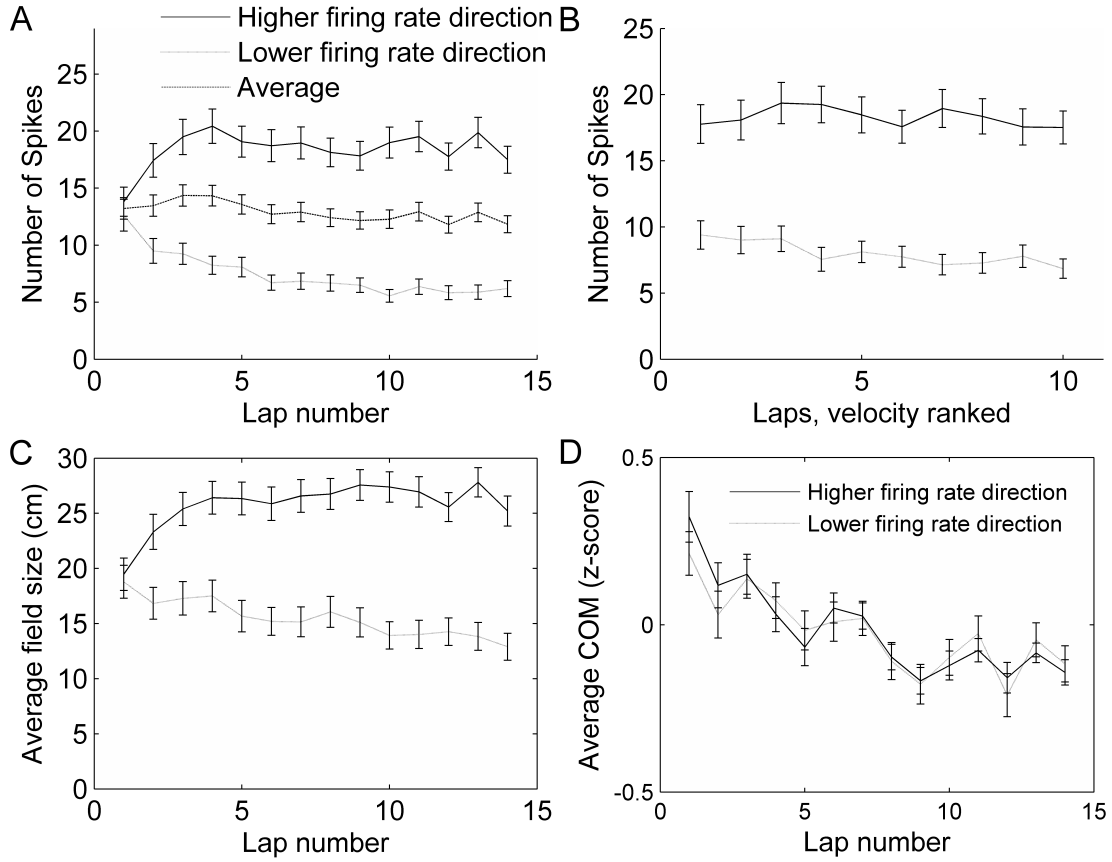


Figure 3.4 Control analyses

A. The average number of spikes fired in all fields did not change with lap number, even though the firing rates in each direction did. **B.** The number of spikes fired within a field decreased slightly with running speed, but not differentially for the two running directions. The average number of spikes fired on the slowest pass through each field, the next slowest, and so on until the fastest pass, was calculated. The first 4 laps were excluded from this analysis, because the running speed was highly correlated with lap number in these laps. The slowest passes through each field (excluding the first 4 laps) were on average 17.7 cm/s (SEM = 0.53), and the fastest passes were on average 31.0 cm/s (SEM = 0.75), covering a range of the same size to the range of the passes during laps 1-10. **C.** Average field size (measured as the distance from the first spike to the last spike) changed in each running direction across laps by about 35%, but not as much as the number of spikes fired (A). **D.** The center of mass (COM) of place fields shifted backwards, in both preferred (higher firing rate) and non-preferred (lower firing rate) directions.

To understand how individual fields changed as the rat gained experience in the environment, we plotted the directionality index during the first 3 laps versus the

directionality index during the last 3 laps for each individual field (figure 3.5A). This plot shows that while, on average, the directionality index increased with lap number, individual fields exhibited a wide range of directionality indices both at the start of exposure to the environment as well as after repeated runs. Consistent with the average results, many fields showed a substantial increase in directionality index during the behavior session, while many fewer fields showed a decrease in directionality index. To check the significance of the directionality index for each individual field, we calculated the chi square statistic comparing the number of spikes in each running direction for each field, both in the first 3 laps, and in the last 3 laps. Of the 194 total fields expressed on day 1, 77 showed significantly directional firing during laps 1-3, and 111 showed significant directionality during the last 3 laps. Fifty-six of these showed directional firing both at the beginning and end of the session. Of those 56 fields, 42 showed an increase in directionality index from the first 3 to the last 3 laps. The last 62 fields did not show significant directionality at the beginning or end of the session. Interestingly, of the 77 fields that showed significantly directional firing at the start of the session, 8 exhibited a reversal in the preferred firing direction. At the beginning of the session, the firing rate in these 8 fields was higher in the direction that became the lower firing rate direction when averaged over the session (the 'lower firing rate', or 'non-preferred' direction). By the end of the session, 7 of these fields showed a significant directionality in the preferred direction, while 1 of them did not show significant directionality. We plotted the number of spikes per lap separately for each of 5 categories of fields: fields that

showed directional firing only at the end of the session (figure 3.5B, blue), fields that showed directional firing (in the preferred direction) both at the start and end of the session (figure 3.5C, green), fields that never showed directional firing (figure 3.5D, cyan), fields that showed significant directional firing (in the preferred direction) only at the start of the session (figure 3.5E, magenta), and fields that showed significant directional firing in the non-preferred (lower firing rate) direction at the start of the session (figure 3.5F, red). Separating the fields into groups that exhibit similar directionality changes during the first session shows that even though different cells exhibit different amounts of directionality throughout the session, there was an average tendency to increase their firing rate in the preferred direction and decrease their firing rate in the non-preferred direction during the first few laps. A substantial number of cells, however, exhibited decreases in firing in the preferred direction or increases in firing in the non-preferred direction while nevertheless increasing overall directionality, due to even greater changes in the opposite direction.

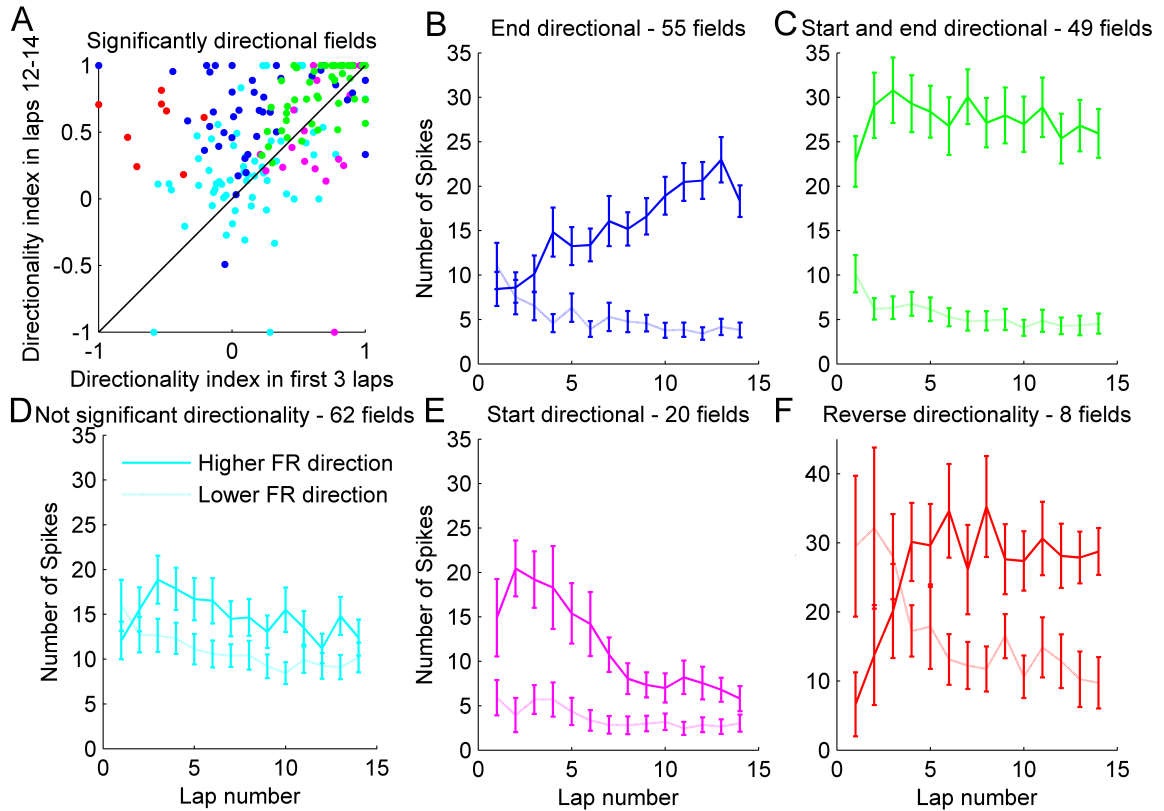


Figure 3.5 Remapping in individual fields

A. To observe the amount of rate remapping exhibited within individual fields, the directionality index during the first 3 laps was plotted against the directionality index during the last 3 laps. Significance of the directionality in individual fields was assessed with a χ^2 test. Fields were classified based on whether they exhibited significant ($p < 0.05$) directionality at the beginning or end of the session or both, and are color-coded based on this classification. **B-F.** For each group of fields, the average firing rates in each running direction are also displayed. Error bars represent standard error of the mean. Additionally, 8 fields were identified that showed significant directionality in the non-preferred direction at the beginning of the session. We addressed the question of whether there may be some form of competition involved in the change in firing rates over the first few laps by assessing whether directionality tended to increase in the direction that was preferred on lap 1. In other words, we tested the hypothesis that initially stronger inputs tended to get stronger while initially weaker ones tended to get weaker. The average directionality during lap 1 was small, but significant ($0.12 \pm \text{SEM } 0.045$, t -test: $p < 0.05$). We computed the signed directionality index $(\text{CW rate} - \text{CCW rate}) / (\text{CW rate} + \text{CCW rate})$ for each field for laps 1 and 14 on day 1 and performed a regression analysis. There was a weak tendency for directionality to increase in the direction of the initial bias ($R^2 = 0.084$, $F = 13.1$, $p < 0.001$). This tendency was true even for the 3 rats that were actually visiting the track for the first time ($R^2 = 0.081$, $F = 8.05$, $p < 0.01$).

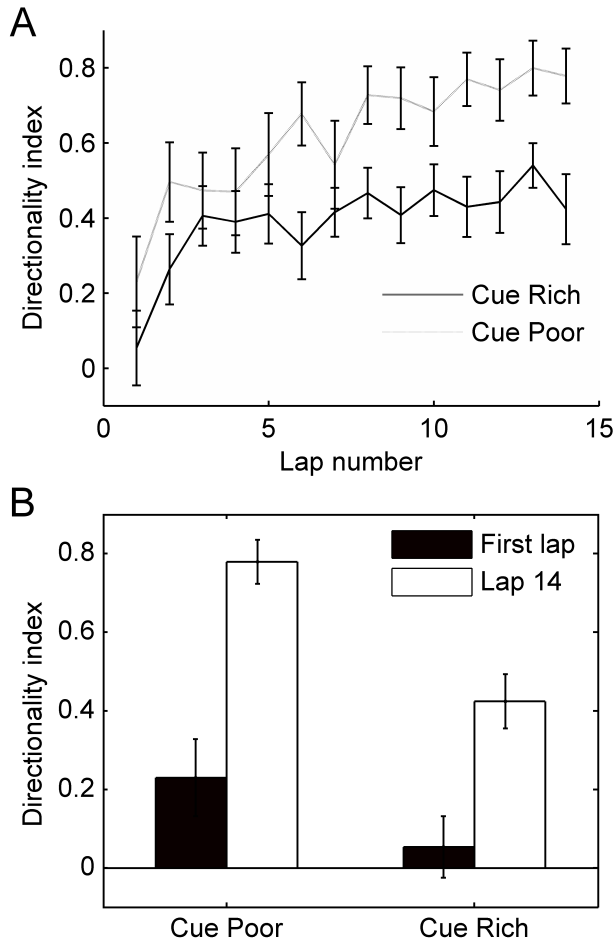


Figure 3.6 Local cues and the development of directionality

Half of the circular track was enriched with small objects and textures (local cues). **A.** The mean directionality index is plotted for fields expressed on the cue-rich and cue-poor halves of the track. **B.** During the first lap, field directionality on the cue-rich and cue-poor halves of the track did not differ significantly (t-test, $p=0.16$). Over the session, fields on both parts of the track became significantly more directional (paired t-tests, $p<0.01$); however, fields on the cue-rich part of the track increased directionality less than fields on the cue-poor side, and directionality was significantly different between regions on the last lap (t-test, $p<0.001$).

Place cells are known to express more bidirectional place fields when local cues are present on the track (Battaglia et al., 2004). To assess how local cues affected the development of directional firing in our experiment, half of the track had small objects

or textures on it, and the other half was bare. During the first lap, fields on either side of the track did not differ significantly (t-test, $p=0.16$), but by the end of the first session, fields expressed on the cue poor half of the track showed higher directionality than fields expressed on the half of the track rich in cues (t-test, $p<0.001$; figure 3.6). An analysis of variance showed a significant effect of cue condition on the directionality index ($F=4.39$, $p<0.05$), and a significant interaction between lap number and cue condition ($F=5.93$, $p<0.05$). Another possible difference between the two halves of the track was the rats' behavior: they ran slower on the cue-rich part of the track, and stepped over and around certain objects and textures in stereotyped ways (running speed through fields on cue rich part of the track: 18.2 ± 4.56 cm/s, cue poor part of track: 29.5 ± 7.99 cm/s, t-test: $p<0.001$). The specific stereotyped movements and the sequence of movements, however, was different between the two running directions on the cue-rich part of the track, and more similar (involving fewer specialized movements) on the cue-poor part of the track.

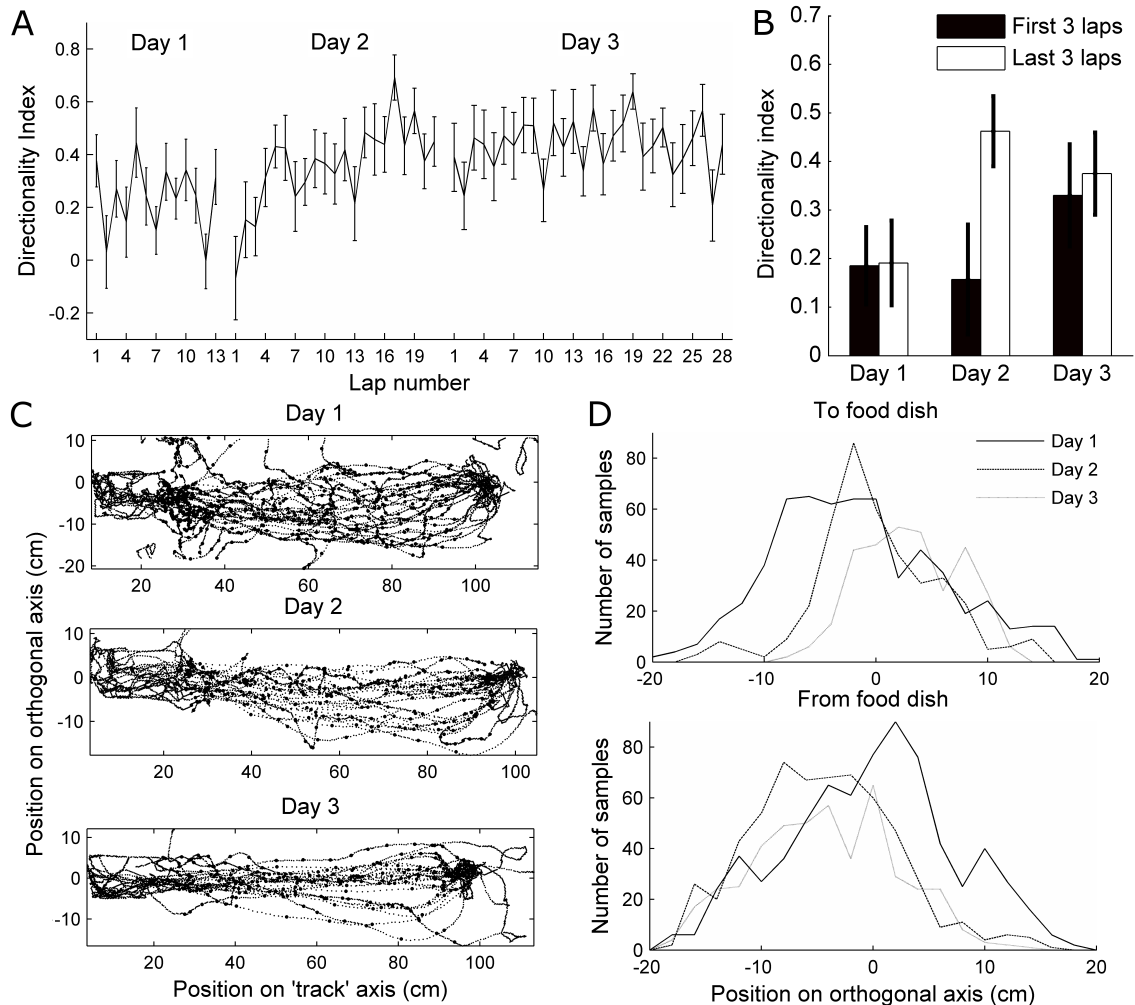


Figure 3.7 Directionality in an open field

A-B. Directionality index in fields expressed on an open-field platform during performance of a shuttle task. Day 1 is the first day each rat ran more than 20 laps (This was actually day 2 in the environment for one rat, and day 4 for the other rat. On this day, rat 4 ran 22 laps, 13 of which were direct, and the rat 5 ran 25, 20 of which were direct.) The day after that, the rats ran 53 and 21 direct laps respectively, and the directionality index started low and increased by laps 18-21. On the following day (3), the directionality index started as high as at the end of day 2, and did not change throughout the session. **B.** Directionality index during the first 3 and last 3 laps of each session. **C.** Paths run by one of the rats during the first 13 direct passes between the start box (left) and the food dish (right). The position was sampled 5 times per second, excluding the times when the rat was in the box or at the food dish, to test for variability (large dots). **D.** Distribution of positions along the axis orthogonal to the direct path from food dish to box at the sampled times is plotted for both rats. Paths toward the food dish and away from the food dish are plotted separately. The distribution is wider on day 1 in both directions.

Directional firing of place cells has also been shown when a rat's path was not physically restricted to a track, but the rat was trained to run a specified path in order to receive rewards at known locations (Markus et al., 1995). To determine whether directional firing in this case also develops from initially omni-directional place fields, we trained rats to run back and forth between a home-box location and a food dish on a circular open-field platform. It took the rats 2-4 days to learn the task, but as soon as they were running >20 laps, we analyzed the directionality of their place fields. On the first that day the rats ran more than 20 laps, the directionality index of the fields was low and did not significantly change during the session (figure 3.7A). The day after that, however, the directionality index started low and increased by the end of the session (figure 3.7A&B; paired t-test between first 3 laps and last 3 laps: $p < 0.01$). The following days the directionality index started as high as at the end of day 2, and did not change throughout the session. As in the circular track task, the speed of running through a field affected the number of spikes fired during that pass slightly, but did not affect passes in the two directions differentially. To determine why directionality only developed on the second day of performing the shuttling task, we analyzed the variability of the paths the rats took to the food dish (the paths for one rat are plotted in figure 3.7C). The first 13 direct laps were analyzed on each day for each rat. The position was sampled 5 times per second during traverses to and from the food dish (excluding times the rat was in the box or at the food dish). The position along the axis orthogonal to the most direct path from home box to food dish (the 'track' axis) was analyzed. On the first day, the

distribution of positions visited by both rats during their runs was wider than on the following days (Brown-Forsythe test for equality of variances: $p < 0.001$, multiple comparison test shows that day 1 is significantly different from days 2 and 3, but day 3 is not different from day 2). Even though the paths were more stereotyped when directionality developed, and were different between the two running directions, the difference in the paths did not predict the directionality index, as in the circular track data. These results show that the differential rate remapping in opposite running directions can develop not only on tracks that constrain the animal's trajectory, but also in an open field environment that is repeatedly traversed along a particular path. In an open field environment, however, the rate remapping develops only once behavior becomes stereotyped.

DISCUSSION

The main finding is that, in rats running on a track, the firing of hippocampal place cells is initially bidirectional, and gradually becomes highly unidirectional. This large increase in directional selectivity involves gradual changes in firing rates in either or both running directions, during approximately the first 5-10 laps on the first day of exposure to the track. This effect is almost entirely due to positive and negative changes in direction-specific firing rates of the neurons, and not to changes in the locations in which the neurons fire (i.e., rate remapping). Thus, while retaining information about the allocentric location of the animal, the network gradually differentiates the direction in

which it is traveling on the track. This finding clarifies a long standing question of why the firing of hippocampal neurons is different in different directions when the rat is following a specified path (McNaughton et al., 1983a; Muller et al., 1994), but the same in each direction when the rat is following random paths (Muller et al., 1987).

The formation of place fields has been hypothesized to depend on one of two separate mechanisms: learning of the sensory details of the environment to construct a map and triangulate one's location in it, or a continuous updating of one's movement trajectory to calculate allocentric position in the environment (path integration), or some combination of the two mechanisms. Models relying on the first mechanism rely on the learning of associations between place cells and their sensory inputs in order to form non-directionally specific place fields. For example, Sharp (1991) modeled a network with sensory inputs relating to the egocentric distance and direction of landmarks projecting to entorhinal and then hippocampal cells, and used competitive learning to establish place fields. A prediction of this model was that place fields would initially be directional, but become direction-independent after exploration in multiple directions. Because exploration was restricted to two directions on a track, place fields on a track would never become omni-directional in this model. Our data, however, show a pattern opposite to that predicted by this model; place fields are initially omni-directional, and increase their direction-specificity with experience. The current findings are more consistent with models that rely on some form of path integration to determine the initial location of place fields.

The assertion that path integration determines the formation of place fields is well supported with previous experimental evidence (reviewed in McNaughton et al., 1996; 2006). For example, symmetry of sensory cues in an environment does not result in symmetrical place cell firing (Sharp et al., 1990) and identical sensory environments located at 180° rotated orientations (Fuhs et al., 2005), or in different rooms (Leutgeb et al., 2005b) result in global remapping of place representations. Further, place fields do not change location when lights are turned on or off (O'Keefe and Speakman, 1987; Quirk et al., 1990; Markus et al., 1994). The inhibition (Kentros et al., 1998) or deficiency (Barnes et al., 1997) of LTP does not disrupt the formation of place fields, but does disrupt the recall of place cell associations with previously visited environments. Global remapping is instantaneous when a large mismatch between sensory cues and vestibular information occurs (Knierim et al., 1998), as is place field realignment to moved landmarks (Gothard et al., 1996), further supporting that learning is not necessary for the establishment of novel or changed place cell representations.

In the framework of path integration models, earlier hypotheses to account for directionality along restricted paths involved a switch of 'reference frames' or maps (now referred to as global remapping) at the arm ends; however, attempts to observe the predicted complete discontinuity in firing patterns at arm-ends were generally unsuccessful (Redish et al., 2000). The symmetrical firing observed during the first traversal of a path, is consistent with typical, non-directional firing during random foraging behavior, and also with the evidence that the selection of which hippocampal

neurons are able to fire at a given location is determined on the basis of path integration rather than exteroceptive cues (presumably by inputs from the medial entorhinal cortex). When the animal travels the same route multiple times, however, it appears that the firing of hippocampal cells gradually becomes conjunctive for the path integrator coordinates and the direction-specific 'local view' (McNaughton et al., 1991). The most plausible source of external landmark information to the hippocampus proper is via the lateral entorhinal cortex (Burwell and Amaral, 1998; Si and Treves, 2009; Renno-Costa et al., 2010; Deshmukh and Knierim, 2011). Lateral entorhinal cortex (LEC) projects to the outer portions of the dendrites of DG and CA3 uniformly along the transverse axis of hippocampus, and to the distal (i.e. nearest to subiculum) CA1 cells. We observed strong increases in directional tuning in both CA3 and CA1 (including the cells located in proximal CA1, which only get direct inputs from MEC and CA3), raising the possibility that the directionality increase in CA1 is largely driven by changes in CA3 itself or in Schafer collateral synapses.

At present, one can only speculate about the possible mechanisms of the increased directionality. The data appear to be generally compatible with the observation that LEC inputs are capable of bidirectional weight changes (LTP/LTD; McNaughton et al., 1978; Abraham and Goddard, 1983) and support the hypothesis that the LEC to CA3 (and/or DG) connections which are active in a given direction either increase or decrease according to some form of competition. Plausibly, the initial mean weights of synapses driven by the novel cues, being drawn effectively at random from

an existing weight distribution, would be approximately equal in the two directions (central limit theorem). Whether the mean weights would increase or decrease might depend on some form of competition (e.g., BCM rule), by which inputs causing strong activation are strengthened whereas those causing weaker activation are weakened. We did observe a slight tendency for directionality to increase in the direction of initial preference, but it accounted for only 8% of the directionality variance by the end of session 1. It is also possible that competition is influenced by the timing of inhibitory inputs from interneurons driven at short-latency by other pyramidal cells (Csicsvari et al., 1998; Marshall et al., 2002; Maurer et al., 2006b). In addition, the firing rates of some hippocampal interneurons are strongly modulated by novelty (Wilson and McNaughton, 1993; Nitz and McNaughton, 2004), which may have an important impact on plasticity over the first few laps. In any case, if the magnitude and direction of weight change is a random variable that is correlated over the active population of inputs onto a given hippocampal cell for a given running direction, then the firing in opposite directions would tend to diverge, resulting in increased directional bias.

On average, there was about a 50% increase or decrease in firing rate over time in a given direction (figure 3.4A); however, there were cases of cells either starting out or ending up with zero spikes in one direction. If the observed changes in firing are indeed due to changes in LEC synaptic efficacy, the complete lack of firing in one direction implies that, at least in some cells, MEC inputs alone are not sufficient to drive spiking. Since MEC inputs are also known to exhibit plasticity, however, it is also possible

that both sets of inputs may undergo experience dependent changes. The effect of local cues on the track, however, which would likely reduce the net difference in external input in the two directions, appears to indicate that the main changes are driven by external inputs.

Other studies have shown that rate remapping occurs when the behavioral goals or context, or internal state of the animal changes (e.g. Frank et al., 2000; Wood et al., 2000; Bower et al., 2005). By teaching the rats a shuttling task, we modified their behavioral goals. This change in behavioral context could explain why remapping occurred in the same environment when the task changed from foraging for randomly placed rewards and running between predictable reward locations (Markus et al., 1995). In our results, this rate remapping didn't occur until the task was so well learned that it was performed stereotypically. This indicates that the development of directionality in the hippocampus does not drive the change in behavioral strategy; instead it may be driven by the shift to a different behavioral state. Some of the studies of rate remapping at identical locations during running toward different goals have been interpreted to mean that mnemonic coding, when it is task-relevant, exists in the hippocampus in addition to spatial coding (Berke et al., 2009). Another interpretation, based on our results, is that the 'context' encoded by the hippocampus can include the particular trajectory being traversed, if traversal of the trajectories becomes highly stereotyped. Studies of the initial place cell activity in these tasks should be performed to differentiate between these two hypotheses. If the rate remapping occurs after the task

is well learned, it would suggest that task demands, including goal locations, are actually learned by a different structure, such as the striatum, and remapping in the hippocampus is driven later by input relating to the task context. Some findings support this second hypothesis, including that Berke et al. (2009) did not see rate remapping in the initial learning trials of their cued goal maze task, even though in those trials the rat was using its prior positions to plan a future route. Additionally, rate remapping of overlapping positions in a sequence task does not occur when the overlapping parts of the trajectories include more than one arm (Lenck-Santini et al., 2001; Bower et al., 2005), and is not necessary for a rat to learn complex sequences (Bower et al., 2005).

Mehta et al., (1997) reported an experience-dependent place field expansion in CA1, with a center of mass shift in the direction opposite the direction of travel, when rats ran unidirectionally around a track. This effect was subsequently shown to occur also in CA3, in a more long lasting form (Lee et al., 2004) and to be dependent (at least in CA1) on NMDA receptor function (Ekstrom et al., 2001). The accepted view of the mechanism of this experience dependent expansion and shift is that it reflects the development of what Hebb (1949) referred to as a “phase sequence”. Synapses from cells that fire earlier in a sequence onto cells firing later become asymmetrically strengthened through spike-timing dependent LTP. In their discussion, Mehta et al. (1997) commented: “A natural question is whether the observed asymmetry would cancel out if the rat ran repeatedly back and forth along a route in both directions. It turns out that this experiment is not possible because, under such circumstances, the hippocampus

encodes the forward and return journeys using different sets of place cells.” The present results show that this conjecture was incorrect; the forward and return journeys apparently are encoded by the same set of place cells, but with substantially direction-dependent firing rates, and we did observe a center of mass shift in both the preferred and the non-preferred directions, on the first day. The fact that field expansion in both directions didn’t cancel out the asymmetric center of mass shift, could be explained by local feedback inhibition, an after-hyperpolarizing current, or another form of depression in each place cell that does not allow a place cell that has recently fired to be activated by connections from other currently active place cells. Another possible implication of this result is that the synapses that mediate rate remapping are not the same as the synapses that mediate the place field shift. Rate remapping typically resulted in fewer spikes fired in the non-preferred direction, suggesting a synaptic depression, yet the field shift is generally attributed to synaptic enhancement.

On the second and third days on the track, place field shift occurred only in CA1 cells, and only in the preferred direction, while directionality increased only slightly, and in both CA1 and CA3 cells. The fact that place field expansion does not occur in CA3 on later days is consistent with previous results (Lee et al., 2004) which suggest that the underlying plasticity is more persistent in CA3 than CA1. A possible explanation for the lack of expansion in the non-preferred direction in CA1 on days 2 and 3 may be that there was insufficient depolarization on the cells to induce LTP in the feed-forward

synapses from CA3. Of course, the foregoing proposals are speculative. Understanding the specific mechanisms involved in these phenomena await further study.

In summary, during the first few traverses of a fixed route in space, place cell activity is almost entirely determined by allocentric position; later the activity becomes modulated by other factors, without significantly affecting the position dependence (rate remapping). The shift is likely due to sensory information at a given position, but could also be partially driven by internal state variables such as memory or goals, or the behavior of the animal at particular locations. We presented evidence that directionality does not develop until behavior becomes stereotyped, suggesting that the performance of a specific task in an environment contributes to changes in place cell activity. Both sensory and motor information makes its way into the hippocampus, in a highly processed form, however. Recordings from the input structures to the hippocampus (especially MEC and LEC) during performance of directional tasks in a novel environment are needed to elucidate what drives the development of directionality of place cells.

Contributions: B.L. McNaughton conceived the project. Z. Navratilova, L.T. Hoang and C.D. Schwindel conducted the experiments. Z. Navratilova performed the analysis. M. Tatsuno helped with discussion of analysis and results. Z. Navratilova and B.L. McNaughton wrote the paper.

Acknowledgements: We would like to thank J.L. Valdes, V. Bouquet, K. Bohne, J. Wang, and J. Bohanick for technical assistance, and C. Barnes for access to facilities and resources. Supported by NS20331 and AHFMR Polaris award.

Chapter 4 Reactivation of Rate Remapping in CA3

C. Daniela Schwindel¹, Masami Tatsuno¹, Bruce L. McNaughton^{1,2,3}

¹University of Lethbridge, Lethbridge, AB, Canada; ²University of California, Irvine, CA;

³Neuroelectronic Research Flanders.

ABSTRACT

The hippocampal CA3 network may contribute to episodic memory by combining spatial and contextual information using a dual coding scheme known (respectively) as 'global' and 'rate'-remapping. In CA3, global remapping exhibits attractor-like dynamics whereas rate-remapping apparently does not, leading to the hypothesis that only the former can be associatively retrieved. This question is key to the general hypothesis that CA3 serves as a general purpose autoassociator. We conducted large-scale single unit recordings from CA3 of rats while they ran on a circular track in different directions (in different sessions), and while they slept. We find that, during off-line, spontaneous reactivation, separation of the two contextual memories associated with the same spatial map occurs.

INTRODUCTION

The hippocampus is thought to play a central role in the formation of episodic-like memory. The general theory behind this idea is that the CA3 network of the hippocampus is a general-purpose autoassociative network (Marr, 1971; McNaughton and Morris, 1987; Treves, 1990; Treves and Rolls, 1992) capable of representing external inputs and encoding them in an attractor framework (Hopfield, 1982; Amit and Treves, 1989) using Hebbian synaptic modification. This allows the whole of the hippocampal representation of an event to be recalled from a reduced or distorted version of the stored pattern, and results in a hysteresis effect whereby the entire system transitions abruptly to a stored state once a critical similarity of the current and stored patterns is achieved. It is generally believed that the spontaneous reactivation during sleep (Wilson and McNaughton, 1994) of patterns stored autoassociatively in the hippocampus serves to assist neocortical memory consolidation (Marr, 1971).

The hippocampus combines spatial and 'contextual' information by means of a dual coding scheme in which the location and spatial extent of 'place fields' appears to be determined by an internally generated mechanism based on path-integration (McNaughton et al., 2006) signals, probably of medial entorhinal origin (Hafting et al., 2005; Fyhn et al., 2007), whereas the intensity of 'in-field' firing is rapidly adjusted on the basis of sensory and internal cues ('context'), probably conveyed via lateral entorhinal cortex (Hargreaves et al., 2005; Lu et al., 2013). Rearrangement of place field location due to changing position is now commonly referred to as 'global remapping',

whereas variations of in-field firing rates is called 'rate-remapping' (Leutgeb et al., 2005b).

Rate-remapping has been observed in various different conditions, such as changing wall colour (Leutgeb et al., 2005b), wall shape (Leutgeb et al., 2005b; Leutgeb and Moser, 2007; Colgin et al., 2010; Lu et al., 2013), changing task demands (Allen et al., 2012) or odors (Anderson and Jeffery, 2003), as well as internal variables such as working memory and/or action plans (Wood et al., 2000; Bower et al., 2005). In a recent study (Navratilova et al., 2012), we showed that the firing rate differences that occur when a rat runs in opposite directions on the same track (McNaughton et al., 1983a) are a result of rate-remapping. Place cells start out with almost symmetrical firing in the two directions, presumably driven by path integrator input. The symmetry is rapidly broken as a consequence of direction-dependent differences in external sensory input, presumably arriving via lateral entorhinal cortex. Directional firing bias develops within the first several laps and is maintained on subsequent days.

One well supported theory is that the path integrator mechanism is based on prewired 'continuous attractor' dynamics in MEC (McNaughton et al., 1996; Redish et al., 1996; Zhang, 1996; Samsonovich and McNaughton, 1997; Fuhs and Touretzky, 2006; McNaughton et al., 2006) which give rise to grid cells at several spatial scales, and that combining grid cell inputs at different spatial scales plays a dominant role in formation of discrete place fields in hippocampus. According to this theory, if an animal explores two spatially separate environments, the two representations formed in the

hippocampus (CA3) will be statistically independent due to different 'locations' of activation on the upstream continuous attractor manifold. Transitioning between the two environments will cause an abrupt shift between the two neural representations (global remapping). On the contrary, sensory/contextual changes within the same environment are associated with the same set of active cells and are encoded by changes in their firing rates (rate-remapping) but not locations.

Recently, Colgin et al. (2010) performed a test of whether both spatial and sensory information can lead to attractor dynamics in CA3. They showed that when the environmental cues were gradually morphed between two familiar end-points, coherent, abrupt transitions occurred in CA3 only if the end-points had been previously learned in different spatial locations and hence were associated with different global mappings. They concluded that "associations among the represented features of the two boxes were not sufficient to produce attractor dynamics in the hippocampus, whereas associations between the features and an internal representation of relative location produced strong attractor dynamics ", and thus, "the available evidence does not favor the theory that CA3 is a standard autoassociative network whose purpose is to encode associations among the sensory features of the environment". A major implication of this conclusion is that spontaneous retrieval of recently experienced patterns might contain only the spatial component of the activity and any component due to rate-remapping would be lost. This result would present difficulties for most

theories of the role of hippocampus in encoding episodic memories that occur at the same place.

In the present study we performed a test of the hypothesis that both the spatial and the rate-remapping components of firing (i.e., the full hippocampal code for the episode) are reactivated during sleep. We took advantage of the pronounced rate remapping that occurs during running in opposite directions around a circular track (Navratilova et al., 2012). Essentially, we asked whether reactivation of firing rate distributions that occurs during rest immediately after running in one direction is more similar to the hippocampal activation for that direction than for the pattern during subsequent running in the opposite direction. Rejection of the null hypothesis (no difference) in the predicted direction would indicate that both the spatial and the sensory features are retrieved in the hippocampus during off-line reactivation.

METHODS

Behavioral training and recording experiment. The animals used for this study were individually housed and kept on a 12h dark/12h light cycle. The training and experiment were conducted during the light phase. The animals were food deprived and kept at 85% of their free feeding body weight in order to be motivated to run for food reward. All animal protocols complied with Federation of Laboratory Animal Science Associations (FELASA) guidelines under the guidance of the Neuro-Electronic Research Flanders (NERF) and KU Leuven institutional animal care.

Four Long Evans and 1 Wistar rat, between 3 and 5 months of age, were pretrained to run back and forth on a linear track for food reward (chocolate sprinkles), which was provided on each end of the track. Training took place once or twice daily for about two to three weeks depending on how quickly the animal acquired the task. During this training period a “hyperdrive” with twelve independently movable recording tetrodes (Gothard et al., 1996) ($<1M\Omega$) and two references was implanted above the right hippocampus (-3.8 AP, -3.0 ML relative to bregma). The tetrodes were lowered into the cortex (1960 microns) right after surgery and then further down to area CA3 of the hippocampus over the course of about two weeks. One tetrode was placed into layer CA1 to record ripple events. Another tetrode was placed close to the hippocampal fissure to record sharp wave events and was used as a visual guide during tetrode turning. A differential signal was recorded from the corpus callosum and was used as neutral reference throughout the recordings. The tetrode turning was based on hippocampal, local field potential landmark features such as theta rhythm during waking and movement and the occurrence of sharp waves and ripples during quiet wakefulness and slow wave sleep (Buzsaki et al., 1992). The anatomical positions of the tetrodes were confirmed histologically using Nissl stains.

Once all tetrodes were in the desired location, the experiment started. The recordings were conducted in a different room than the pretraining, using a circular track elevated ca. 15 cm above the floor with low (1 cm) railings along the in- and

outside (diameter: 170 cm). The room and experimental apparatus were novel on day one of recording.

The recording procedure for four (3 animals) to five days (2 animals) was conducted as follows. The animal first rested in a high-walled towel-padded black wooden box, placed in the center of the track for about 45 minutes. It then ran the first session of continuous laps in one direction for food reward at a fixed location on the track. The animal ran a total of four sessions of 15 minutes with the first and last sessions in the same direction (A, A') and the second and third sessions (B, B') in the same direction but opposite to A. The running sequence was alternated between clockwise (CW) - counter clockwise (CCW) - counter clockwise (CCW) - clockwise (CW) and CCW-CW-CW-CCW over the course of 4-5 recording days. That is, CW-CCW-CCW-CW was used on the days 1, 3 and 5 and CCW-CW-CW-CCW on the days 2 and 4. The reward location remained the same for each animal. Between the run sessions the animal rested for about 20 minutes in the box, and after the fourth session it rested for 45 minutes. The recording arena was surrounded by black curtains, which were not fully closed, to allow the experimenter to go in and out between sessions. The gap in the curtains at the door together with an illuminated emergency exit light above the door also provided a constant distant cue for the animal to polarize the environment. In addition, the experimenter sat on a chair close to the food dish to deliver the reward. The light was dimmed during recordings.

The thresholded spike signals were recorded with a Cheetah Data Acquisition System (Neuralynx), digitized at 32 kHz and bandpass filtered between 600 Hz and 6 kHz. The continuous local field potential traces (LFP) were filtered between 1 Hz and 300 Hz and sampled at 2.4 kHz. The animal's position was tracked at 60 frames/s using LEDs mounted on the headstage that were detected by a color camera that was mounted on the ceiling of the recording room (approximately 0.33 cm/pixel).

Spike sorting. Spiking activity was analyzed offline using an automated spike-sorting algorithm (Klustakwik by K. D. Harris) to isolate units and separate them from noise. The resulting clusters were manually refined using cluster cutting software (MClust 3.1SE by A. D. Redish, with customizations by P. Lipa, S. Cowen, and D. Euston) in a multiparameter space including features such as energy (area under the waveform), peak-to-trough distance, principal component, time (to control for stability of the recording of the unit over the entire length of recording) and cross correlograms. Only units with less than 0.2 % interspike intervals (ISI) falling within 2 ms refractory period were accepted. Also, the median of the z-scored waveforms of the last sleep session had to be within 1 standard deviation of the median of the z-scored waveforms of the first sleep session on at least three out of four channels to exclude units that underwent drift. Units that fired with less than 0.05 Hz in any of the behavioral or sleep sessions were excluded from the analysis except for the ripple characterization (see *Cross correlation analysis between CA3 unit activity and ripple peak times* and *Number of spikes and proportion of active neurons per ripple*), which left a total of 349 neurons.

Place field analysis. The video tracked position of the rat during the run session was extracted at each video frame by fitting a circle to the ring of LEDs on the headstage. The 2D position was deconstructed into a 1D position along the track. The food dish location was defined as 0. The rat's velocity was calculated by smoothing the 2-dimensional position with a 1 s hamming window and calculating the distance the animal had moved between subsequent frames. Any periods in which the animal moved less than 2 cm/s were removed. Place fields were defined along the linearized track by smoothing (with a hanning window of 7 bins) the firing rate in 5 cm position bins for each cell. The smoothed firing rates were z-scored to 0 mean with a standard deviation of 1. Any peaks exceeding a z-score of 2 for at least 6 cm were detected as fields. All adjacent bins on either side of the peak were included until the z-score dropped to 0, which is where the boundaries of the place field were set. Fields that were less than 20 cm apart were merged and fields with peaks within 30 cm before or after the food dish location were deleted. First, sessions of same direction were combined and then field boundaries were determined in each direction independently. If the fields overlapped in the two directions, they were matched and considered as one field. If no opposite direction match was found, then the same boundaries were used for both directions. This procedure ensured that all spikes of the fields were considered even when fields showed a backward shift in the running direction. All fields detected by the algorithm were checked manually and deleted if they did not show phase precession in at least one of the two directions. Ca. 36.6% of fields detected by the automated algorithm were

deleted in the manual step and a total of 260 fields remained. Ca. 6% of place field boundaries were manually adjusted.

Spatial correlations. The spatial correlations were computed by correlating the linearized spatial maps of a cell in sessions of same or different running directions with each other. For different running directions, sessions A and B and sessions B' and A' were compared.

Population vector correlations in the mazes. The similarity of the spatial maps for same and different running directions was estimated by computing the population vector correlations. The linearized spatial maps of all n cells were used to construct an n cells (rows) by t spatial bins (columns) matrix of firing rates for each condition (A, A', i.e. first and last session and B, B', i.e., second and third session). For the different direction comparison, the two sessions of same running directions were combined (A and A', as well as B and B') and the rows in the spatial matrices were normalized by their maximum. The bins within the field boundaries in B (combined with B') were flipped and shifted. The amount by which the fields were shifted was determined by what shift resulted in the highest mean spatial correlation over all cells per data set. All cells within one data set were shifted by the same amount. The population vector correlations were computed for each position bin in one spatial matrix with all position bins in another spatial matrix.

Global remapping simulation. Global remapping was simulated by moving the place fields of one direction randomly around the track and calculating the spatial correlations. This procedure was repeated 1000 times.

Directionality index. The directionality index was computed by taking the absolute difference of the mean place field firing rates of a cell in the two running directions divided by the sum of the mean place field firing rates in the two directions of comparison. The DI can range between 0 and 1, with 0 indicating identical rates in the two directions of comparison and 1 indicating maximally different rates in the two directions of comparison. Note that 0 DI can only occur in the limit of zero sampling error.

EEG analysis. The LFP signal recorded in the hippocampal fissure was filtered offline between 6-10 Hz to determine the theta signal. To identify ripple events, the local field potential recorded in the cell layer of CA1 was band pass filtered offline between 100 and 300 Hz and the envelope of the signal was determined by a Hilbert transform and smoothed using a 30 ms sliding time window. Ripples were detected when the signal continuously exceeded the mean + 2 SD for at least 15 ms. Ripple epochs that were closer than 25 ms were merged.

Rate reactivation analysis. The mean firing rates of all neurons on each recording day were computed for each maze session during running periods (speed of rat > 2cm/s) and for each sleep session during ripple periods. As the firing rate distribution is lognormal (Figure 4.2e), the mean rates were log transformed. The data of all rats were combined. The correlations between the log transformed firing rate vectors during sleep 2 was computed with the preceding (A) and following maze session (B).

Cross correlation analysis between CA3 unit activity and ripple peak times. Spike times of individual CA3 neurons (n = 1058) were cross-correlated with the ripple peak times recorded on that day as reference events. The correlograms were computed with a bin size of 5 ms over a window of 400 ms centered around 0. The mean and standard error of the mean per bin were computed.

Number of spikes and proportion of active neurons per ripple. The number of spikes that occurred per ripple was summed regardless of neuron identity. The proportion of active neurons per ripple was calculated by taking the ratio of the number of neurons that fired during a ripple over all simultaneously recorded neurons.

RESULTS

To test whether hippocampal CA3 neurons reactivate the sensory/contextual modulation of their rates within a stable spatial map, we recorded from five rats (346 neurons) while they were running on a circular track for 15 minutes per session in clockwise and counter clockwise directions in an A-B-B'-A' paradigm (A' and B' are repeated recordings in the A and B directions). Sleep epochs were recorded while the animal was resting in a box in the center of the track (but not on the track) between run sessions for 20 minutes (S2-S4). Sleep sessions before the first (S1) and after the last running session (S5) were 45 minutes long. It should be stated here that 'sleep' is used as a label for epochs before and after run sessions and does not exclude possible awake periods during these epochs.

Firing rates encode running direction within a stable spatial code

CA3 neurons with place fields on the circular track show direction dependent firing rate differences (Figure 4.1). The selected examples (Figure 4.1) show phase precession in their fields in both direction but the absolute rates are direction specific. The location is largely constant except for an asymmetry due to phase precession effects. For a quantitative assessment of whether the spatial maps for the two running directions are not different (i.e., no global remapping, Figure 4.2a-c), we assessed the similarity using population vector correlations. For same direction comparisons (Figure 4.2a, A with A' and Figure 4.2b, B with B') the population vector correlations show a narrow band with values close to 1 along the diagonal. This indicates that both field locations and within field firing rates are similar in repeated recordings in the same direction. Correlation values further away from the diagonal correspond to positions further apart on the track and therefore appear more and more dissimilar. For different direction comparisons (Figure 4.2c, A vs. B), all rows in the binned spatial maps of all cells were normalized by their maximum to alleviate the influence of rate difference and to emphasize the similarity of the two spatial maps. The bins within field boundaries in one direction were flipped and rotated by an optimal amount assessed per data set to compensate for the field asymmetry. This improved the spatial correlations significantly (0.06 ± 0.30 compared to 0.18 ± 0.36 after flipping and rotating, $p < 0.000001$, ttest, one-tailed), especially compared to a simulated global remapping situation, in which the

fields in one direction where randomly shifted along the track (0.0009 ± 0.30 , $p < 0.000001$, ttest, one-tailed).

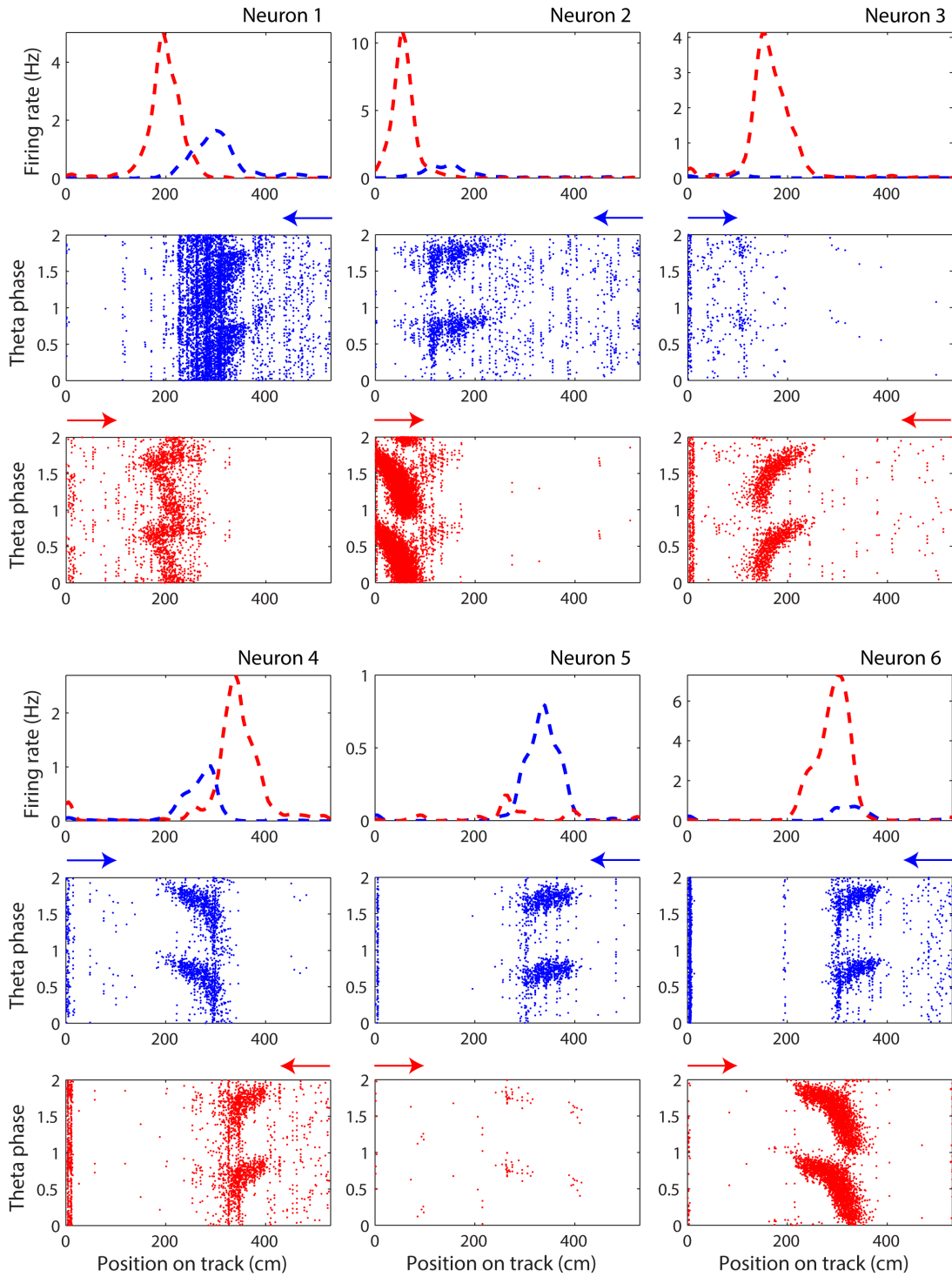


Figure 4.1 Rate remapping in different running directions on a circular track

Six examples taken from 2 different rats on 3 different days to illustrate the rate differences within place fields in different directions (indicated by colors blue and red). For each neuron the

normalized (i.e., occupancy corrected) firing rate is plotted in the two directions (blue and red dashed lines in first row) against the linearized position in cm on the track. The reward location is at 0 cm. The theta phases of the spikes discharged in the two directions are plotted below. Two full cycles of theta phase are plotted for illustration purposes. Arrows over theta phase plots indicate running direction. Theta phase plots are not occupancy corrected, which is why there is an accumulation of spikes around the reward zone at the beginning of the track.

Next, we quantified the effect of rate remapping using a directionality index (Leutgeb et al., 2005b; Navratilova et al., 2012) that measures the similarity of firing rates of a cell in two conditions. We calculated the DI by comparing the mean firing rates within the place fields in opposite directions (Figure 4.2d, crosses) with the mean firing rates within the place fields in same directions (Figure 4.2d, diamonds). The DI for opposite directions is significantly different from the DI for same directions already on the first day (Wilcoxon rank sum test, one-tailed, $p < 0.0001$). Thus, the rate-remapping was established on the first day (Leutgeb et al., 2005b; Navratilova et al., 2012) and increased over subsequent recording days (Wilcoxon rank sum test, one-tailed, $p < 0.00001$ for opposite vs. same direction), reaching about a 2-fold difference.

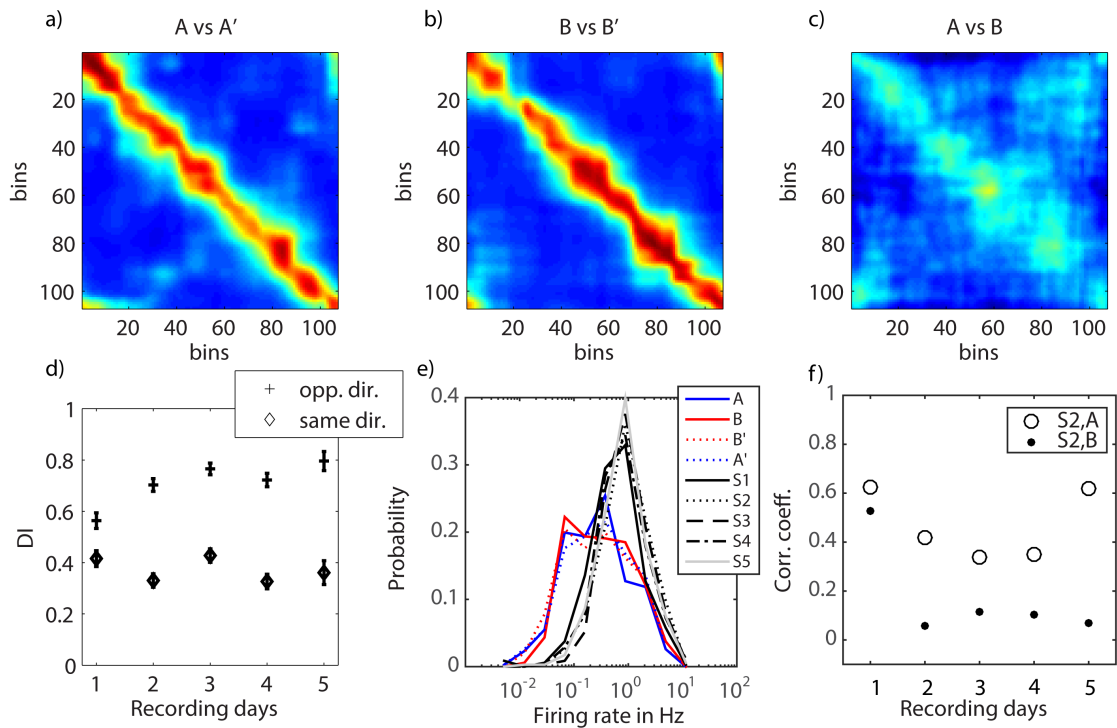


Figure 4.2 Similarity between spatial maps, directionality index, lognormal firing rate distributions and reactivation of rate remapping

a) The population vector correlations of the binned spatial maps of all neurons of the pooled data of all rats in session A and A' (repeated recording in the same running direction) and B and B' (b) are plotted with cool – warm colorscale ranging between -0.17 and 0.97). Population vector correlations of corresponding positions on the track (plotted along diagonal) show the highest values, while the values decrease with increasing offset between population vector locations. c) The population vector correlation matrix for sessions in opposite directions after normalizing each row to their maximum, flipping spatial bins within field boundaries and alignment of fields, shows lower values along the diagonal as well as a broader band. This effect arises from differences in firing rates as caused by rate remapping, asymmetric field expansion and phase precession effects, which result in place fields in opposite directions being offset slightly when the rat's head is taken as the position reference (Skaggs et al., 1996), Figure 14E). However, the spatial structure of field location in the two directions is preserved. d) The directionality index (DI) is plotted for all animals pooled over 5 recording days. The mean and SEM of the DI in the different direction comparison (crosses, A vs B and A' vs B') and same direction comparison (diamonds, A vs A' and B vs B') are plotted. e) The firing rate distribution of all recorded neurons is plotted for all behavioral (red and blue solid and dashed lines) and all sleep sessions during ripple events (black and grey solid, dashed and dotted dashed lines). Note the log scale on the x-axis. f) The mean firing rates of all cells of session A, B and sleep 2 of all animals were pooled and log transformed. The correlation between S2 and A (open circles) as well as between S2 and B (closed circles) were computed over 5 recording days. The correlations between S2 and A are significantly higher than between S2 and B (Wilcoxon rank sum test, one-tailed, $p=0.03$).

Reactivation in CA3 includes contextual modulation of firing rates

To determine whether the firing rates are faithfully reactivated in sleep after behavior, we tested the following null hypothesis. If CA3 only reactivates the spatial information, which is identical in both sessions, we expect that activity in session A explains activity in the following sleep (S2) no better than activity in the subsequent run session B (order: A – sleep (S2) – B). The specific alternative hypothesis is that both spatial and rate-remapped components are reactivated and therefore activity (i.e., firing rates) in A explains activity in subsequent sleep better than activity in B does. As the firing rate distributions in behavior and sleep are lognormal (Figure 4.2e), we computed the correlations between the log transformed mean firing rate vectors (Battaglia et al., 2005; Mizuseki and Buzsaki, 2013) during running periods in sessions (A and B) and during ripple periods in sleep S2 (Figure 4.2f). The correlation $r(S2, A)$ was significantly higher than $r(S2, B)$ (Wilcoxon rank sum test, one-tailed, $p=0.03$) over the course of all five recording days. On day 1, the difference between $r(S2,A)$ and $r(S2,B)$ is the smallest (0.53 and 0.63, respectively). On that day, rate remapping was also the least expressed (Figure 4.2d). On days 2-5, values for $r(S2,A)$ ranged between 0.34 and 0.62 and values for $r(S2,B)$ fell between 0.06 to 0.12. We can therefore reject the null hypothesis. The log transformed mean rate correlations between the remaining sleep and maze sessions are included in the Appendix.

A classical approach to assess reactivation is to compute the pairwise correlation coefficients between neurons during sleep and behavior (Wilson and McNaughton, 1994; Kudrimoti et al., 1999). In our case, the critical comparisons would be the correlation coefficients for neuron pairs in maze A and for neuron pairs in S2 (same for maze B and S2). However, this approach is biased towards rejecting the null hypothesis due to the asymmetry of place fields (Mehta et al., 1997), which can result in differences in the overlap of neighboring fields in opposite running directions, even in the absence of rate remapping. In figure 4.3., the schematic illustrates that two asymmetric place fields (neuron 1 in blue and neuron 2 in green) with constant firing rates in the two directions (i.e., no rate remapping) and constant Euclidean distance between their peak firing positions (double sided arrow) in the two directions and different tuning curves, show different amounts of overlap (red filled area). This would affect the correlation coefficients for this neuron pair in the two directions differently, suggesting rate remapping, when there is none. We computed the analysis and obtained significant results consistent with our conclusion; however, given the potential bias we decided to not rely on this approach.

Another type of analysis that seeks to identify recurring patterns or sequences of neural activity has been developed using Bayesian decoding (Davidson et al., 2009), combinatorial methods (Lee and Wilson, 2002), or template matching (Tatsuno et al., 2006). These methods have not been applied to this data as the place field representation in most data sets is too sparse to design a useful template or use

Bayesian decoding. The attempt was made to detect sequences according to Lee and Wilson's (2002) method, however, in data sets with >15 place fields the number of possible combinations calculated to assess significance exceeds our current computational power. As the scientific question in this study is addressable with a simple correlation between mean firing rates of neurons in behavior and sleep, which gives a robust result, this was the method of choice. In addition, it is reasonable to assume that the spatial sequences are identical, albeit in reverse order. A simple reversal of the sequence in the opposite direction would likely introduce a certain degree of error due to phase precession effects. It is therefore not a straightforward comparison to match sequences of opposite running directions with sequences in sleep and likely gives a noisier result than a simple rate correlation.

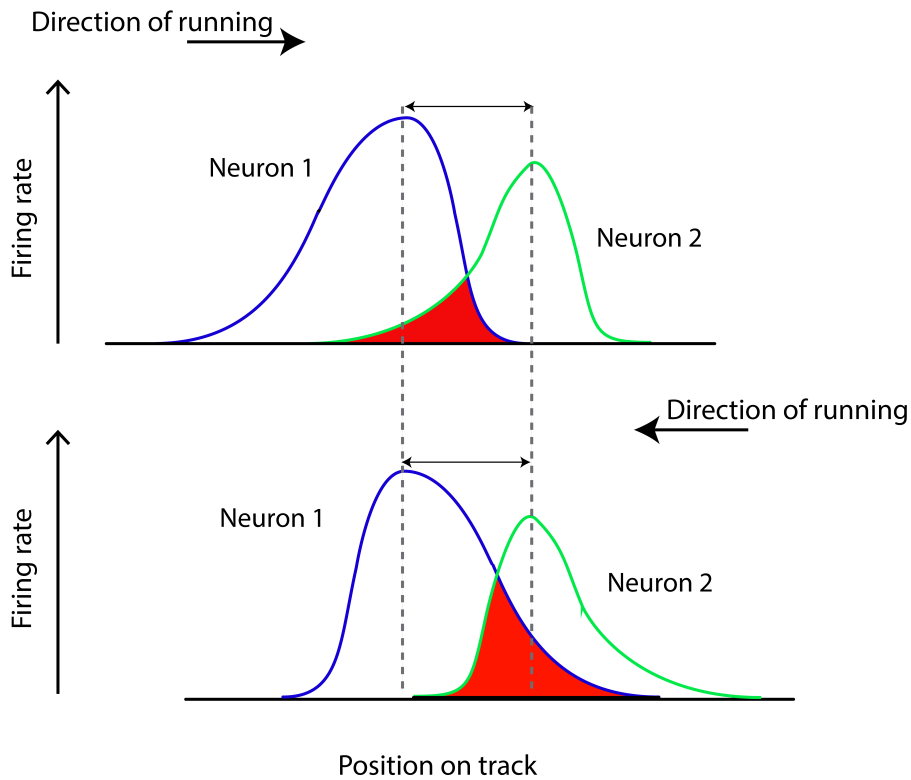


Figure 4.3 Asymmetry of place fields and its effect on their overlap

Two asymmetric place fields of two neurons (blue and green) are drawn on the track (x-axis) that show expansion of the field opposite to the animal's running direction (black arrow on top left and right of schematic). The two fields show different tuning, but each shows the same tuning and firing rate (on y-axis) for both directions. The Euclidean distance (double sided arrow) between their peak firing locations (dashed line) is kept constant in the two directions. The area, in which the firing of the two place cells overlaps, is indicated in red and differs in the two directions. This difference will affect the correlation coefficient between the neuron pair in the two directions and bias the result toward finding a difference between the two directions and rejecting the null hypothesis, when it is true (i.e., the individual neurons do not show rate remapping).

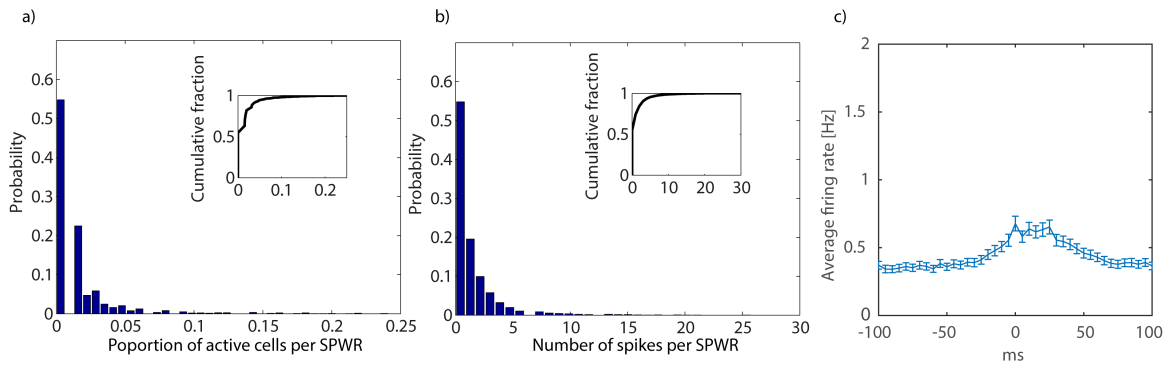


Figure 4.4 Relationship between CA3 unit activity and ripple events

a) The proportion of neurons active out of the total number of simultaneously recorded neurons in any given sharp wave/ripple (SPWR) is plotted as the probability distribution and the cumulative probability distribution (inset). The activation probability among the recorded cells per ripple is extremely low. b) The probability distribution of the total number of spikes per sharp wave ripple shows that the majority of ripples in CA1 entrain only very few spikes in the recorded CA3 population. c) CA3 unit activity cross correlated with peak ripple times in the EEG with a bin size of 5 ms. The mean and SEM are plotted for each bin. CA3 neurons show elevated firing within a window of -25 to +75 ms around the peak of ripple oscillations recorded in the CA1 pyramidal layer. The broad peak of the cross correlogram is likely due to the differences in the timing of spikes in CA3 b and c.

CA3 unit activity was very sparse during sharp wave ripple complexes. The proportion of active cells and the number of spikes fired was extremely low (Singer and Frank, 2009). Elevated firing was observed within a time window of about 100 ms (between -25 ms to +75 ms) around the peak times of CA1 ripples (Figure 4.4 c). The peak firing occurred between 0 and 25 ms after the peaks of the detected ripples in pyramidal layer CA1. The broad peak in the spike timing likely reflects the fact that the recording tetrodes were located in CA3 b and c, which show an offset in spike timing relative to CA1 ripples (Csicsvari et al., 2000). The peak firing rate was around 0.7Hz, which is considerably lower than in CA1 (Csicsvari et al., 2000), but is consistent with previous reports (Csicsvari et al., 2000). This effect might imply that the ripple selection

criterion may have been fairly stringent, which possibly caused the loss of spikes fired around the edges of the ripple events, especially around the onset of ripples. Relaxing the thresholds for start and end times of ripples could potentially help to get more accuracy for CA3 firing rates during ripples. Nevertheless, the result clearly indicates that firing rates during ripples in S2 resemble more closely the preceding experience (Figure 4.2f).

DISCUSSION

CA3 has been shown to encode contextual information flexibly onto a single spatial map without affecting other independent spatial maps (Gothard et al., 1996; Anderson and Jeffery, 2003; Leutgeb et al., 2005b; Leutgeb et al., 2007; Allen et al., 2012). In addition, it has been demonstrated that CA3 reactivates pattern sequences in sleep after the experience, but lack of perfect fidelity in this reactivation and the apparent lack of attractor dynamics for the sensory components during waking, left open the question of whether reactivation during sleep contains both sensory and spatial components, or only the latter. We found that firing rates in sleep were significantly more similar to the previously experienced episode than to a future episode of identical spatial content with different sensory context, confirming that both determinants of the collective activity are reactivated.

How can the present result be rationalized with the apparent lack of attractor dynamics for sensory/contextual information in CA3? Recent experimental evidence

showed that there are abrupt attractor-like transitions in the population output of CA3 in response to sensory input that is gradually morphed between two spatially independent stored memories (Leutgeb et al., 2005b; Leutgeb et al., 2007; Colgin et al., 2010), whereas spatially overlapping but visually distinct memories cause diverse and non-coherent changes in CA3 neuron firing (Leutgeb et al., 2005b; Leutgeb et al., 2007; Colgin et al., 2010; Lu et al., 2013). Some cells do show abrupt transitions but do so at different points, some cells show smooth transitions and others show hysteresis; but as a population the transition in the output appears gradual. This suggested that there might not be attractor dynamics for spatial/contextual information in CA3. Recent modelling studies, however, suggest that episodic memory could possibly be supported by a combination of discrete and continuous attractor dynamics (Renno-Costa et al., 2014; Solstad et al., 2014). The possibility of discrete attractor dynamics in the recurrent collaterals of CA3 and hysteresis effects in some cells suggests that different sensory/episodic events that occur in the context of the same spatial map may be stored in the synapses of CA3 neurons and be amenable to retrieval during off-line reactivation.

CONCLUSION

This study shows that CA3 combines and stores spatial and episodic components of memories. It is able spontaneously to retrieve specific episodic information related to a single spatial location. Rate remapping therefore may be an effective way of encoding

and separating different experiences associated with the same location and using this separation to index the different memory components in the neocortex.

Contributions: B.L. McNaughton and C.D. Swindel conceived the project. C.D. Swindel conducted the experiment and analysis. M. Tatsuno helped with discussion of analysis and results. C.D. Swindel and B.L. McNaughton wrote the manuscript.

Acknowledgements: We thank Karim Ali for technical assistance with Matlab and Zaneta Navratilova for sharing Matlab code regarding video processing and place field analysis, as well as Lilia Mesina for help with cluster cutting. This work was supported by the grants from Alberta Innovates Health Solutions (Polaris Award), NSERC, and Neuroelectronic Research Flanders to BLM, NSERC DG 386522-2010 to MT and an Alberta Innovates Health Solutions Graduate Fellowship to CDS.

**Chapter 5 Long-term Recordings Improve the Detection of Weak Excitatory-Excitatory
Connections in Rat Prefrontal Cortex**

C Daniela Schwindel, Karim Ali, Bruce L McNaughton, Masami Tatsuno

Department of Neuroscience, Canadian Centre for Behavioural Neuroscience, The
University of Lethbridge, 4401 University Dr W, Lethbridge, AB, T1K 3M4, Canada

published in: Schwindel et al. (2014) The Journal of Neuroscience 34 (16):5454-5467.

ABSTRACT

Characterization of synaptic connectivity is essential to understanding neural circuit dynamics. For extracellularly recorded spike trains, indirect evidence for connectivity can be inferred from short-latency peaks in the correlogram between two neurons. In spite of their predominance in cortex, however, significant interactions between excitatory neurons (E) have been hard to detect because of their intrinsic weakness. By taking advantage of long duration recordings, up to twenty-five hours, from rat prefrontal cortex, we found that 7.6% of the recorded pyramidal neurons are connected. This corresponds to approximately 70% of the local E-E connection

probability that has been reported by paired intracellular recordings (11.6%). This value is significantly higher than previous reports from extracellular recordings, but still a substantial underestimate. Our analysis showed that long recording times and strict significance thresholds are necessary to detect weak connections while avoiding false positive results, but will likely still leave many excitatory connections undetected. In addition, we found that hyperreciprocity of connections in prefrontal cortex that was shown previously by paired intracellular recordings was only present in short-distance, but not in long distance (~300 microns or more) interactions. As hyperreciprocity is restricted to local clusters, it might be a minicolumnar effect. Given the current surge of interest in very high-density neural spike recording (e.g., NIH BRAIN Project) it is of paramount importance that we have statistically reliable methods for estimating connectivity from cross-correlation analysis available. We provide an important step in this direction.

INTRODUCTION

Characterization of synaptic interactions on a large scale is essential to understand information processing in neural circuits. In an attempt to characterize local circuit dynamics, combined electrophysiological and imaging techniques have started to map out neocortical circuits (Bock et al., 2011; Ko et al., 2011). With recent developments in multi-electrode recording technology, it has also become possible to

monitor large numbers of neurons simultaneously with high temporal resolution (McNaughton et al., 1983b; Csicsvari et al., 2003a; Buzsaki, 2004). Even though this number is still small relative to the total number of neurons, one advantage of ensemble recordings is that it can greatly facilitate the study of spike-train interactions, because the number of neuron pairs increases as the square of the number of units recorded. The obtained spike trains are often analyzed by cross correlations to infer synaptic interactions (Alonso and Martinez, 1998; Ostojic et al., 2009). The cross correlogram, a well-established technique to investigate temporal relationships between neural spikes, describes the co-variance between the binned spike trains of two neurons at various time lags (Perkel et al., 1967b; Kirkwood, 1979; Aertsen and Gerstein, 1985; Brown et al., 2004). A plausible argument for synaptic connectivity can be made from the presence of short-latency peaks in the correlogram within the range of central glutamatergic EPSP and gabaergic IPSP rise times (Csicsvari et al., 1998; Bartho et al., 2004; Fujisawa et al., 2008).

Despite the potential usefulness of the cross-correlation method, the detection of excitatory interactions between pyramidal neurons (E-E interaction) has been difficult (Bartho et al., 2004; Fujisawa et al., 2008), because these interactions are generally weak (McNaughton, 1980; Mason et al., 1991; Deuchars et al., 1994; Markram et al., 1997; Thomson and Deuchars, 1997; Reyes and Sakmann, 1999; Thomson et al., 2002). Excitatory synaptic strength of intracellularly measured cortical connections has been shown to follow a lognormal distribution (Song et al., 2005), suggesting that a very small

number of strong connections are embedded in a large number of weak connections. In addition, the duration of typical ensemble recordings is not long (up to a few hours). The consequence is a limited sampling of spike occurrences and also a poor sampling of the possible state-space occupancy distribution (Perkel et al., 1967a, b). Cells are tuned to respond to a given set of input vectors and some vectors in the set may never occur during the sampling epoch. Thus, for some connected cells in the sample, the input which brings them close enough to threshold to allow synaptic interaction may not occur during the sampling period. In other words, the effective contribution of cell A to the firing of cell B is not independent of the activity of other cells in the network. Hence, some connections may not be visible in spike cross-correlograms from a given sample epoch.

To explore these issues, we analyzed neural ensembles from rat prefrontal cortex and estimated the asymptotic detection probability of excitatory connections and investigated the nature of the distribution of the detected excitatory connections.

MATERIALS AND METHODS

Recording experiment. Twenty-five hour continuous, multi neuron recording data sets were collected from three adult male Brown-Norway/Fischer 344 hybrid rats that were trained to run a spatial sequence task (Euston et al., 2007) and were also subjected to a novel object exposure procedure (Tatsuno et al., 2006). The recording sessions were divided into two 12h sleep/rest sessions interrupted by 1h behavior, which was either

the sequence task or the novel object exposure, to yield a total recording duration of 25h per recording session. The animals were implanted with a hyperdrive with 12 independently movable tetrodes (Gothard et al., 1996) ($<1\text{M}\Omega$ impedance) in the left medial prefrontal cortex (3.2 mm AP, 1.3 mm ML relative to bregma) to record from dorsal anterior cingulate cortex (ACd) and prelimbic cortex (PL). The tetrodes were used to record extracellular single units. The anatomical positions of the tetrodes were confirmed histologically.

Two additional probes were placed 4-5 mm deep in the medial prefrontal cortex to record a differential reference signal. The animal's position was tracked at 60 frames/s using LEDs mounted on the headstage that were detected by a color camera that was mounted on the ceiling of the recording room (approximately 0.33 cm/pixel). The thresholded signals were recorded with a Cheetah Data Acquisition System (Neuralynx), digitized at 32 kHz and bandpass filtered between 600 Hz and 6 kHz. Local field potential (LFP) data were filtered between 1 and 475 Hz and sampled at 2 kHz.

Animal care and surgeries were conducted in accordance with National Institutes of Health guidelines and approved Institutional Animal Care and Use Committee protocols. After surgery, rats were administered 26 mg of acetaminophen (children's Tylenol; McNeil, Fort Washington, PA) and also received 2.7 mg/ml acetaminophen in the drinking water for 1-2 d after surgery. In addition, they were given oral ampicillin on a 10 d on/10 d off regimen for the duration of the experiment.

Spike sorting. Spiking activity was analyzed offline using an automated spike-sorting algorithm (KlustaKwik by K. D. Harris) to isolate units and separate them from noise. The resulting clusters were manually refined using cluster cutting software (MClust 3.0 by A.D. Redish, with customizations by P. Lipa, S. Cowen, and D. Euston) in a multi-parameter space including features such as energy (area under the waveform), peak to trough distance, principal component, time (to control for stability of the recording of the unit over the entire recording duration) and cross correlograms. In addition, all units were verified by waveform visualization software (WaveformCutter 1.0 by S. Cowen). Only units with less than 0.3% interspike intervals (ISI) falling within 2 ms refractory period were accepted.

During long recording times, the position of the electrode can shift and, consequently, the shape of the recorded waveform can change. This can lead to errors in spike sorting and can cause false temporal firing relationships between neuron pairs. For this reason, we only included neurons that show good isolation and little variance in their waveforms and z-scored peak amplitudes over the entire length of recordings (Figure 5.1a). As a measure for the stability of the neurons, we calculated the fractional change of firing rate between the first and the last 4 hour periods. We found that the fractional change for the majority (95%) of the neurons that were selected by the first criteria was less than 80%, suggesting that the neurons were stable for the 25 hour period of recordings.

In addition, inspired by the recent finding by Mizuseki and Buzsaki (2013) that the distribution of firing rates follows a lognormal distribution in the hippocampal formation, we also calculated the distribution of firing rate of our data. Figure 5.2c shows the firing rate distribution during the first and last 4 hours of recording. We found that not only does the firing rate follow a lognormal distribution, but also the shape of the distribution did not change between the two periods. We also confirmed that the firing rate calculated of the entire recording follows a log-normal distribution.

Neuron classification. Neurons are classified into excitatory, inhibitory or unclassified based on statistical dependency with other neurons. Firstly, for each reference neuron, cross correlations against all other neurons were calculated with a bin size of 1 ms and a window size of +/-50 ms. Secondly, each cross correlation was converted to a z-score with its mean and standard deviation. This alleviated the problem of spike rate differences. Next, we calculated the moving average (window size: 15 ms) of the z-scored cross correlations and subtracted it from the original signal to obtain a detrended z-scored cross correlation. This procedure removed modulations in intermediate temporal ranges that are slower than monosynaptic interactions. Correlations that showed putative common input (measured as a peak or trough encompassing lag [-1:1]) were excluded from further cell classification analysis. Cross correlation pairs that did not contain relevant information were also removed (if none of the z-scored correlation values within [-4, 4] exceeded 2 or -2, the pair was removed). Finally, the average cross correlation of the remaining pairs was calculated (Figure 5.1b). Mean and one standard

deviation of the average cross correlation for the bins outside of $[-4, 4]$ ms were used as a threshold to determine whether a bin within $[1, 4]$ ms has a relevant correlation signal for cell classification; if at least one bin exceeded the upper threshold (mean + 1std) and no bin undershot the lower threshold (mean - 1std), the reference neuron was classified as a putative excitatory neuron. If at least one bin undershot the lower threshold (mean - 1std) and no bin exceeded the upper threshold (mean + 1std), the reference neuron was classified as a putative inhibitory neuron. Otherwise, the reference neuron was left unclassified. We also inspected all individual cross correlations visually to verify whether the decision of the algorithm we applied on the average detrended z-scored cross correlations was consistent with the judgment made by human observers. In summary, this procedure aims at classifying a reference neuron based on the average statistical influence of the reference neuron to all possible postsynaptic target neurons.

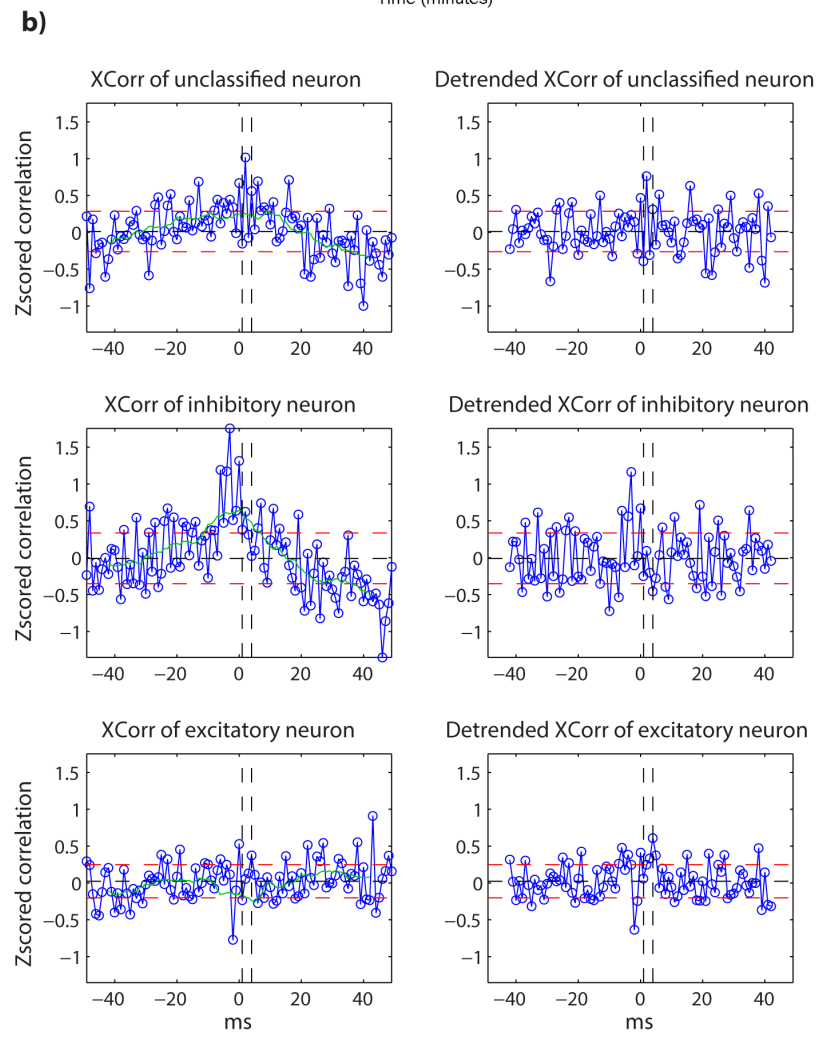
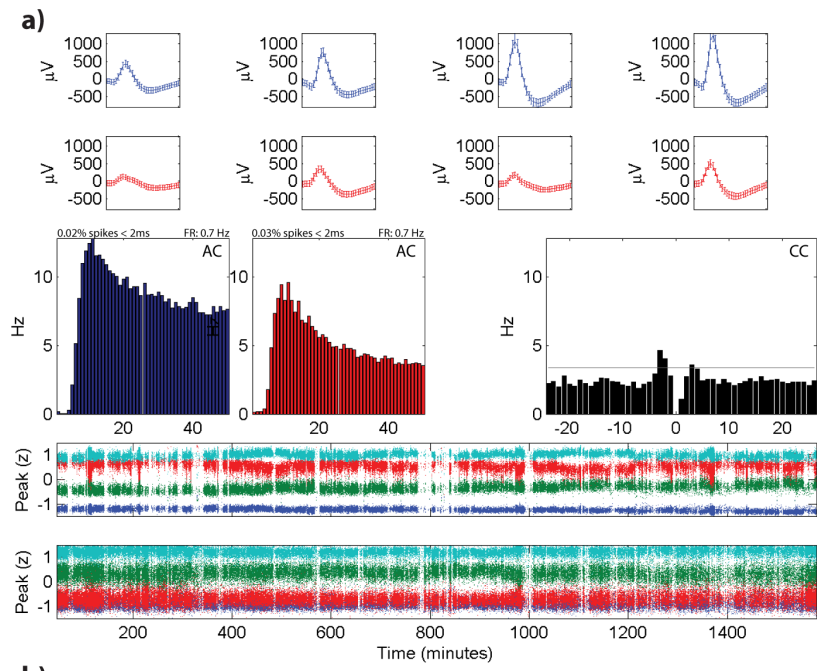


Figure 5.1 Neuron classification

a) Stability of neurons and cleanness of clusters recorded on the same tetrode. Average waveforms (top two rows), autocorrelograms (AC, two middle left panels), cross correlogram (CC, middle right panel) and time plots (two bottom panels) of two excitatory neurons recorded on the same tetrode are depicted. The percent of spikes within 2 ms of refractory period included in the cluster and the firing rate are indicated above the autocorrelograms. Both clusters show distinct waveforms (each waveform is depicted for a 1 ms window) and have clean refractory periods (0.02% and 0.03%, respectively, spikes within 2 ms of refractory period). Their cross correlogram is reciprocally significant (EE2) at a significance threshold of $\alpha = 10^{-5}$ (grey horizontal line). b) Classification of neurons. In the left column, the average z-scored cross correlations of three different neurons, without the detrending procedure, are depicted in blue. In the right column, the corresponding detrended average z-scored cross correlations are plotted. The black horizontal dashed line depicts the mean, the red horizontal dashed lines depict one standard deviation above and below the mean, respectively, and the green line is the moving average of the z-scored cross correlation computed with a moving window of 15 ms. The vertical black dashed lines represent the limits of the window of interest between 1 and 4 ms, within which short-latency peaks or troughs are assessed for classification. The top row represents an unclassified neuron that, without detrending, would have been classified possibly falsely as excitatory. The middle row shows an inhibitory neuron that without detrending, would have been classified as excitatory. The last row represents an excitatory neuron that would have been left unclassified without detrending.

Cross correlation analysis. All simultaneously recorded neurons from each animal were cross correlated with each other with a bin size of 1 ms. The cross correlation values were normalized by the firing rate of the reference neuron. This procedure resulted in $n*(n-1)/2$ correlation pairs (n = number of recorded units. Self-correlation was excluded). For each neuron pair, the spikes of one spike train were jittered randomly within an interval of [-5, 5] ms to break up the short-latency relationships between spikes. The bin size and jitter interval were chosen based on synaptic integration times in frontal cortex neurons in vivo (Leger et al., 2005). Then, the jittered spike trains were cross-correlated with a bin size of 1 ms. This procedure was repeated 1000 times to compute a surrogate data set of cross correlations. Various significance thresholds (α -

levels) were computed from the distribution of jittered data to detect peaks or troughs with short latency and duration (≤ 2 ms) in the cell pair correlations (Bartho et al., 2004; Fujisawa et al., 2008): α levels used are 0.5, 0.2, 0.1, 0.05, 0.02, 0.01, 5×10^{-3} , 2×10^{-3} , 1×10^{-3} , 5×10^{-4} , 2×10^{-4} , 1×10^{-4} , 5×10^{-5} , 2×10^{-5} , 1×10^{-5} and the global min/max value (referred to as absolute limit: abs) which corresponds to the overall maximum and minimum values of all bins in the surrogate data set. If a single bin exceeded the significance level within the first 4 ms before or after lag 0, the correlation was scored as significant excitation and the pair was considered monosynaptically connected. Similarly, if two neighboring bins undershot the significance level within the first 4 ms before or after lag 0, the connection was scored as significant inhibition (Bartho et al., 2004). This way, significance was tested for both possible directions of interaction between the two neurons. To verify our method and temporal window within which we assess significance of the short-latency peaks, we repeated the same analysis as described above for 4 ms windows around ± 25 ms and ± 50 ms.

The length of the recording period used for the cross correlogram calculation was varied from one hour to 25 hours with one-hour increments. Firstly, for each hour segment and for a given significance level α , we constructed a matrix of significant cross-correlations for all possible non-overlapping blocks (i.e. 25 blocks for 1 hour segments, 12 blocks for 2 hour long segments, etc.). This resulted in a matrix with an entry for each significant correlation type EE1, EE2, EI1, EI2, IE1, II1, EU1 and IU1; EE1 represents unidirectional excitation between two excitatory neurons; EE2 represents reciprocal

excitation between excitatory neurons; E11 represents unidirectional excitation from an excitatory neuron onto an inhibitory neuron; E12 represents reciprocal connection between an inhibitory and an excitatory neuron; IE1 represents unidirectional inhibition from an inhibitory neuron onto an excitatory neuron; I11 represents unidirectional inhibition between two inhibitory neurons; EU1 represents unidirectional excitation from an excitatory neuron onto an unclassified neuron; IU1 represents unidirectional inhibition from an inhibitory neuron onto an unclassified neuron. Since swapping reference- and target-neurons results in the mirror image of the original cross correlogram, only the upper triangle of the result matrix was considered. We then summed the number of significant correlations for each correlation type. In order to estimate the distribution of the number of detected correlations for each hour segment, we used bootstrapping with replacement (Mooney, 1993; Hoffman and McNaughton, 2002). The matrix was randomly resampled with replacement as many times as needed to obtain 1000 samples for each hour segment. For instance, for the 1-hour segment, each upper triangle of the 25 result matrices was resampled 40 times. For the 25 hour segment, only one result matrix was obtained and was therefore resampled 1000 times. The median, 84th and 16th percentile were calculated to characterize the distribution. For the tetrode-wise analysis, the connection matrix of each tetrode was resampled with replacement 1000 times. The result was summed across tetrodes and data sets. Again, the median, 84th and 16th percentile of the bootstrapped sample distribution were calculated.

The experimentally derived detection probability of excitatory connections p_{α}^n for the significance level α and the recording length of n hours was defined as

$$p_{\alpha}^n = \frac{\#(EE1) + 2 \times \#(EE2)}{2N}, \quad (1)$$

where $\#(EE1)$ is the number of significant unidirectionally connected pairs, $\#(EE2)$ is the number of significant reciprocally connected pairs, and N is the total number of neuron pairs.

Extrapolation by fitting the statistical power function using simulated annealing. In order to investigate how the experimentally derived detection probability of weak E-E connections p_{α}^n may improve beyond the recording duration of 25 hours, we applied curve fitting based on statistical power. To obtain a reasonable estimate, we used a framework for the case that both the data from the alternative hypothesis and the data from the null hypothesis follow the normal distribution with a known standard deviation. The statistical power function, defined as the probability of rejecting the null hypothesis when the alternative is true, is written as:

$$power = 1 - ncdf\left(cutoff \mid \mu_1, \frac{\sigma}{\sqrt{n}}\right), \quad (2)$$

where the *cutoff* is the threshold value for rejecting the null hypothesis when the alternative is true, μ_1 is the mean of the alternative hypothesis (the mean peak cross-

correlation value within -4 to +4 ms excluding 0), σ is the standard deviation of the null and alternative hypotheses, n is the sample size (the length of recording (hours)), and

$$ncdf = p = F(x | \mu, \sigma) = \frac{1}{\sigma\sqrt{2\pi}} \int_{-\infty}^x e^{-\frac{(t-\mu)^2}{2\sigma^2}} dt. \quad (3)$$

Using the significance level α , the *cutoff* is written:

$$cutoff = ninv\left(1 - \alpha, \mu_0, \frac{\sigma}{\sqrt{n}}\right), \quad (4)$$

where μ_0 is the mean of the null hypothesis (chance-level cross-correlation value estimated by spike-jittering) and

$$ninv = x = F^{-1}(p | \mu, \sigma) = \{x : F(x | \mu, \sigma) = p\}. \quad (5)$$

Plugging equation 4 into equation 2 yields:

$$power = 1 - ncdf\left(ninv\left(1 - \alpha, \mu_0, \frac{\sigma}{\sqrt{n}}\right), \mu_1, \frac{\sigma}{\sqrt{n}}\right). \quad (6)$$

We conjectured that the probability of detecting a significant cross correlation between two neurons, if a connection exists and the conditions for its making a contribution to post-synaptic spiking are realized, follows the same form of statistical power. The fitted detection probability of excitatory connections C_α^n for the significance level α and the recording length of n hours can be obtained as:

$$C_\alpha^n = CEE_\alpha \cdot power = CEE_\alpha \left(1 - ncdf \left(ninv \left(1 - \alpha, \mu_0, \frac{\sigma}{\sqrt{n}} \right), \mu_1, \frac{\sigma}{\sqrt{n}} \right) \right), \quad (7)$$

where CEE_α is the asymptotic detection probability of excitatory connections p_α^n at the significance level α . Finally, in order to obtain a better fit, the significance level α and the standard deviation σ in the right hand side in equation 7 were treated as fitting parameters α_{param} and σ_{param} , respectively. This gives the final fitting equation:

$$C_\alpha^n = CEE_\alpha \left(1 - ncdf \left(ninv \left(1 - \alpha_{param}, \mu_0, \frac{\sigma_{param}}{\sqrt{n}} \right), \mu_1, \frac{\sigma_{param}}{\sqrt{n}} \right) \right). \quad (8)$$

In summary, CEE_α , α_{param} and σ_{param} in equation 8 were optimized to fit the data of the experimentally derived detection probability of weak E-E connections p_α^n . This yields the fitted detection probability of excitatory connections C_α^n . Note that in a standard testing of a normal mean with a known standard distribution, α and α_{param}

are identical and they represent the significance level of the test. Similarly, σ and σ_{param} are identical and they represent the standard distribution of the null and alternative hypotheses. In this study, however, α_{param} was separated from α and σ_{param} was separated from σ , and they were treated as fitting parameters. This distinction was necessary to obtain a good fit to our experimental data. We speculate that it might be partly due to the fact that μ_1 follows a skewed continuous distribution rather than a normal distribution. Given the fact that many different fitting functions were indeed able to fit our experimental data almost equally well, but would produce greatly different asymptotes, we chose a fitting function that is based on statistical power.

Actual curve fitting was conducted by simulated annealing (Metropolis et al., 1953; Kirkpatrick et al., 1983) using MATLAB Global Optimization Toolbox (MathWorks). Simulated annealing is a well-established, general optimization method that has been used as a powerful optimizer for n-body problems including the classic traveling salesman problem (Metropolis et al., 1953; Kirkpatrick et al., 1983). The method can be pictured as the physical process of first heating a material and then lowering the temperature slowly, which corresponds to minimizing the system's energy. More precisely, at a sufficiently high temperature, the system is slightly perturbed and the change of energy, ΔE , is calculated. The new state is accepted if ΔE is negative. If the energy increases, the new state is accepted under a certain probability ($p = \exp[-\Delta E / (k_B T)]$ where k_B = Boltzmann constant and T = temperature) to avoid that the system

gets stuck in local minima. This process is repeated many times at the current temperature. The temperature is slowly decremented until the system is frozen (Kirkpatrick, 1983). The method may not find the optimum solution but is most likely to find one of the near-optimum solutions. We ran 1000 optimization trials to select the best parameter values that would give the least sum of squares. See table 2 for optimization results for all α levels. The r-squares, R^2_{AllEx} and R^2_{AllExtT} , were computed to estimate the goodness of fit of the optimized function to the data.

Calculation of the effect size h . In order to compare the size of the short-latency peak across neuron pairs, we introduced the effect size h that was defined as the normalized significant peak,

$$h = \frac{h_{\text{peak}} - \mu_{\text{jitter}}}{\sigma_{\text{jitter}}} \quad (9)$$

where h_{peak} is the height of the maximum peak in the cross correlogram in [-4,-1] ms and [1,4] ms (i.e., the maximum peak taken of this 8 ms window) for unidirectional excitatory connections (EE1) and the height of the maximum peaks in the cross correlogram in [-4,-1] ms and [1,4] ms for reciprocal excitatory connections (EE2) (i.e. the maximum peak taken of each 4 ms window), and μ_{jitter} and σ_{jitter} are the mean and the standard deviation of the jittered data for the corresponding cross correlation, respectively (Fujisawa et al., 2008).

RESULTS

Long-term recordings of 25-hour length were analyzed using cross correlations to identify excitatory connections between prefrontal putative pyramidal neurons. Six data sets obtained from three rats that were subjected to both a repeated sequence running task and novel object experience, were analyzed (Two novel-object data sets were described previously (Tatsuno et al., 2006)). Table 5.1 shows the number of neuron pairs in each session. In total, we analyzed 237 neurons and 4787 correlation pairs. An example of units included in the analysis is shown in Figure 5.1a. We classified the neurons into excitatory (54%), inhibitory (8%) and unclassified neurons (38%) based on their overall short latency effects on postsynaptic neurons (see methods, Figure 5.1b), as the different classes were not unambiguously differentiable based on their waveform characteristics. This may be due to our recording parameters, e.g. using a rather tight band-pass filter between 600 Hz-6 kHz, which affects the shape of the recorded spikes.

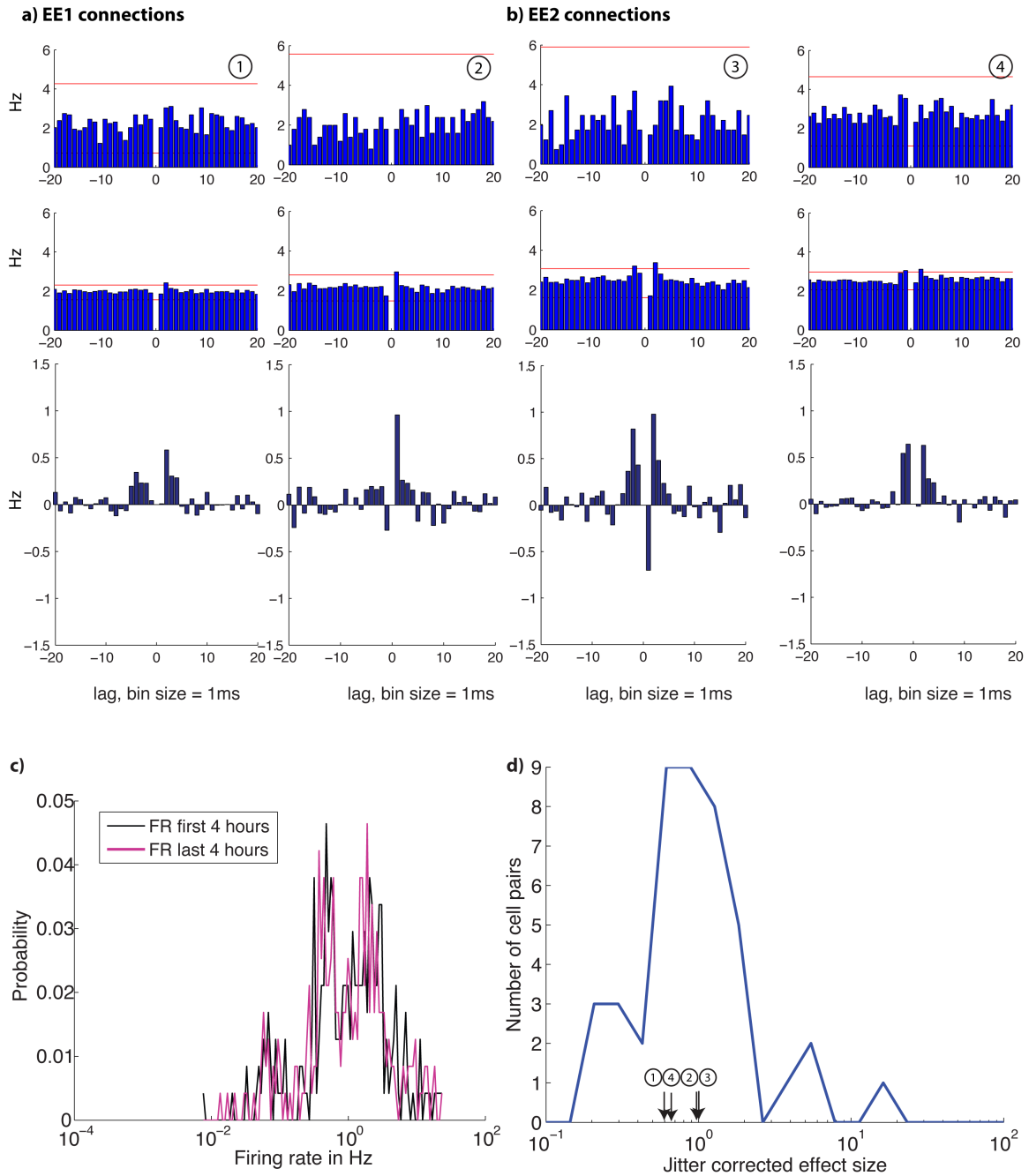


Figure 5.2 Examples of cross correlograms for detected excitatory connections, firing rate distribution and the distribution of the jitter corrected effect size

Examples of cross correlograms between two putative pyramidal neurons that are unidirectionally connected (a, EE1 connections) or reciprocally connected (b, EE2 connections).

In the top row, cross correlations for 1 hour long spike trains and in the second row, cross correlations for the same neurons pairs for 25 hour long spike trains are shown with a window size of 20 ms and a bin size of 1 ms. The red horizontal lines depict the significance level (α =

abs) determined by 1000 spike-jittered cross-correlations. Note the improved signal to noise ratio in the 25 hour cross correlograms (middle row), which enables the detection of small, short latency peaks. The bottom row shows the jitter corrected correlograms for 25 hours obtained by subtracting the mean of the jittered cross correlograms of each cell pair from the original cross correlogram (middle row). c) The distribution of firing rate probability among all neurons for the first 4 hours (black) and last 4 hours (pink) of recording. The firing rate distribution for both recording intervals is lognormal. Note the log scale on the x-axis. d) The distribution of the jitter corrected effect size for EE1 and EE2 connections. The distribution of the jitter corrected peaks of the significant cross correlations is lognormal as previously shown by Mizuseki et al. (2013). The peaks of the neuron pairs shown in a) and b) are indicated in the plot.

Changes of detection probability over various lengths of recordings

Significant excitatory connections between neuron pairs were detected by using a spike train jitter method (Bartho et al., 2004; Fujisawa et al., 2008). As the threshold for significant interactions is chosen somewhat arbitrarily by the experimenter and influences the size of the type I error (false-positives), we investigated a wide range of significance levels; 16 different α levels ranging from 0.5 to absolute limit (abs). The absolute limit is derived from the absolute maximum value of all bins in the jittered data for each neuron pair and represents the strictest α level. Note that it is not much smaller than 10^{-5} (the smallest used before abs).

Figures 5.2a and 5.2b show four examples of cross correlograms between two putative pyramidal neurons with the absolute limit. While no significant short-latency peak was detected with a one-hour recording (Figure 5.2a, b, top row), it was detected with a 25-hour recording (Figure 5.2a, b, middle row). The reduced fluctuations in the correlogram reflect the improved signal to noise ratio and enable the detection of small peaks. As expected, longer recording times increase the chance of detecting weak

excitatory connections. In addition, we also calculated the jitter-corrected cross corelograms (Figure 5.2a, b, bottom row) (Hirabayashi et al., 2013; Mizuseki and Buzsaki, 2013). This is obtained by subtracting the mean jittered cross correlations for each bin from the original cross correlation. The results show that the significant peaks clearly stand out. The firing rate distribution of the analyzed data set follows a lognormal distribution as previously shown (Mizuseki and Buzsaki, 2013) and does not change between the first and last 4 hours of recordings (Figure 5.2c). The distribution of the jitter corrected significant peaks follows a lognormal distribution as well (Figure 5.2d), which is also consistent with previous findings (Mizuseki and Buzsaki, 2013).

Table 5.1 The number of neuron pairs, significant excitatory connections and the experimentally derived detection probability of excitatory connection pairs

The number of neuron pairs, the number of unidirectional excitatory connections (EE1), the number of reciprocal excitatory connections (EE2) and the number of unconnected neuron pairs (NO) as well as the connection probability (detection probability of excitatory connections, p_{25}^{α} , equation 1) for the 25 hour recordings are reported in 3 different ways in order to compare them to intracellular recording studies (Song et al., 2005) and to extracellular recordings (Fujisawa et al., 2008 and the counting method in this paper, in which we only consider excitatory neurons across all tetrodes). Therefore, all three columns contain our data, simply reported according to three different counting methods, which are detailed below.

Formula for calculating the number of neuron pairs for Song et al. (2005) criteria:

$$\# \text{ of neuron pairs} = N_{AllExTT} = \sum_{i=1}^{N_{TT}} \frac{n_{EE,i}(n_{EE,i} - 1)}{2},$$

where $n_{EE,i}$ is the total number of excitatory neurons within tetrode i and N_{TT} is the total number of tetrodes.

Formula for calculating the number of neuron pairs for our criteria:

$$\# \text{ of neuron pairs} = N_{AllEx} = \frac{n_{EE}(n_{EE} - 1)}{2},$$

where n_{EE} is the total number of excitatory neurons.

Formula for calculating the number of neuron pairs for Fujisawa et al. (2008) criteria:

$$\# \text{ of neuron pairs} = N_{All} = \frac{n_{all}(n_{all} - 1)}{2},$$

where n_{all} is the total number of all recorded neurons, including inhibitory and unclassified neurons.

The formula for calculating the connection probability of excitatory neuron pairs p_{α}^n was provided by equation (1) in the main text.

Data Sets		Counting method			
		Song et al.	Present study	Fujisawa et al.	
Rat 1	Novel	# of neuron pairs	36	276	820*
		# of EE1 connections	5	6	6
		# of EE2 connections	1	1	1
		# of unconnected pairs	30	269	813*
		p_{α}^{25} (connectivity)**	0.10	0.01	0.00
	Sequence	# of neuron pairs	22	210	528*
		# of EE1 connections	9	12	12
		# of EE2 connections	2	3	3
		# of unconnected pairs	11	195	513*
		p_{α}^{25} (connectivity)**	0.30	0.04	0.02
Rat 2	Novel	# of neuron pairs	26	153	780*
		# of EE1 connections	2	2	2
		# of EE2 connections	1	1	1
		# of unconnected pairs	23	150	777*
		p_{α}^{25} (connectivity)**	0.08	0.01	0.00
	Sequence	# of neuron pairs	5	55	325*
		# of EE1 connections	1	1	1
		# of EE2 connections	0	0	0
		# of unconnected pairs	4	54	324*
		p_{α}^{25} (connectivity)**	0.10	0.01	0.00
Rat	Novel	# of neuron pairs	77	253	903*

3	# of EE1 connections	4	4	4
	# of EE2 connections	0	0	0
	# of unconnected pairs	73	249	899*
	p_{α}^{25} (connectivity)**	0.03	0.01	0.00
	<hr/>			
Sequence	# of neuron pairs	109	496	1431*
	# of EE1 connections	6	10	10
	# of EE2 connections	9	3	3
	# of unconnected pairs	100	483	1418*
	p_{α}^{25} (connectivity)**	0.11	0.02	0.01
<hr/>				
	Total # of neuron pairs	275	1443	4787*

*includes inhibitory and unclassified neurons as well as excitatory neurons, while all other counts contain excitatory neurons only

** $\alpha = \text{abs}$

The experimentally derived detection probability of excitatory connections p_{α}^n for the significance level α and the recording length of n hours was given by equation 1. To make the results comparable to paired intracellular recordings between pyramidal neurons (Song et al., 2005), N was taken as the total number of possible excitatory neuron pairs ($N_{AIEEx} = 1443$, Table 5.1). In addition, since intracellular recordings are typically done in slices and are limited to a smaller volume of tissue, we also calculated N as the number of possible excitatory neuron pairs per tetrode ($N_{AIEExTT} = 275$, Table 5.1). While the results for both N_{AIEEx} and $N_{AIEExTT}$ are presented, we consider that $N_{AIEExTT}$ is more directly comparable to previous intracellular recordings (Song et al., 2005). The results of detection probabilities normalized by all recorded neuron pairs

(Bartho et al., 2004; Fujisawa et al., 2008) ($N_{All} = 4787$), including connection types other than excitatory interactions are shown in Figure 5.9.

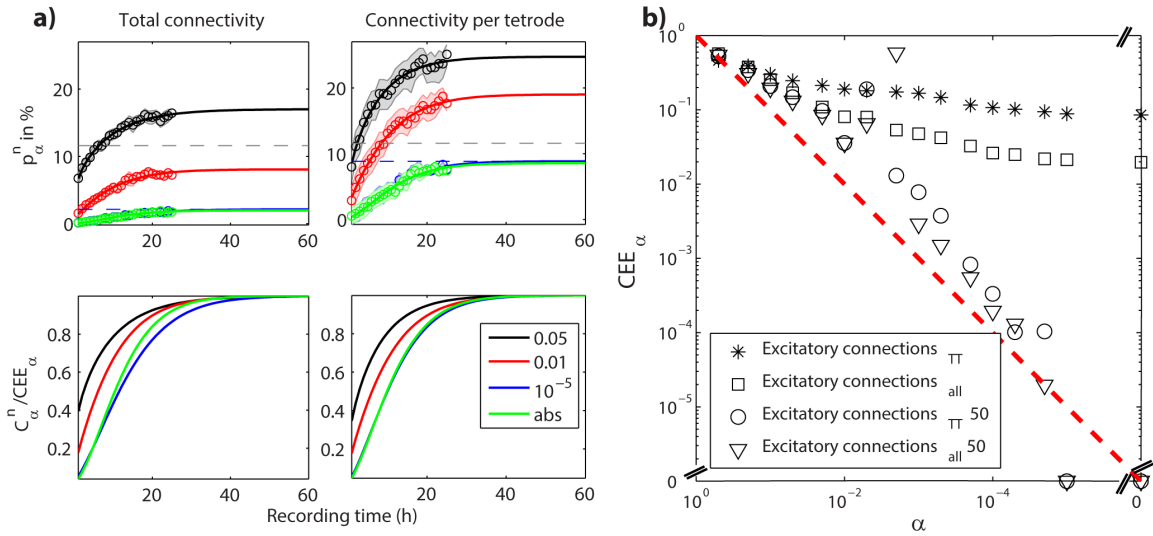


Figure 5.3 The experimentally derived detection probability

a) (Top) The experimentally derived detection probability p_{α}^n of excitatory connections. The median (circles) and 16th and 84th percentile (shaded area) of the detection probability are plotted for recording lengths of 1-25 hours. The data in the left plot was normalized by the total number of possible excitatory neuron pairs (N_{AllEx}) and the data in the right plot by the total number of possible excitatory neuron pairs per tetrode ($N_{AllExTT}$). The results for four different significance α -levels (color coded) are shown: 0.05, 0.01, 10^{-5} , abs (note: the curves for the latter two levels largely overlap). The detection probabilities (C_{α}^n , solid lines) were extrapolated until asymptote (CEE_{α}) as estimated by the fitting of the statistical power function. The gray dashed horizontal line at 11.6% denotes the local connectivity as detected by Song et al. (2005) between pyramidal neurons in layer 5 of rat visual cortex. The blue dashed line indicates the asymptote as approached by $\alpha=10^{-5}$. All R^2 values indicating the goodness of fit are between 0.98 and 0.99.

(Bottom) The fitted detection probabilities (C_{α}^n) divided by CEE_{α} are plotted for N_{AllEx} normalization (left) and for $N_{AllExTT}$ normalization (right). **b)** The asymptotes (CEE_{α}) are plotted against the α levels on a log-log scale. Open squares and asterisks correspond to CEE_{α} normalized by N_{AllEx} and by $N_{AllExTT}$, respectively. Both ways of CEE_{α} estimation seem to approach a lower limit. Triangles and circles correspond to CEE_{α} normalized by N_{AllEx} and by $N_{AllExTT}$, respectively, for the alternative window at +/- 50 ms. CEE_{α} approaches zero as α becomes stricter. This is expected because no monosynaptic interactions are expected to be detected in the time interval of +/- 50 ms.

Figure 5.3a (top panels, data points) shows how the experimentally derived detection probabilities of excitatory connections p_{α}^n changes from one hour recordings to 25 hour recordings for four representative α levels: 0.05, 0.01, 10^{-5} and the absolute limit. The data points represent the median and the background band shows the range for the 84th and 16th percentile estimated by bootstrapping. The detection probabilities increased with longer recording times for both ways of calculating the connection probability. For $\alpha = 0.05$, the detection probability increased from 6.7% (N_{AllEx}) and 8% ($N_{AllExTT}$) for one hour long recording segments to 16.4% (N_{AllEx}) and 25% ($N_{AllExTT}$) for 25 hour long recording segments, respectively. For $\alpha = 0.01$, the detection probability increased from 1.6% (N_{AllEx}) and 2.9% ($N_{AllExTT}$) to 7.2% (N_{AllEx}) and 17.6% ($N_{AllExTT}$), respectively. For the stricter α values, 10^{-5} and the absolute limit, which show very similar trends for both ways of normalization, the detection probability increased from 0.1% (N_{AllEx}) and 0.5% ($N_{AllExTT}$), to 1.7% (N_{AllEx}) and 7.6% ($N_{AllExTT}$), respectively.

Table 5.2 Optimization results for fitting the statistical power function to the experimental data

a) Optimization results for fitting the statistical power function (equation 8) to the experimental data p_{α}^n for all investigated α levels. The table shows the optimization results for all 16 α levels using simulated annealing for fitting the data p_{α}^n normalized by the number of excitatory neuron pairs per tetrode ($N_{AllExTT}$). The left column represents the significance thresholds (α) that were applied to count the number of significant cross correlations. The parameter $CEE_{\alpha, AllExTT}$ (the asymptotic detection probability of excitatory connections p_{α}^n), $\alpha_{param, AllExTT}$ as well as $s_{param, AllExTT}$ were optimized using simulated annealing. μ_0 and μ_1 were estimated from the data; μ_0 is the mean of the jittered cross correlations of all EE pairs. μ_1 is the mean of the peaks within the window [-4;4] of all significant EE cross correlations. $LSS_{AllExTT}$ (least sum of squares)_{AllExTT} shows the smallest LSS that was used to select the best fit out of the 1000 optimization trials. $R^2_{AllExTT}$ provides a measure for the goodness of the optimization result. **b)** The table shows the simulated annealing optimization results for all 16 α levels for fitting the data normalized by the

total number of excitatory neuron pairs (N_{AllEx}). $CEE_{\alpha, AllEx}$, $\alpha_{param, AllEx}$ and $s_{param, AllEx}$ were optimized using simulated annealing. The columns for α , μ_0 , μ_1 , LSS and R^2_{AllEx} are as described in a).

a)

α	$CEE_{\alpha, AllExTT}$	$\alpha_{param, AllExTT}$	μ_0	μ_1	$\sigma_{param, AllExTT}$	LSS _{AllExTT}	$R^2_{AllExTT}$
0.5	46.29	0.415	1.83	2.2	0.267	62.649	0.36
0.2	39.18	0.470	1.83	2.2	1.042	20.919	0.94
0.1	30.09	0.271	1.83	2.2	0.691	10.824	0.98
0.05	24.73	0.166	1.83	2.2	0.631	8.583	0.98
0.02	21.39	0.090	1.83	2.19	0.612	6.378	0.99
0.01	19.01	0.060	1.83	2.2	0.582	4.222	0.99
5×10^{-3}	18.13	0.040	1.83	2.2	0.572	3.806	0.99
2×10^{-3}	17.43	0.032	1.83	2.2	0.606	4.147	0.99
1×10^{-3}	16.74	0.026	1.83	2.2	0.617	3.488	0.99
5×10^{-4}	14.70	0.020	1.83	2.2	0.578	2.834	0.99
2×10^{-4}	11.63	0.014	1.83	2.2	0.508	3.092	0.99
1×10^{-4}	10.73	0.012	1.83	2.2	0.507	2.555	0.99
5×10^{-5}	10.20	0.009	1.83	2.2	0.487	3.307	0.98
2×10^{-5}	9.45	0.010	1.83	2.2	0.506	2.507	0.98
1×10^{-5}	8.85	0.009	1.83	2.2	0.489	2.952	0.98
abs.	8.56	0.007	1.83	2.2	0.470	3.056	0.98

b)

α	$CEE_{\alpha, AllEx}$	$\alpha_{param, AllEx}$	μ_0	μ_1	$\sigma_{param, AllEx}$	LSS _{AllEx}	R^2_{AllEx}
0.5	57.02	0.7	1.83	2.2	0.804	4.706	0.97
0.2	37.85	0.49	1.83	2.2	0.913	5.264	0.98

0.1	25.53	0.35	1.83	2.2	0.864	2.539	0.99
0.05	17.00	0.22	1.83	2.2	0.741	1.858	0.99
0.02	10.94	0.11	1.83	2.19	0.649	1.577	0.99
0.01	8.06	0.06	1.83	2.2	0.577	1.383	0.98
5×10^{-3}	8.02	0.06	1.83	2.2	0.573	1.739	0.98
2×10^{-3}	5.34	0.02	1.83	2.2	0.583	0.478	0.99
1×10^{-3}	4.76	0.02	1.83	2.2	0.629	0.214	0.99
5×10^{-4}	4.21	0.02	1.83	2.2	0.637	0.189	0.99
2×10^{-4}	3.27	0.02	1.83	2.2	0.603	0.102	0.99
1×10^{-4}	2.65	0.02	1.83	2.2	0.603	0.056	0.99
5×10^{-5}	2.53	0.01	1.83	2.2	0.554	0.063	0.99
2×10^{-5}	2.18	0.01	1.83	2.2	0.529	0.083	0.99
1×10^{-5}	2.15	0.01	1.83	2.2	0.535	0.076	0.99
abs.	1.97	0	1.83	2.2	0.455	0.112	0.99

Curve fitting and extrapolation of the relationship between statistical power and sample size

Next, we investigated how the detection probability of excitatory connections between putative pyramidal neurons would improve beyond the recording duration of 25 hours. The fitting of equation 8 was applied to the experimentally derived detection probabilities p_{α}^n with 16 different α levels (0.5 to the absolute limit) to obtain the fitted detection probabilities C_{α}^n beyond 25 hours. The optimization results are summarized in Table 5.2. Figure 5.3a (top panels) show the fitted results for 4 representative significance thresholds (α levels for 0.05, 0.01, 10^{-5} and abs). The corresponding power

function, defined by C_α^n / CEE_α , where CEE_α is the asymptotic value of p_α^n , was also obtained (Figure 5.3a, bottom panels). We found that the fitted functions converge to different asymptotic values of the experimentally derived detection probability of excitatory connections p_α^n but the difference becomes very small for stricter α levels (10^{-5} and absolute limit). There indeed appears to exist a lower limit asymptote as the threshold becomes stringent ($\sim 2\%$ (N_{AIEx}) and $\sim 8.5\%$ (N_{AIExTT})), indicated by the blue dashed lines in the plots. The CEE_α values for the stricter α levels ($\sim 2\%$ with N_{AIEx} and $\sim 8.5\%$ with N_{AIExTT}) reach about 20% and 70% of the local connectivity as reported by Song (Song et al., 2005), respectively. As was discussed in the previous section, we consider that N_{AIExTT} is more directly comparable to their study. Therefore, we conclude that approximately 70% of local E-E connections could be detected by long extracellular recordings.

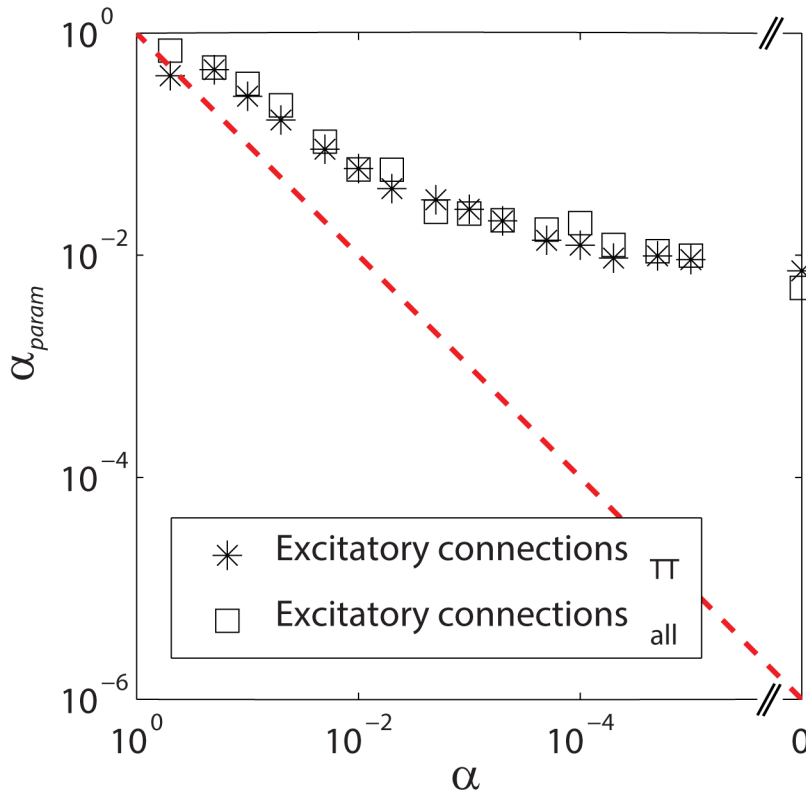


Figure 5.4 The relationship between the significance level α and the fitting parameter α_{param}
 The relationship between the significance level α and the fitting parameter α_{param} , obtained from equation 8. Asterisks depict the results obtained with N_{AllEx} and open squares depict the results obtained with $N_{AllExTT}$. α_{param} deviates gradually when α gets smaller. This is likely due to the fact that μ_1 is not a single value, but a distribution, which is not accounted for in equation 8. However, α and α_{param} maintained a monotonically decreasing relationship. This suggests that separating α_{param} from α does not violate the original relationship of $\alpha = \alpha_{param}$ substantially.

For α levels of 0.05 and 0.01, the power function ($C_{\alpha}^n / CEE_{\alpha}$) approaches 1 more quickly than that of 10^{-5} and absolute limit (Figure 5.3a, bottom panels); approximately 90% of power could be achieved with 20 hours of recording. However, their detection probability also increases quickly and exceeds Song et al.'s (2005) detection probability of 11.6%; $\alpha = 0.05$ with N_{AllEx} normalization and $\alpha = 0.05$ and 0.01 with $N_{AllExTT}$

normalization (Figure 5.3a, top panels). Since intracellular recordings have intrinsically a higher chance of detecting monosynaptic connections, as the presynaptic neurons are stimulated and even subthreshold responses in the postsynaptic neurons recorded, the overshoot for α levels 0.05 and 0.01 suggests that these acceptance criteria detect excessive false-positives.

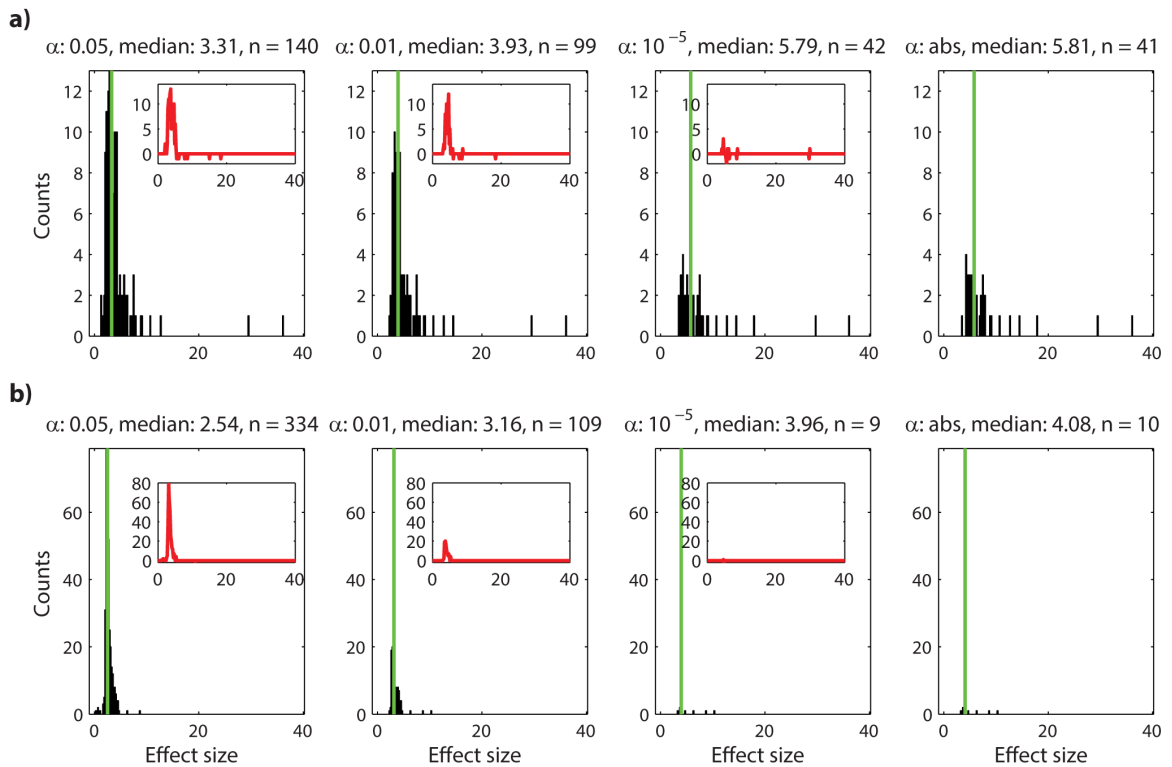


Figure 5.5 The distribution of effect sizes for short-range and long-range connections

The distribution of effect sizes (h) for short-range (a) and long-range (b) connections plotted for four different α values. The distribution of effect size for both unidirectional and reciprocal connections (EE1 and EE2) recorded within tetrodes (a) and between tetrodes (b) for four different α levels (0.05, 0.01, 10^{-5} and abs) are depicted. The number of peaks included as well as the medians of the distributions are indicated above each histogram. The median is also plotted as a green vertical line. The results for α levels 10^{-5} and absolute limit are comparable. The distributions of effect size for α levels 0.05 and 0.01 are also similar. The insets show the difference between the most stringent group (α abs) and the less stringent groups (α levels 0.05 and 0.01). These counts correspond to weak effect sizes (< 5) and most likely false-positives. The strong effect sizes (>10) are found in correlations between excitatory neurons recorded on the same tetrode, indicating that the strongest connections are mostly local.

To assess how the same asymptote could be possibly reached, CEE_α are plotted against the α levels in percent on a log-log scale (Figure 5.3b). We found that as α levels get stricter, the slope of the consecutive data points for both ways of the CEE_α estimation gets increasingly smaller (open square and asterisk correspond to N_{AIEEx} and $N_{AIEExTT}$ normalization, respectively). This result indicates there is a lower limit asymptote. In contrast, when choosing a window of identical size at longer latency lags (± 50 ms), the CEE_α estimation approaches zero almost following a diagonal line (open circle and open triangle correspond to N_{AIEEx} and $N_{AIEExTT}$ normalization, respectively). A similar result was also obtained for the latency lags of ± 25 ms. These results demonstrate that the windows at the latency lags outside of monosynaptic interactions (e.g., ± 25 ms or ± 50 ms) do not contain monosynaptic interactions.

In the final form of the fitting function (equation 8), the significance level α was treated as a fitting parameter α_{param} to obtain a better fit. We confirmed that α and α_{param} were monotonically related, indicating that fitting α_{param} does not violate the original relationship of $\alpha = \alpha_{param}$ significantly (Figure 5.4). However, α_{param} deviates gradually when α gets smaller. This could be due to the fact that μ_1 will follow a skewed distribution, which is not accounted for in equation 8. Equation 8 would need to be rewritten accordingly but it is beyond the scope of the present paper. Taken together, these results show that our method using short-latency peaks of cross correlations with

strict α levels and using the approach of fitting a statistical power function is valid for detecting monosynaptic E-E interactions and estimating their asymptotic detection probability in local networks.

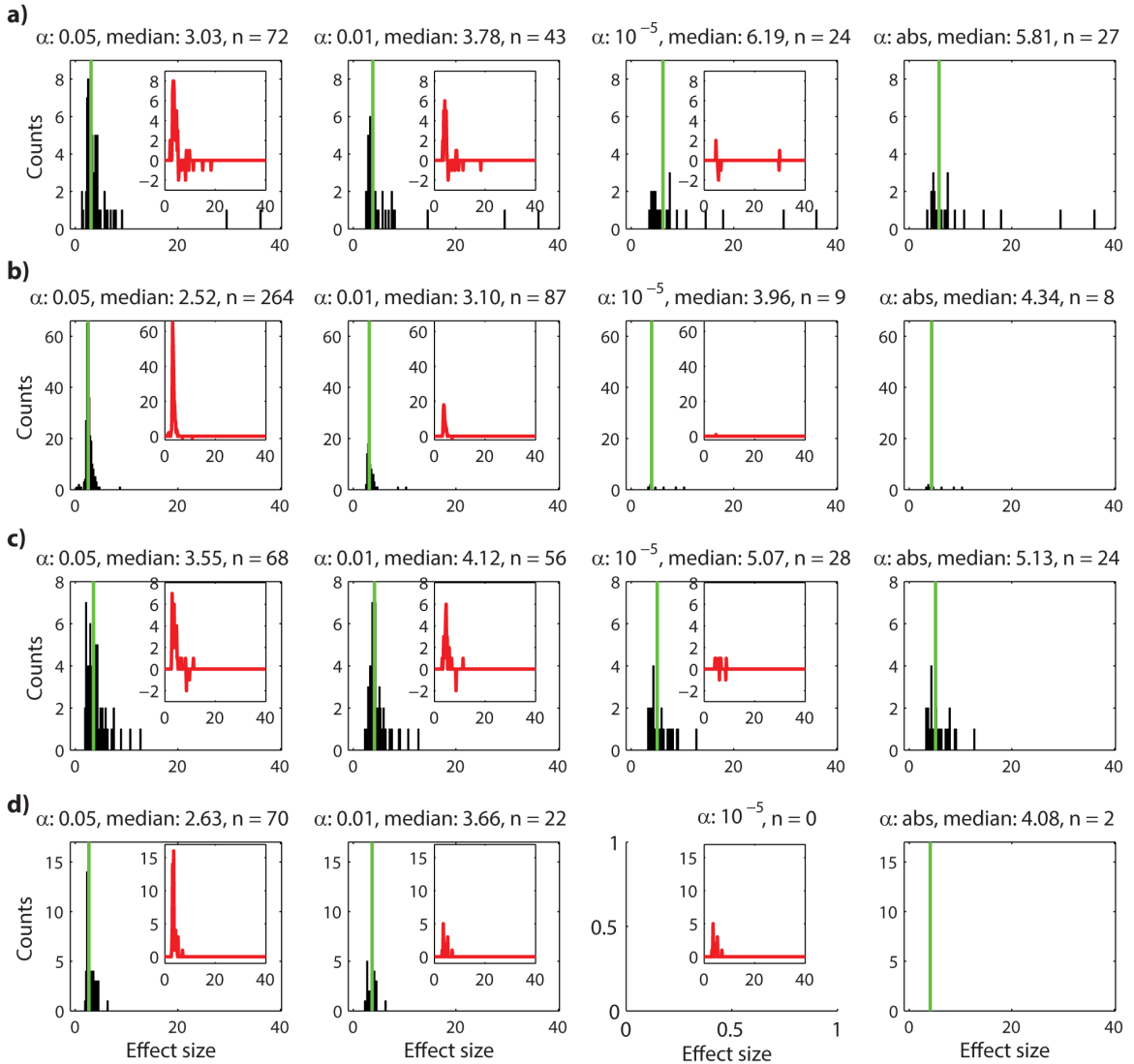


Figure 5.6 The distribution of effect sizes for unidirectional connections (EE1) and for reciprocal connections (EE2) within and between tetrodes

The distribution of effect sizes (λ) for unidirectional connections (EE1) within (a) and between (b) tetrodes and for reciprocal connections (EE2) within (c) and between (d) tetrodes for α levels 0.05, 0.01, 10^{-5} and abs. The significance levels as well as the median of the distributions are indicated above the histograms. The insets show the difference between higher α (0.05, 0.01 and 10^{-5}) and α abs, indicating the amount of likely false-positives included in the counts. The

strongest effect sizes of unidirectional connections seem to be distributed among short-range connections rather than long-range connections (**a**). The long-range connections appear to be predominantly single directed excitatory connections (**b**). As the significance level is determined by a jitter method over a distribution of 1000 jitter trials that can differ for different α levels, it is possible that not all pairs detected with α abs are included in the pairs detected with $\alpha 10^{-5}$ (even though they are mostly identical). In other words, occasionally a few more pairs can be detected with α abs than with $\alpha 10^{-5}$, which in the extreme case leads to no peaks detected at $\alpha 10^{-5}$, but still two peaks detected at α abs (**d**). Reciprocal excitatory connections seem to be mostly local (**c**) and according to α levels 10^{-5} and abs, there are hardly any reciprocal excitatory connections detectable between excitatory neurons recorded on different tetrodes (**d**). This also suggests that the peaks in α levels 0.01 and 0.05 are likely to be false-positives.

False-positives and the distribution of effect size

We investigated whether the connections detected by less stringent α levels (e.g., 0.05 and 0.01) were contaminated by false-positives by plotting the distribution of the effect size h (equation 9). The distribution of the effect size within tetrodes (short range) and between tetrodes (long range) for four representative α levels (0.05, 0.01, 10^{-5} and abs.) are plotted in Figures 5.5a and 5.5b, respectively. Both unidirectional (EE1) and reciprocal excitatory connections (EE2) are included in the analysis. The results show that the distributions for the stricter α levels (10^{-5} and abs) were almost identical and contained strong effects only (two most right panels in Figure 5.5). On the contrary, less strict α levels (0.05 and 0.01) contained additional large counts of smaller effect sizes (two most left panels in Figure 5.5). Subtraction of the most stringent distribution ($\alpha =$ abs.) from less stringent groups ($\alpha = 10^{-5}$, 0.01 and 0.05) confirmed that the stricter α levels (10^{-5} and abs) are very similar to each other but less stringent α levels (0.05 and 0.01) have higher counts of weak effect sizes (Figure 5.5, insets). This is likely

due to peak counts being contaminated by a large proportion of false-positives. Since false-positives would occur randomly, their distribution is expected to be Gaussian-like, which is consistent with what we obtained (Figure 5.5, insets). In addition, most of the stronger effects are found in short range interactions (within tetrodes, Figure 5.5a), not in long-range interactions (between tetrodes, Figure 5.5b), suggesting that the strongest connections are mostly local. We also investigated the distribution of the effect size for unidirectional (EE1) and bidirectional connections (EE2) separately; Figure 5.6a for EE1 (within tetrodes), Figure 5.6b for EE1 (between tetrodes), Figure 5.6c for EE2 (within tetrodes) and Figure 5.6d for EE2 (between tetrodes). We found that the majority of strong effects for both EE1 and EE2 are local and that the long-range excitatory connections are predominantly unidirectional (EE1).

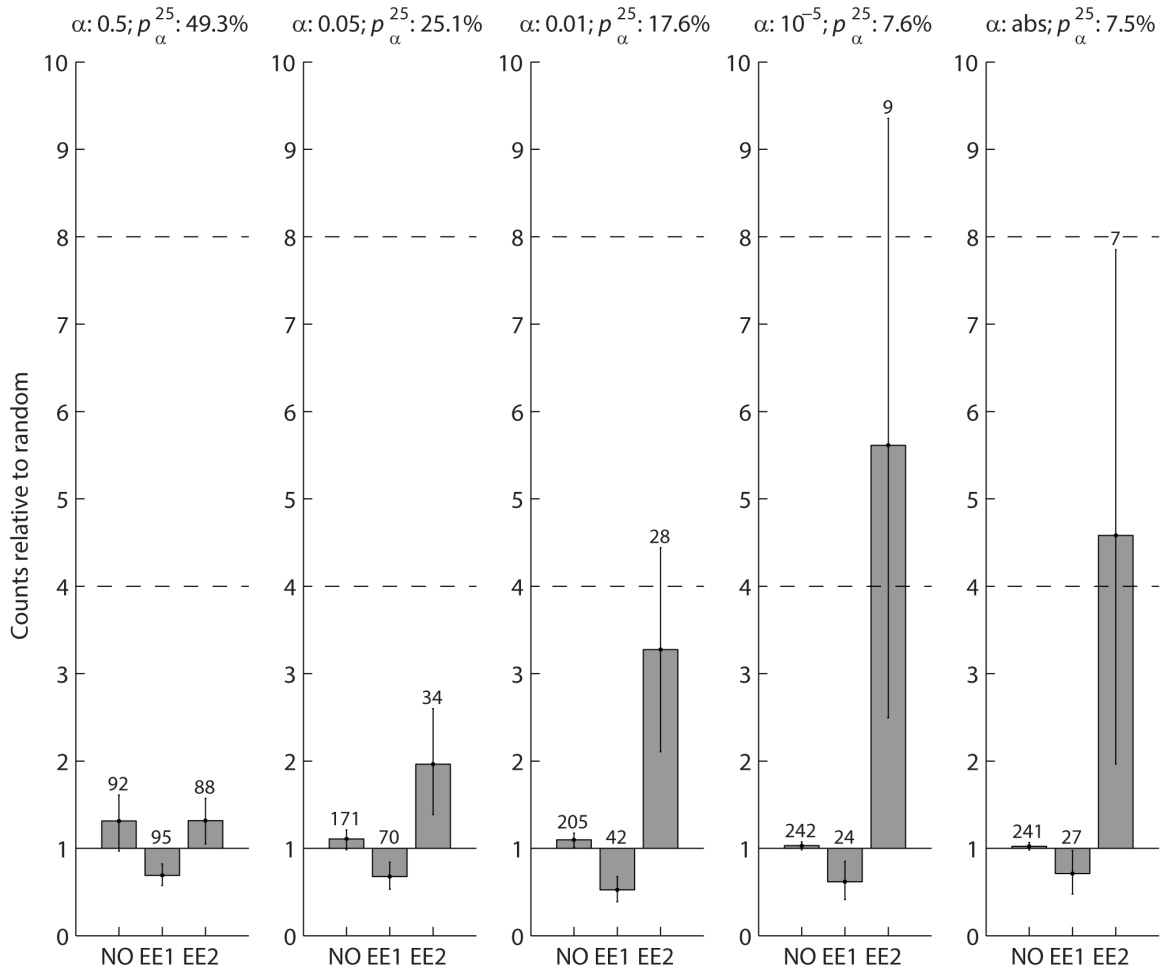


Figure 5.7 Counts of unconnected and excitatory connected neuron pairs relative to the random-connection null hypothesis

The counts of unconnected (NO), single directed excitatory (EE1) and reciprocal excitatory (EE2) neuron pairs for 5 representative α levels (left to right; 0.5, 0.05, 0.01, 10^{-5} and abs), relative to the prediction of the random-connection null hypothesis are shown. The connection probability p_{α}^{25} as well as the α levels are indicated above the individual bar plots. The absolute counts of connections are indicated above the bars. Error bars represent the 2.5th and 97.5th percentiles of the medians of 1000 bootstrapped distributions. The dashed horizontal lines at 4 and 8 indicate the expected counts of observed EE2 connections relative to the null hypothesis in the Song et al. (2005) and Wang et al. (2006) studies. For stricter α levels (abs and 10^{-5}), reciprocally connected excitatory neuron pairs (EE2) with the $N_{AllExTT}$ normalization are 4.6-5.6 times more likely than expected. This is in the four to eight times range calculated from Song et al. (2005) and Wang et al. (2006). As α becomes less stringent (0.01, 0.05 and 0.5), the difference becomes less striking because more false-positive counts are likely to be included. The counts of single directed excitatory neuron pairs (EE1) and of unconnected neuron pairs (NO) are close to the expected numbers.

Hyperreciprocity in mPFC

Further support of the conclusion that less stringent α levels (e.g., 0.01 and 0.05) are massively contaminated by false-positives came from comparing the counts of significant connection pairs at different α levels and the number of connection pairs predicted by a random connection assumption (Figure 5.7). Given that a network is randomly connected by a connection probability p_α^n (equation 1), the expected number of unconnected pairs is $N(1 - p_\alpha^n)^2$, the expected number of unidirectionally connected pairs is $2Np_\alpha^n(1 - p_\alpha^n)$ and the expected number of reciprocally connected pairs is $N(p_\alpha^n)^2$. Song et al. (2005) reported that the count of reciprocally connected excitatory neuron pairs (EE2) in rat visual cortex is four times higher than the number predicted. Wang et al. (2006) report 3.5 times and 7.9 times more EE2 connections than predicted in visual cortex and prefrontal cortex, respectively, in young ferrets. The ratios of observed EE2 to predicted EE2 are comparable in visual cortex for both rodent studies (4 in rat and 3.5 in ferret). EE2 connections are twice as likely in ferret medial prefrontal cortex than in visual cortex ($7.9/3.5 = 2.3$) and if the relationship holds true for rat, we would expect the EE2 connection probability in rat medial prefrontal cortex to be up to 8 times higher than predicted by a random connectivity assumption. Based on these considerations, we predicted that the EE2 connection in rat medial prefrontal cortex would be four to eight times higher than predicted. For the stringent α levels of the absolute limit and 10^{-5} , we found that medians of observed EE2 connections are 4.6 and 5.6 times higher than the number predicted, respectively (Figure 5.7, right columns). In

addition, their 95% confidence intervals (Figure 5.7, error bars) overlap with the predicted four to eight times range, suggesting that these results are consistent with what we predicted based on the numbers by Song et al. (2005) and Wang et al. (2006). However, for less stringent α levels, the difference between observed EE2 counts and predicted EE2 counts became lower than predicted; 3.2 times for $\alpha = 0.01$, 2 times for $\alpha = 0.05$ and 1.3 for $\alpha = 0.5$ (Figure 5.7, left three columns). Furthermore, their 95% confidence intervals do not overlap with the four to eight times range, except for $\alpha = 0.01$, where there is a small overlap, indicating that the statistics of the observed EE2 connections were different for less stringent α levels. Because false-positives detected in cross correlograms are expected to occur randomly, the observed decrease of hyper-reciprocity suggests that more false-positives are included if less stringent α levels were used. We therefore conclude that stricter α levels together with long-term recordings are necessary for reliable detection of weak E-E interactions in extracellular recordings.

Excitatory connectivity in mPFC is predominantly local

The relationship between local excitatory connectivity (within tetraode connections, normalized by N_{AIExTT}) and total excitatory connectivity (within and between tetraode connections, normalized by N_{AIEx}) can be further investigated by plotting them against each other for different α levels (Figure 5.8). For stricter α levels, observed connections were localized within the upper-left triangle, suggesting that

predominantly local connections were detected. With increasingly relaxed α levels the difference between local and total connectivity disappeared (at $\alpha = 0.2$), indicating that the difference was masked by an increasing number of false-positives. Interestingly, total connectivity became larger than local connectivity for $\alpha = 0.5$. If there was a general tendency of underestimating the local connectivity and overestimating the total connectivity, then this could explain why the total connectivity is larger than the local connectivity for $\alpha = 0.5$. One could speculate that over-elimination of spikes during spike sorting resulting in decreased correlations (Cohen and Kohn, 2011) could lead to the observed effect as this would affect the detection of significant cross correlations within tetrodes more than between tetrodes. Incapability of recording overlapping spikes within tetrodes may also enhance this tendency.

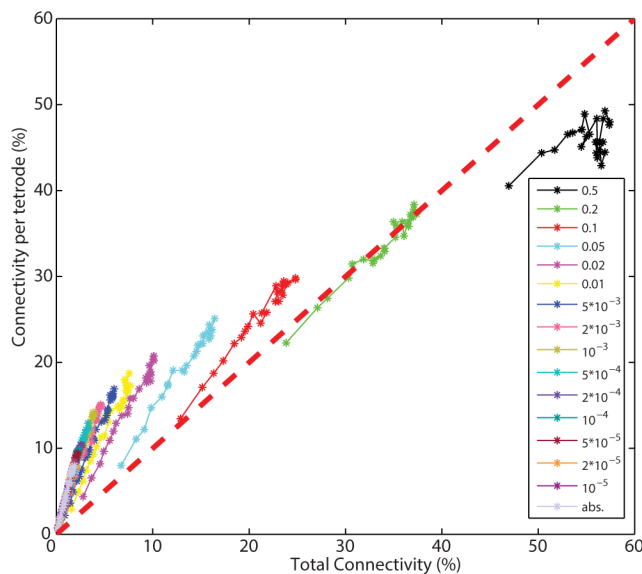


Figure 5.8 Number of excitatory connections per tetrode versus the total number of excitatory connections

The number of excitatory connections per tetrode (local connectivity, normalized with $N_{AUE \times TT}$) is plotted against the total number of excitatory connections (total connectivity, normalized with

N_{AllEx}) for all investigated α levels. The red diagonal dashed line indicates equal probability between local and total connectivity (including within and between tetrode connections). The detected connections are predominantly local.

Various types of excitatory connections are the most abundant in mPFC and their detection probability increases with sample size.

In addition to E-E interactions (EE1 and EE2), our 25-hour recordings also allowed us to investigate six additional connection categories (EI1, EI2, IE1, II1 and EU1 and IU1, see methods); Although, II2, reciprocal inhibition between putative inhibitory neurons, could be defined as well, we excluded this connection probability from our analysis because its cross-correlation cannot be easily distinguished from the case of common inhibitory input. The detection probabilities of connection categories involving excitatory neurons (EE1, EE2, EI1, EI2, IE1 and EU1) change with increased recording duration for two representative α levels (10^{-5} and abs., Figure 5.9). Note that the normalization by all recorded neuron pairs (N_{All}) was used because all neuron types (excitatory, inhibitory and unclassified) were included. We also found that EE1 (Figure 5.9b) and EU1 (Figure 5.9g) are the most abundant connection types followed by EE2 (Figure 5.9c), EI1 (Figure 5.9a) and EI2 (Figure 5.9d), suggesting that excitatory interactions are the major portion of cortical connections in rat prefrontal cortex. Inhibitory interactions, IE1 (Figure 5.9e), II1 (Figure 5.9f) and IU1 (Figure 5.9h), are detected much less frequently.

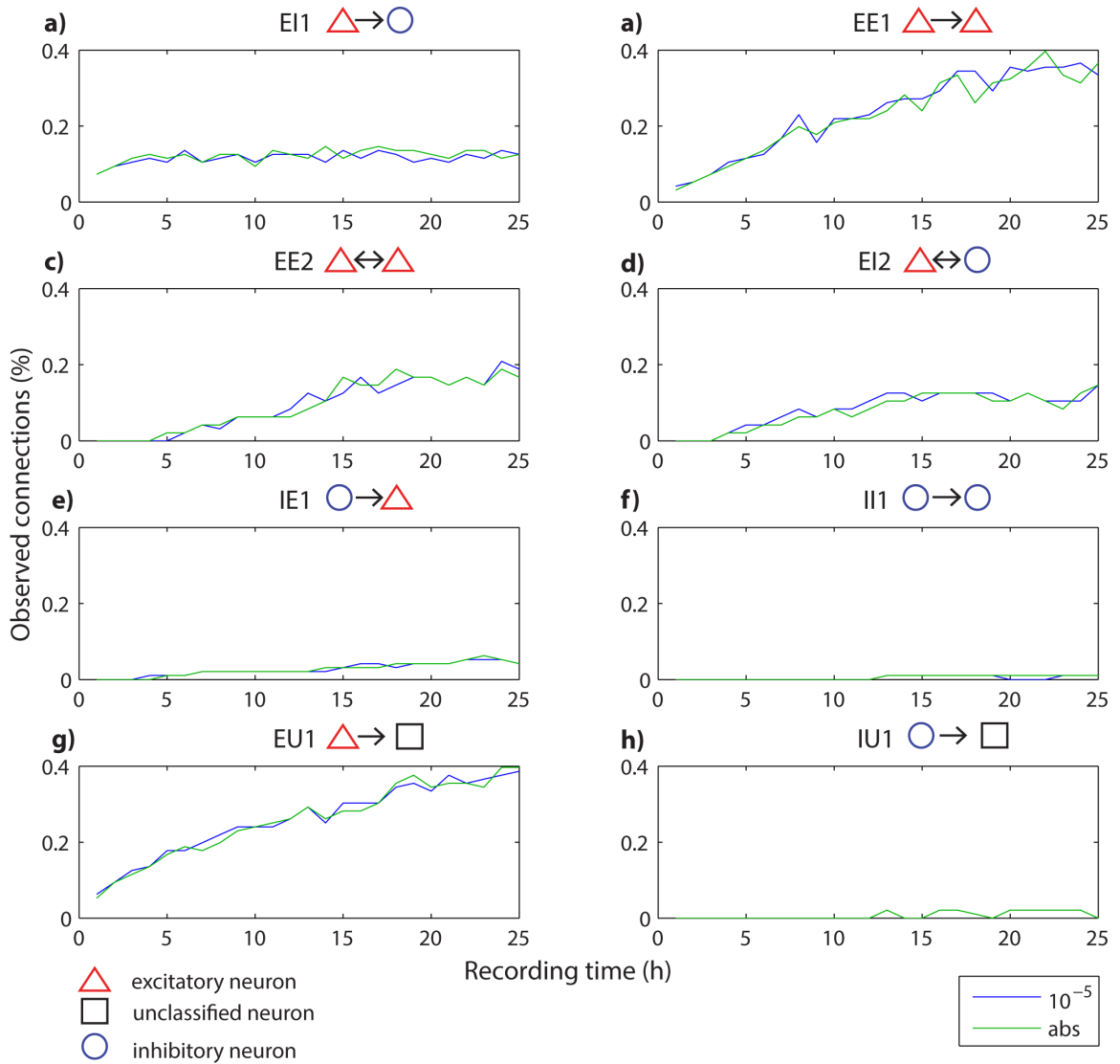


Figure 5.9 Detection probabilities over different hour segments for different categories of connection types

Significance thresholds ($\alpha 10^{-5}$ and abs) are color coded and indicated at the bottom right of the figure panel. The median of the bootstrapped detection probabilities, normalized by the total number of neuron pairs (4787) including excitatory, inhibitory and unclassified neurons for 1 to 25 hours are plotted for the two different significance thresholds for eight different types of connections: a) unidirectional excitation from an excitatory neuron onto an inhibitory neuron, E1; b) unidirectional excitation between two excitatory neurons, EE1; c) reciprocal excitation between excitatory neurons, EE2; d) reciprocal connection between an inhibitory and an excitatory neuron, EI2; e) unidirectional inhibition from an inhibitory neuron onto an excitatory neuron, IE1; f) unidirectional inhibition between two inhibitory neurons, II1; g) unidirectional excitation from an excitatory neuron onto an unclassified neuron, EU1; h) unidirectional inhibition from an inhibitory neuron onto an unclassified neuron, IU1. The most abundant

connection types in mPFC are excitatory connections (a-d, g). Their detection probability increases with longer recording times except for EI1, which seem to be already reliably detected at shorter recording times (a). Inhibitory connections are rarely detected in our data set and their detection probability does not improve significantly with longer recording times.

DISCUSSION

Pyramidal neurons are the most abundant cell type in neocortex. Pyramid-pyramid connections (E-E interactions) provide the majority of intracortical and extracortical projections. However, most E-E synapses are extremely weak (McNaughton, 1980; Mason et al., 1991; Deuchars et al., 1994; Markram et al., 1997; Thomson and Deuchars, 1997; Reyes and Sakmann, 1999; Thomson et al., 2002). With long-term continuous recordings, we tried to capture weak connections between pyramidal neurons. As opposed to most electrophysiological studies that generally record for about 0.5 - 2 hr per session, we were able to detect excitatory interactions between putative pyramidal cells in 8.5% of cell pairs with recording lengths up to 25 hours. This connection probability of 8.5%, estimated using the number of putative excitatory neuron pairs per tetrode, corresponds to approximately 70% of the local E-E connections reported in Song et al. (2005). As was discussed, this normalization is considered to be most comparable to Song et al. (2005). The smaller connection probability (2%) found for the total excitatory connectivity indicates that on average the connection probability falls off with distance (Song et al., 2005; Fujisawa et al., 2008). In addition, 1 hour fragments of our recordings yielded a consistent number of

monosynaptically coupled pairs (0.2% for strictest α levels: abs and 10^{-5} and 1.04% for α 0.01; counts were normalized using all recorded neuron pairs, Figure 5.9) to previously reported studies (0.2 - 0.8%; (Csicsvari et al., 1998; Bartho et al., 2004; Maurer et al., 2006b; Fujisawa et al., 2008).

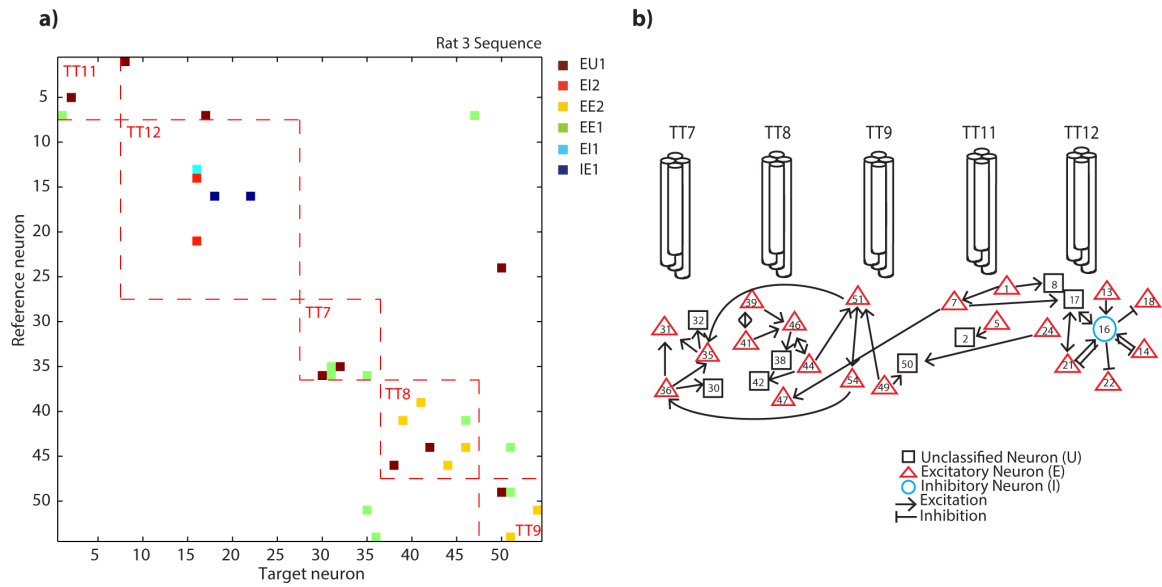


Figure 5.10 The cross correlogram matrix for all simultaneously recorded neurons

a) The cross correlogram matrix for all ($n=54$) simultaneously recorded neurons in one session (rat 3, sequence task). Red dashed lines indicate correlations between neurons recorded on the same tetrode. Different colors denote different types of connections (see figure legend for Figure 5.9) based on significant short-latency peaks or troughs in the cross correlogram at α abs.

(b) Schematic mapping of the connections in the cross correlogram matrix in a) between the neurons recorded on 5 different tetrodes. This animal had a ‘split bundle’ hyperdrive with 6 recording tetrodes targeting the hippocampus (not included in this paper) and 5 tetrodes targeting the medial prefrontal cortex (shown in b).

The strength of a pyramidal-pyramidal connection is partly determined by the location of the synapse and the type of receptors activated (Deuchars et al., 1994). For instance, since lateral connections between pyramidal neurons in cortex are predominantly on distal parts of the dendrites, they are weakened as the potential propagates towards the

soma. Those inputs are nearly only transferred if they coincide with other inputs (Deuchars et al., 1994). Therefore the E-E interactions detected by relatively short duration electrophysiological recordings are presumably the strongest ones. However, those are embedded in a much larger matrix of weak connections, which are difficult to capture with extracellular recordings that only detect action potential transmission. With regard to successful spike transmission, pyramidal – interneuron pairs have been shown to be more reliable (Mizumori et al., 1989; Marshall et al., 2002; Holmgren et al., 2003; Swadlow, 2003). Using a less stringent detection threshold such as 1%, as used in many previous studies, is therefore less likely to be severely affected by false-positives. A higher convergence of excitatory inputs among pyramidal neurons is necessary to bring a postsynaptic pyramidal neuron to firing threshold (McNaughton et al., 1981; Markram et al., 1997). In this respect, long-term recordings dramatically increased the detection probability of the statistically rare E-E events.

In Figure 5.5, we reported that most connections are local, i.e. both pre- and postsynaptic neurons are within the recording radius of a single tetrode. In the hippocampus, monosynaptically coupled pairs of pyramidal neurons and interneurons were also more frequently observed on the same tetrode than on different tetrodes (Csicsvari et al., 1998; Maurer et al., 2006b). Connection strength tends to cluster around a few neurons (Bartho et al., 2004; Song et al., 2005; Fujisawa et al., 2008), often referred to as hub neurons. We also observed that many connections converge onto a few neurons. The majority of detected connections are local (Figure 5.10a, Figure 5.11),

recorded on the same tetode (Figure 5.10a, red dashed lines). A schematic diagram created from Figure 5.10a also confirmed that there exists a hub neuron (Figure 5.10b, neuron #16). Its inhibitory property (a hub neuron is an inhibitory neuron) is consistent with previous studies (Bartho et al., 2004; Fujisawa et al., 2008).

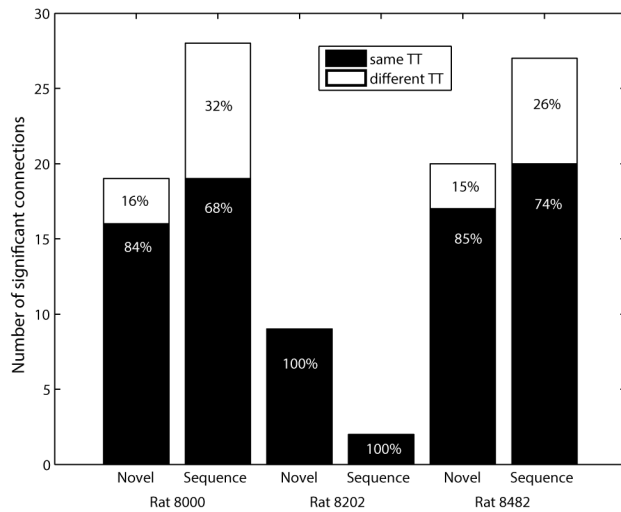


Figure 5.11 Summary of local and long-range connections per dataset

The number of significant excitatory connections within (same TT) and between (different TT) tetodes for the individual data sets for α abs. Numbers are given in absolute (y-axis) and percent (written on bars) values.

In this study, we showed that the detection probability of weak E-E connections can be significantly improved by long-term recordings (25 hours) due to the substantially improved signal to noise ratio reflected in smoother cross-correlation signals for 25 hours compared to 1 hour long recordings (Fig. 5.2). We were also able to detect the hyperreciprocity of excitatory connections in medial prefrontal cortex with our long-term extracellular recordings (Song et al., 2005; Wang et al., 2006) (Fig. 7). This strongly suggests that connectivity is not random, but highly structured. Despite the fact that

increased recording times improve the detection of connections among excitatory neurons, extracellular recordings still underestimate the local connectivity as is reported by paired intracellular recordings. At best, they identify about 70% of local excitatory connections at an α level that is strict enough to exclude most type I errors (Fig. 3). This limitation can be partly attributed to the fact that extracellular recordings in behaving and resting animals are bound to the brain state spaces visited over the duration of recordings, which the experimenter has only limited control over. In contrast, through direct stimulation of the presynaptic neuron, any subthreshold response in the postsynaptic neuron can be monitored in paired intracellular recordings. In addition, our analysis indicates that, in order to estimate reliably an asymptotic value for the local connectivity, stable recordings of at least 20-25 hours, ideally longer, have to be used. This can be a challenge under many experimental conditions. A further caveat of the correlation method is the fact that the nature of the measure is a correlation and therefore reflects synaptic interactions only indirectly. Consequently, the cross correlation analysis of extracellularly recorded spike trains should not be considered a definitive tool for estimating connectivity and should be used with caution. In spite of this caveat, the method can provide important preliminary information for within- and inter-regional circuit connectivity and changes in their connectivity due to experimental manipulations that may not be obtainable with other current methods.

The cross correlogram, like all other statistical methods, has limitations in terms of its applicability to the interference of causal interactions from spike-train data. Firstly,

the method assumes that the spike trains are stationary, meaning that their stochastic properties do not change over time. This assumption is not always easy to justify; for example, with repeated stimulus presentations neurons tend to adapt their responses (Fairhall et al., 2001). Secondly, cross correlations are affected by firing rate differences between the neurons (de la Rocha et al., 2007; Amari, 2009). Appropriate normalization, however, can alleviate this problem (Hirase et al., 2001). It has been proposed that the information-geometric measure could be an alternative correlation measure that is statistically orthogonal to the change of firing probability (Amari and Nagaoka, 2000; Amari, 2001). In addition, recent theoretical studies show that an information-geometric measure could be more directly related to synaptic interactions (Tatsuno and Okada, 2004; Tatsuno et al., 2009; Nie and Tatsuno, 2012) and that it can be applied to non-stationary data (Shimazaki et al., 2012). Other promising methods would include a Bayesian approach (Brown et al., 2004; Eldawlatly et al., 2010) and a regularized logistic approach (Zhao et al., 2012). These measures may perform well in identifying causal, non-linear relationships between neurons. Further investigation of long-term electrophysiological data by such statistical methods would promote the detection of neural interaction and hence contribute to the understanding of the circuit dynamics underlying complex behavior.

Author contributions: B.L. McNaughton conceived the project. C.D. Schwindel, M. Tatsuno, and K. Ali analyzed the data. M. Tatsuno conducted the experiments. C.D. Schwindel, M. Tatsuno and B.L. McNaughton wrote the manuscript.

Acknowledgements: We thank Francesco Battaglia for helpful comments on a previous version of the manuscript. This work was funded by an Alberta Innovates Health Solutions Polaris Award and National Institute of Mental Health R01MH46823-16 grant awarded to B.L. McNaughton, an Innovates Centre of Research Excellence SCH001 grant awarded to M. Tatsuno and an AIHS graduate fellowship awarded to C.D. Schwindel. The funders had no role in study design, data collection and analysis, decision to publish, or preparation of the manuscript.

Chapter 6 General Discussion

SUMMARY

The hippocampus as a main player in episodic memory formation has been described as a structure that forms a conjunctive representation for space and context. Earlier studies however, suggested that the contextual component might not actually be stored in an associatively retrievable form. Here it was shown that the contextual component of the code is learned through experience and can be retrieved in subsequent sleep. The spatial component is thought to be determined by intrinsic dynamics, such as path integration, in a specially configured network for generating a coordinate representation. The combined hippocampal output pattern can be understood as an index code that is stored in distributed neocortical modules and can be used to retrieve different memory attributes stored there. Through coordinated reactivation of neurons in different cortical columns, the connectivity matrix in the cortex can be modified to optimize storage capacity. However, in *chapter 5*, the challenges of measuring the excitatory connectivity matrix from extracellular spike train correlations was shown. The difficulty is due to the inherent weakness of excitatory connections in neocortex. This hurdle was to some degree overcome by using long sampling times (25 hours), but this places a serious limit on the temporal resolution over

which plastic changes might be assessed with these methods, and, moreover, achieving stability over such long recording times is technically difficult.

DISCUSSION

It is generally accepted that the hippocampus contributes to the encoding and retrieval of episodic memory. However, how the hippocampus fulfills this role is still poorly understood. A large body of evidence supports the notion that the hippocampus forms spatial maps for different environments in a retrievable manner. However, little is known as to whether the hippocampus can retrieve different events associated with identical spatial information, which is a critical feature for episodic memory.

Understanding rate remapping in the context of attractor dynamics

Area CA3 has often been proposed to act as an autoassociator network (Marr, 1971; McNaughton and Morris, 1987; Treves, 1990; Treves and Rolls, 1992), which creates representations by binding together external input features through hebbian connections to form discrete attractors representing the collective of stimulus features (Hopfield, 1982; Amit and Treves, 1989). A degraded or fractionated version of the stored pattern can then be sufficient to retrieve associatively the entire pattern (referred to as pattern completion or error correction) (Hopfield, 1982). In a recent study, Colgin et al. (2010) tried to understand why it is that in some cases attractor dynamics (i.e., abrupt transitions between network states) are observed in the output of

CA3 and in other cases not. To address this issue, two familiar representations were morphed successively over a series of intermediate shapes (Leutgeb et al., 2005a). Two groups of animals were familiarized with the end shapes according to two training paradigms. The critical difference between the two training regimes was that, in one scenario, the end shapes (square and circle) were acquired at a common spatial location, and in the other, they were acquired in different spatial locations. The general autoassociation theory predicts attractor dynamics during the morph sequence in both cases. According to the attractor-map theory, the cue configuration in the first training paradigm should be associated with identical path integrator coordinates, while in the latter the cue configuration should be associated with different path integrator coordinates. In the common location training, gradual transitions were observed, suggesting that contextual cues are insufficient for associative recall. Attractor dynamics were only observed when the end shapes were associated originally with different spatial coordinates, indicating that differences in spatial input are necessary for associative retrieval of the two maps. From this study, it was concluded that the attractor dynamics observed in the hippocampus do not result from hebbian associations between external input features within the hippocampus (CA3) that form discrete attractors, but rather from a continuous attractor network upstream in the medial entorhinal cortex onto which landmark features can be linked (McNaughton et al., 2006). The assumption that a continuous path integration system rather than cue configurations are determinant of hippocampal spatial maps was already based on data

from previous studies that show the persistence of place fields against cue removal (O'Keefe and Speakman, 1987) and in darkness (Quirk et al., 1990; Markus et al., 1994), or the realignment of fields following conflicting configurations of vestibular and visual cues (Knierim et al., 1998). Coherent realignment in grid fields with simultaneous global remapping in CA3 between representations associated with light and dark (Fyhn et al., 2007), but no change in the grid population response during rate remapping, further strengthened the support for the attractor-map based theory of path integration. Grid cells show the same grid phase and orientation relative to landmarks independent of the animal's starting position (Hafting et al., 2005). Once external cues have been anchored to path integrator coordinates, they can exert strong control over which representation is retrieved without active locomotion of the animal between the two environments (Wills et al., 2005; Colgin et al., 2010; Jezek et al., 2011). Such linking between spatial and contextual information could take place in the hippocampus (Rolls et al., 2002; McNaughton et al., 2006; Solstad et al., 2014). However, it is not clear whether the rate distributions that differentiate cue configurations within constant maps (i.e., rate remapping) are stored and retrieved within CA3 or whether they are reinstated during behavior due to external input from e.g., lateral entorhinal input (Lu et al., 2013). In *chapter 4*, I addressed the question whether the rate distributions for different running directions with identical spatial information are reactivated in sleep when external input is largely absent. The presented results clearly indicate that the firing rate distribution during sharp wave ripple complexes is explained significantly better by the preceding

running direction than by the following and not yet experienced running direction on the respective recording day. Significant rate differences are observed on the track already on the first day; however, the differences become more pronounced on subsequent days. This implies that rate remapping develops with increasing experience within the first day, which has also been demonstrated in *chapter 3*. Similarly, the firing rates during sharp wave ripple complexes are better correlated with the firing rates during the preceding run session than with the ones in the following run session on days 2-5. This suggests that the active group of CA3 cells reinstates the firing rate distribution associated with the experienced context.

A proposed mechanism could be as follows. An initially generic, non-directional map is created for the space, based on path integrator input from medial entorhinal cortex. Upon repeated traversing through the space in opposite directions, a different distribution of synaptic input from lateral entorhinal cortex in response to the two different contexts/cue configurations associated with the two directions drives the firing rates of CA3 cells within their place fields up and down. Fewer local cues on the track will make the “local view” more different. This results likely in more heterogeneous lateral entorhinal cortex input in the two directions and increased directionality of the hippocampal place fields (Battaglia et al., 2004a). Upon repeated activation of place cells, the synaptic weights at the LEC-CA3 (and possibly LEC and DG) synapses are adjusted and eventually could activate the map based on the cue configuration. In addition, sequential activation of CA3 neurons will lead to plasticity between neurons

with neighboring fields at the recurrent collaterals and adjust the synaptic weights. The two firing rate distributions are thought to be stored associatively within CA3 that could form discrete context attractors within a continuous spatial attractor framework (Renno-Costa et al., 2014; Solstad et al., 2014). Solstad et al. (2014) constructed a model that could achieve the experimentally observed population and single cell responses in the morphing experiment (Leutgeb et al., 2005a; Colgin et al., 2010) during rate remapping. They demonstrate that a recurrent system such as CA3 can exhibit a smooth transition as averaged population response along the morph sequence and yet show hysteresis and abrupt transitions in individual cell responses, typical for discrete attractor states. This model reconciles that CA3 acts as an autoassociative network, forming discrete attractor states for context, but does so within a continuum of spatial attractors, likely located in MEC. Thus, rate remapping can be understood as switching between context attractors within a single spatial map. This enables the network to use maps flexibly and update them rapidly on a one-trial basis (Monaco et al., 2014) without affecting members of different maps encoding remote locations as has been reported in cases when short cuts or local barriers were introduced (Muller and Kubie, 1987; Alvernhe et al., 2008; Alvernhe et al., 2011).

Is there simultaneous reactivation of multiple episodic events encoded through rate remapping?

An interesting follow up question on the presented result is whether multiple events anchored to the same spatial map can be retrieved at the same time or whether the most recent entry overwrites the previous one. With the data at hand, I could explore potentially whether two memories (context A and B, with context referring to as running direction) can coexist in the synaptic network of CA3. Hippocampal ensembles are organized on a theta time scale (phase precession/sequence compression) during behavior. A theta cycle matches approximately the duration of a sharp wave ripple complex, in which place cell sequences are faithfully expressed during reactivation in sleep (Skaggs and McNaughton, 1996; Nadasdy et al., 1999; Lee and Wilson, 2002; Ji and Wilson, 2007). First, hippocampal activity could be parsed into theta cycles in both running directions. Each theta cycle would constitute a number of cells (N) x number of bins (T) matrix (NxT). Similarly, place cell activity during sleep sessions could be parsed into sharp wave ripple complexes, creating NxT matrices for each sharp wave ripple complex. The sharp wave ripple complexes of a sleep session (e.g., the last sleep session in the day that occurs after both running directions have been experienced twice) could then be used as templates and 'moved' along the theta cycles of each running direction to find the best match (i.e., highest correlation value between sharp wave ripple matrix and theta cycle matrix) according to a template matching procedure (Tatsuno et al., 2006; Euston et al., 2007). The distributions of best matches of sharp wave ripple

complexes with session A and with session B could be compared and tested whether they are significantly different. However, there may be a large number of sharp wave ripple complexes that are unrelated to A and B.

Alternatively, a classification approach such as the k-nearest neighbor classification algorithm could be applied (Cover and Hart, 1967). In this analysis, each sharp wave ripple complex would be assigned to the category of its nearest neighbor or the majority vote of k nearest neighbors based on a distance metric (e.g., Mahalanobis distance). Three categories could be defined. Sharp wave ripple complexes that are 'close' to theta cycles in A or B could define the first two categories. The last category would contain all sharp wave ripple complexes that are neither close to context A nor B. Those sharp wave ripple complexes are presumably replaying a different event. This type of analysis could reveal whether, within one sharp wave ripple complex, one context representation dominates reactivation as is the case in theta cycles in which information about only one environment is expressed (Jezek et al., 2011). Future experiments could address the capacity of the network by exposing the animal to a number of different contexts and test how many episodic memories can be unambiguously retrieved within a common spatial map. A difficulty with all these analyses is the extreme sparsity of the CA3 output (i.e., very few cells are active over the time frame of a theta cycle or a sharp-wave ripple). With even ~100 simultaneously recorded neurons, observing even 2-3 neurons coactive within a sharp-wave ripple is

rare. This makes vector matching very noisy. Perhaps when we are able to record from >100 neurons, these problems may be alleviated.

CONCLUSION

The reactivation of the rate distribution in the hippocampus supports the notion that reactivation processes play a role in memory formation and consolidation. One function of CA3 may be to encode indices to access distributed data stored in the cortex and assist in episodic recall. It remains to be explored whether multiple episodic events linked to the same place can coexist in the network at the same time or whether the most recent representation erases the previous one.

References

- Abraham WC, and Goddard GV (1983) Asymmetric relationships between homosynaptic long-term potentiation and heterosynaptic long-term depression. *Nature* 305:717-719.
- Acsady L, Kamondi A, Sik A, Freund T, and Buzsaki G (1998) GABAergic cells are the major postsynaptic targets of mossy fibers in the rat hippocampus. *J Neurosci* 18:3386-3403.
- Aertsen AM, and Gerstein GL (1985) Evaluation of neuronal connectivity: sensitivity of cross-correlation. *Brain Res* 340:341-354.
- Allen K, Rawlins JN, Bannerman DM, and Csicsvari J (2012) Hippocampal place cells can encode multiple trial-dependent features through rate remapping. *J Neurosci* 32:14752-14766.
- Alme CB, Buzzetti RA, Marrone DF, Leutgeb JK, Chawla MK, Schaner MJ, Bohanick JD, Khoboko T, Leutgeb S, Moser EI, Moser MB, McNaughton BL, and Barnes CA (2010) Hippocampal granule cells opt for early retirement. *Hippocampus* 20:1109-1123.
- Alme CB, Buzzetti RA, Marrone DF, Leutgeb JK, Chawla MK, Schaner MJ, Bohanick JD, Khoboko T, Leutgeb S, Moser EI, Moser MB, McNaughton BL, and Barnes CA (2010) Hippocampal granule cells opt for early retirement. *Hippocampus* 20:1109-1123.
- Alonso JM, and Martinez LM (1998) Functional connectivity between simple cells and complex cells in cat striate cortex. *Nat Neurosci* 1:395-403.
- Alvernhe A, Van Cauter T, Save E, and Poucet B (2008) Different CA1 and CA3 representations of novel routes in a shortcut situation. *J Neurosci* 28:7324-7333.
- Alvernhe A, Save E, and Poucet B (2011) Local remapping of place cell firing in the Tolman detour task. *Eur J Neurosci* 33:1696-1705.

- Amaral D, and Lavenex P (2007) Hippocampal neuroanatomy. . In P. Andersen, R. Morris, D. Amaral, T. Bliss, & J. O'Keefe (Eds.), The hippocampus book. New York: Oxford University Press, Inc. 37-114.
- Amari S (2009) Measure of correlation orthogonal to change in firing rate. *Neural Comput* 21:960-972.
- Amari Si, and Nagaoka H (2000) *Methods of information geometry*. Editor: American Mathematical Society.
- Amari Si (2001) Information geometry on hierarchy of probability distributions. *IEEE Transactions on Information Theory* 47:1701-1711.
- Amit DJ (1989) *Modeling Brain Function: The World of Attractor Neural Networks*. . New York: Cambridge UP.
- Amit DJ, and Treves A (1989) Associative memory neural network with low temporal spiking rates. *Proc Natl Acad Sci U S A* 86:7871-7875.
- Andersen P, Bliss TV, and Skrede KK (1971) Lamellar organization of hippocampal pathways. *Exp Brain Res* 13:222-238.
- Anderson MI, and Jeffery KJ (2003) Heterogeneous modulation of place cell firing by changes in context. *J Neurosci* 23:8827-8835.
- Barnes CA, McNaughton BL, Mizumori SJ, Leonard BW, and Lin LH (1990) Comparison of spatial and temporal characteristics of neuronal activity in sequential stages of hippocampal processing. *Prog Brain Res* 83:287-300.
- Barnes CA, Suster MS, Shen J, and McNaughton BL (1997) Multistability of cognitive maps in the hippocampus of old rats. *Nature* 388:272-275.
- Bartho P, Hirase H, Monconduit L, Zugaro M, Harris KD, and Buzsaki G (2004) Characterization of neocortical principal cells and interneurons by network interactions and extracellular features. *J Neurophysiol* 92:600-608.
- Battaglia FP, Sutherland GR, and McNaughton BL (2004a) Local sensory cues and place cell directionality: additional evidence of prospective coding in the hippocampus. *J Neurosci* 24:4541-4550.
- Battaglia FP, Sutherland GR, and McNaughton BL (2004b) Hippocampal sharp wave bursts coincide with neocortical "up-state" transitions. *Learn Mem* 11:697-704.

- Battaglia FP, Sutherland GR, Cowen SL, Mc Naughton BL, and Harris KD (2005) Firing rate modulation: a simple statistical view of memory trace reactivation. *Neural Netw* 18:1280-1291.
- Berke JD, Breck JT, and Eichenbaum H (2009) Striatal versus hippocampal representations during win-stay maze performance. *J Neurophysiol* 101:1575-1587.
- Bliss TV, and Gardner-Medwin AR (1973) Long-lasting potentiation of synaptic transmission in the dentate area of the unanaesthetized rabbit following stimulation of the perforant path. *J Physiol* 232:357-374.
- Bliss TV, and Lømo T (1973) Long-lasting potentiation of synaptic transmission in the dentate area of the anaesthetized rabbit following stimulation of the perforant path. *J Physiol* 232:331-356.
- Bock DD, Lee WC, Kerlin AM, Andermann ML, Hood G, Wetzel AW, Yurgenson S, Soucy ER, Kim HS, and Reid RC (2011) Network anatomy and in vivo physiology of visual cortical neurons. *Nature* 471:177-182.
- Bower MR, Euston DR, and McNaughton BL (2005) Sequential-context-dependent hippocampal activity is not necessary to learn sequences with repeated elements. *J Neurosci* 25:1313-1323.
- Brandon MP, Bogaard AR, Libby CP, Connerney MA, Gupta K, and Hasselmo ME (2011) Reduction of theta rhythm dissociates grid cell spatial periodicity from directional tuning. *Science* 332:595-599.
- Brown EN, Kass RE, and Mitra PP (2004) Multiple neural spike train data analysis: state-of-the-art and future challenges. *Nat Neurosci* 7:456-461.
- Burke SN, Chawla MK, Penner MR, Crowell BE, Worley PF, Barnes CA, and McNaughton BL (2005) Differential encoding of behavior and spatial context in deep and superficial layers of the neocortex. *Neuron* 45:667-674.
- Burwell RD, and Amaral DG (1998) Cortical afferents of the perirhinal, postrhinal, and entorhinal cortices of the rat. *J Comp Neurol* 398:179-205.
- Buzsaki G (1986) Hippocampal sharp waves: their origin and significance. *Brain Res* 398:242-252.

- Buzsaki G, Horvath Z, Urioste R, Hetke J, and Wise K (1992) High-frequency network oscillation in the hippocampus. *Science* 256:1025-1027.
- Buzsaki G (2004) Large-scale recording of neuronal ensembles. *Nat Neurosci* 7:446-451.
- Clark RE, Broadbent NJ, Zola SM, and Squire LR (2002) Anterograde amnesia and temporally graded retrograde amnesia for a nonspatial memory task after lesions of hippocampus and subiculum. *J Neurosci* 22:4663-4669.
- Cohen MR, and Kohn A (2011) Measuring and interpreting neuronal correlations. *Nat Neurosci* 14:811-819.
- Colgin LL, Moser EI, and Moser MB (2008) Understanding memory through hippocampal remapping. *Trends Neurosci* 31:469-477.
- Colgin LL, Leutgeb S, Jezek K, Leutgeb JK, Moser EI, McNaughton BL, and Moser MB (2010) Attractor-map versus autoassociation based attractor dynamics in the hippocampal network. *J Neurophysiol* 104:35-50.
- Cover T, and Hart P (1967) Nearest neighbor pattern classification. *Information Theory, IEEE Transactions on.* 13:21-27.
- Csicsvari J, Hirase H, Czurko A, and Buzsaki G (1998) Reliability and state dependence of pyramidal cell-interneuron synapses in the hippocampus: an ensemble approach in the behaving rat. *Neuron* 21:179-189.
- Csicsvari J, Hirase H, Mamiya A, and Buzsaki G (2000) Ensemble patterns of hippocampal CA3-CA1 neurons during sharp wave-associated population events. *Neuron* 28:585-594.
- Csicsvari J, Henze DA, Jamieson B, Harris KD, Sirota A, Bartho P, Wise KD, and Buzsaki G (2003a) Massively parallel recording of unit and local field potentials with silicon-based electrodes. *J Neurophysiol* 90:1314-1323.
- Csicsvari J, Jamieson B, Wise KD, and Buzsaki G (2003b) Mechanisms of gamma oscillations in the hippocampus of the behaving rat. *Neuron* 37:311-322.
- Davidson TJ, Kloosterman F, and Wilson MA (2009) Hippocampal replay of extended experience. *Neuron* 63:497-507.
- de la Rocha J, Doiron B, Shea-Brown E, Josic K, and Reyes A (2007) Correlation between neural spike trains increases with firing rate. *Nature* 448:802-806.

- Derdikman D, Whitlock JR, Tsao A, Fyhn M, Hafting T, Moser MB, and Moser EI (2009) Fragmentation of grid cell maps in a multicompartiment environment. *Nat Neurosci* 12:1325-1332.
- Deshmukh SS, and Knierim JJ (2011) Representation of non-spatial and spatial information in the lateral entorhinal cortex. *Front Behav Neurosci* 5:69.
- Deuchars J, West DC, and Thomson AM (1994) Relationships between morphology and physiology of pyramid-pyramid single axon connections in rat neocortex in vitro. *J Physiol* 478 Pt 3:423-435.
- Diekelmann S, and Born J (2010) The memory function of sleep. *Nat Rev Neurosci* 11:114-126.
- Dragoi G, and Buzsaki G (2006) Temporal encoding of place sequences by hippocampal cell assemblies. *Neuron* 50:145-157.
- Dragoi G (2013) Internal operations in the hippocampus: single cell and ensemble temporal coding. *Front Syst Neurosci* 7:46.
- Dupret D, O'Neill J, Pleydell-Bouverie B, and Csicsvari J (2010) The reorganization and reactivation of hippocampal maps predict spatial memory performance. *Nat Neurosci* 13:995-1002.
- Ego-Stengel V, and Wilson MA (2010) Disruption of ripple-associated hippocampal activity during rest impairs spatial learning in the rat. *Hippocampus* 20:1-10.
- Eichenbaum H, Dudchenko P, Wood E, Shapiro M, and Tanila H (1999) The hippocampus, memory, and place cells: is it spatial memory or a memory space? *Neuron* 23:209-226.
- Ekstrom AD, Meltzer J, McNaughton BL, and Barnes CA (2001) NMDA receptor antagonism blocks experience-dependent expansion of hippocampal "place fields". *Neuron* 31:631-638.
- Ekstrom AD, Kahana MJ, Caplan JB, Fields TA, Isham EA, Newman EL, and Fried I (2003) Cellular networks underlying human spatial navigation. *Nature* 425:184-188.
- Eldawlatly S, Zhou Y, Jin R, and Oweiss KG (2010) On the use of dynamic Bayesian networks in reconstructing functional neuronal networks from spike train ensembles. *Neural Comput* 22:158-189.

- Euston DR, Tatsuno M, and McNaughton BL (2007) Fast-forward playback of recent memory sequences in prefrontal cortex during sleep. *Science* 318:1147-1150.
- Euston DR, Tatsuno M, and McNaughton BL (2008) Prefrontal cortex leads hippocampus during reactivation of spike coincidences in sleep following performance of a well learned task: Further evidence for an orchestrating role of mPFC in retrieval of consolidated memory. *SfN Abstracts* 391.20
- Fairhall AL, Lewen GD, Bialek W, and de Ruyter Van Steveninck RR (2001) Efficiency and ambiguity in an adaptive neural code. *Nature* 412:787-792.
- Frank LM, Brown EN, and Wilson M (2000) Trajectory encoding in the hippocampus and entorhinal cortex. *Neuron* 27:169-178.
- Fuhs MC, Vanrhoads SR, Casale AE, McNaughton B, and Touretzky DS (2005) Influence of path integration versus environmental orientation on place cell remapping between visually identical environments. *J Neurophysiol* 94:2603-2616.
- Fuhs MC, and Touretzky DS (2006) A spin glass model of path integration in rat medial entorhinal cortex. *J Neurosci* 26:4266-4276.
- Fujisawa S, Amarasingham A, Harrison MT, and Buzsaki G (2008) Behavior-dependent short-term assembly dynamics in the medial prefrontal cortex. *Nat Neurosci* 11:823-833.
- Fyhn M, Molden S, Witter MP, Moser EI, and Moser MB (2004) Spatial representation in the entorhinal cortex. *Science* 305:1258-1264.
- Fyhn M, Hafting T, Treves A, Moser MB, and Moser EI (2007) Hippocampal remapping and grid realignment in entorhinal cortex. *Nature* 446:190-194.
- Gerrard JL, Burke SN, McNaughton BL, and Barnes CA (2008) Sequence reactivation in the hippocampus is impaired in aged rats. *J Neurosci* 28:7883-7890.
- Giocomo LM, Stensola T, Bonnevie T, Van Cauter T, Moser MB, and Moser EI (2014) Topography of head direction cells in medial entorhinal cortex. *Curr Biol* 24:252-262.
- Girardeau G, Benchenane K, Wiener SI, Buzsaki G, and Zugaro MB (2009) Selective suppression of hippocampal ripples impairs spatial memory. *Nat Neurosci* 12:1222-1223.

- Gothard KM, Skaggs WE, and McNaughton BL (1996) Dynamics of mismatch correction in the hippocampal ensemble code for space: interaction between path integration and environmental cues. *J Neurosci* 16:8027-8040.
- Guzowski JF, McNaughton BL, Barnes CA, and Worley PF (1999) Environment-specific expression of the immediate-early gene *Arc* in hippocampal neuronal ensembles. *Nat Neurosci* 2:1120-1124.
- Hafting T, Fyhn M, Molden S, Moser MB, and Moser EI (2005) Microstructure of a spatial map in the entorhinal cortex. *Nature* 436:801-806.
- Hargreaves EL, Rao G, Lee I, and Knierim JJ (2005) Major dissociation between medial and lateral entorhinal input to dorsal hippocampus. *Science* 308:1792-1794.
- Harris KD, Csicsvari J, Hirase H, Dragoi G, and Buzsaki G (2003) Organization of cell assemblies in the hippocampus. *Nature* 424:552-556.
- Hebb DO (1949) *The organization of behavior: a neuropsychological theory*. Editor: Wiley.
- Henze DA, Urban NN, and Barrionuevo G (2000) The multifarious hippocampal mossy fiber pathway: a review. *Neuroscience* 98:407-427.
- Henze DA, Wittner L, and Buzsaki G (2002) Single granule cells reliably discharge targets in the hippocampal CA3 network in vivo. *Nat Neurosci* 5:790-795.
- Hetherington PA, and Shapiro ML (1997) Hippocampal place fields are altered by the removal of single visual cues in a distance-dependent manner. *Behav Neurosci* 111:20-34.
- Hirabayashi T, Takeuchi D, Tamura K, and Miyashita Y (2013) Microcircuits for hierarchical elaboration of object coding across primate temporal areas. *Science* 341:191-195.
- Hirase H, Leinekugel X, Csicsvari J, Czurko A, and Buzsaki G (2001) Behavior-dependent states of the hippocampal network affect functional clustering of neurons. *J Neurosci* 21:RC145.
- Hoffman KL, and McNaughton BL (2002) Coordinated reactivation of distributed memory traces in primate neocortex. *Science* 297:2070-2073.

- Holmgren C, Harkany T, Svennenfors B, and Zilberter Y (2003) Pyramidal cell communication within local networks in layer 2/3 of rat neocortex. *J Physiol* 551:139-153.
- Hopfield JJ (1982) Neural networks and physical systems with emergent collective computational abilities. *Proc Natl Acad Sci U S A* 79:2554-2558.
- Hori E, Tabuchi E, Matsumura N, Tamura R, Eifuku S, Endo S, Nishijo H, and Ono T (2003) Representation of place by monkey hippocampal neurons in real and virtual translocation. *Hippocampus* 13:190-196.
- Huxter J, Burgess N, and O'Keefe J (2003) Independent rate and temporal coding in hippocampal pyramidal cells. *Nature* 425:828-832.
- Insausti R, Herrero MT, and Witter MP (1997) Entorhinal cortex of the rat: cytoarchitectonic subdivisions and the origin and distribution of cortical efferents. *Hippocampus* 7:146-183.
- Jeffery KJ, Gilbert A, Burton S, and Strudwick A (2003) Preserved performance in a hippocampal-dependent spatial task despite complete place cell remapping. *Hippocampus* 13:175-189.
- Jezek K, Henriksen EJ, Treves A, Moser EI, and Moser MB (2011) Theta-paced flickering between place-cell maps in the hippocampus. *Nature* 478:246-249.
- Ji D, and Wilson MA (2007) Coordinated memory replay in the visual cortex and hippocampus during sleep. *Nat Neurosci* 10:100-107.
- Johnson LA, Euston DR, Tatsuno M, and McNaughton BL (2010) Stored-trace reactivation in rat prefrontal cortex is correlated with down-to-up state fluctuation density. *J Neurosci* 30:2650-2661.
- Jouvet M (1969) Biogenic amines and the states of sleep. *Science* 163:32-41.
- Jung MW, Wiener SI, and McNaughton BL (1994) Comparison of spatial firing characteristics of units in dorsal and ventral hippocampus of the rat. *J Neurosci* 14:7347-7356.
- Karlsson MP, and Frank LM (2009) Awake replay of remote experiences in the hippocampus. *Nat Neurosci* 12:913-918.

- Kentros C, Hargreaves E, Hawkins RD, Kandel ER, Shapiro M, and Muller RV (1998) Abolition of long-term stability of new hippocampal place cell maps by NMDA receptor blockade. *Science* 280:2121-2126.
- Kirkpatrick S, Gelatt CD, Jr., and Vecchi MP (1983) Optimization by simulated annealing. *Science* 220:671-680.
- Kirkwood PA (1979) On the use and interpretation of cross-correlations measurements in the mammalian central nervous system. *J Neurosci Methods* 1:107-132.
- Kjelstrup KB, Solstad T, Brun VH, Hafting T, Leutgeb S, Witter MP, Moser EI, and Moser MB (2008) Finite scale of spatial representation in the hippocampus. *Science* 321:140-143.
- Knierim JJ, Kudrimoti HS, and McNaughton BL (1998) Interactions between idiothetic cues and external landmarks in the control of place cells and head direction cells. *J Neurophysiol* 80:425-446.
- Knierim JJ, Neunuebel JP, and Deshmukh SS (2014) Functional correlates of the lateral and medial entorhinal cortex: objects, path integration and local-global reference frames. *Philos Trans R Soc Lond B Biol Sci* 369:20130369.
- Ko H, Hofer SB, Pichler B, Buchanan KA, Sjostrom PJ, and Mrcic-Flogel TD (2011) Functional specificity of local synaptic connections in neocortical networks. *Nature* 473:87-91.
- Koenig J, Linder AN, Leutgeb JK, and Leutgeb S (2011) The spatial periodicity of grid cells is not sustained during reduced theta oscillations. *Science* 332:592-595.
- Kudrimoti HS, Barnes CA, and McNaughton BL (1999) Reactivation of hippocampal cell assemblies: effects of behavioral state, experience, and EEG dynamics. *J Neurosci* 19:4090-4101.
- Lansink CS, Goltstein PM, Lankelma JV, Joosten RN, McNaughton BL, and Pennartz CM (2008) Preferential reactivation of motivationally relevant information in the ventral striatum. *J Neurosci* 28:6372-6382.
- Lansink CS, Goltstein PM, Lankelma JV, McNaughton BL, and Pennartz CM (2009) Hippocampus leads ventral striatum in replay of place-reward information. *PLoS Biol* 7:e1000173.

- Le Duigou C, Simonnet J, Telenczuk MT, Fricker D, and Miles R (2014) Recurrent synapses and circuits in the CA3 region of the hippocampus: an associative network. *Front Cell Neurosci* 7:262.
- Lechner HA, Squire LR, and Byrne JH (1999) 100 years of consolidation--remembering Muller and Pilzecker. *Learn Mem* 6:77-87.
- Lee AK, and Wilson MA (2002) Memory of sequential experience in the hippocampus during slow wave sleep. *Neuron* 36:1183-1194.
- Lee I, Rao G, and Knierim JJ (2004) A double dissociation between hippocampal subfields: differential time course of CA3 and CA1 place cells for processing changed environments. *Neuron* 42:803-815.
- Leger JF, Stern EA, Aertsen A, and Heck D (2005) Synaptic integration in rat frontal cortex shaped by network activity. *J Neurophysiol* 93:281-293.
- Lenck-Santini PP, Save E, and Poucet B (2001) Place-cell firing does not depend on the direction of turn in a Y-maze alternation task. *Eur J Neurosci* 13:1055-1058.
- Leutgeb JK, Leutgeb S, Treves A, Meyer R, Barnes CA, McNaughton BL, Moser MB, and Moser EI (2005a) Progressive transformation of hippocampal neuronal representations in "morphed" environments. *Neuron* 48:345-358.
- Leutgeb JK, Leutgeb S, Moser MB, and Moser EI (2007) Pattern separation in the dentate gyrus and CA3 of the hippocampus. *Science* 315:961-966.
- Leutgeb JK, and Moser EI (2007) Enigmas of the dentate gyrus. *Neuron* 55:176-178.
- Leutgeb S, Leutgeb JK, Treves A, Moser MB, and Moser EI (2004) Distinct ensemble codes in hippocampal areas CA3 and CA1. *Science* 305:1295-1298.
- Leutgeb S, Leutgeb JK, Barnes CA, Moser EI, McNaughton BL, and Moser MB (2005b) Independent codes for spatial and episodic memory in hippocampal neuronal ensembles. *Science* 309:619-623.
- Leutgeb S, Leutgeb JK, Moser EI, and Moser MB (2006) Fast rate coding in hippocampal CA3 cell ensembles. *Hippocampus* 16:765-774.
- Louie K, and Wilson MA (2001) Temporally structured replay of awake hippocampal ensemble activity during rapid eye movement sleep. *Neuron* 29:145-156.

- Lu L, Leutgeb JK, Tsao A, Henriksen EJ, Leutgeb S, Barnes CA, Witter MP, Moser MB, and Moser EI (2013) Impaired hippocampal rate coding after lesions of the lateral entorhinal cortex. *Nat Neurosci* 16:1085-1093.
- Magee JC, and Johnston D (1997) A synaptically controlled, associative signal for Hebbian plasticity in hippocampal neurons. *Science* 275:209-213.
- Markram H, Lubke J, Frotscher M, Roth A, and Sakmann B (1997) Physiology and anatomy of synaptic connections between thick tufted pyramidal neurones in the developing rat neocortex. *J Physiol* 500 (Pt 2):409-440.
- Markus EJ, Barnes CA, McNaughton BL, Gladden VL, and Skaggs WE (1994) Spatial information content and reliability of hippocampal CA1 neurons: effects of visual input. *Hippocampus* 4:410-421.
- Markus EJ, Qin YL, Leonard B, Skaggs WE, McNaughton BL, and Barnes CA (1995) Interactions between location and task affect the spatial and directional firing of hippocampal neurons. *J Neurosci* 15:7079-7094.
- Marr D (1970) A theory for cerebral neocortex. *Proc R Soc Lond B Biol Sci* 176:161-234.
- Marr D (1971) Simple memory: a theory for archicortex. *Philos Trans R Soc Lond B Biol Sci* 262:23-81.
- Marshall L, Henze DA, Hirase H, Leinekugel X, Dragoi G, and Buzsaki G (2002) Hippocampal pyramidal cell-interneuron spike transmission is frequency dependent and responsible for place modulation of interneuron discharge. *J Neurosci* 22:RC197.
- Martin SJ, de Hoz L, and Morris RG (2005) Retrograde amnesia: neither partial nor complete hippocampal lesions in rats result in preferential sparing of remote spatial memory, even after reminding. *Neuropsychologia* 43:609-624.
- Mason A, Nicoll A, and Stratford K (1991) Synaptic transmission between individual pyramidal neurons of the rat visual cortex in vitro. *J Neurosci* 11:72-84.
- Maurer AP, Vanrhoads SR, Sutherland GR, Lipa P, and McNaughton BL (2005) Self-motion and the origin of differential spatial scaling along the septo-temporal axis of the hippocampus. *Hippocampus* 15:841-852.

- Maurer AP, Cowen SL, Burke SN, Barnes CA, and McNaughton BL (2006a) Organization of hippocampal cell assemblies based on theta phase precession. *Hippocampus* 16:785-794.
- Maurer AP, Cowen SL, Burke SN, Barnes CA, and McNaughton BL (2006b) Phase precession in hippocampal interneurons showing strong functional coupling to individual pyramidal cells. *J Neurosci* 26:13485-13492.
- McClelland JL, McNaughton BL, and O'Reilly RC (1995) Why there are complementary learning systems in the hippocampus and neocortex: insights from the successes and failures of connectionist models of learning and memory. *Psychol Rev* 102:419-457.
- McCloskey M, and Cohen NJ (1989) Catastrophic interference in connectionist networks: The sequential learning problem. In G.H. Bower (Ed.), *The psychology of learning and motivation*. New York: Academic Press 24:109-164.
- McNaughton BL, Douglas RM, and Goddard GV (1978) Synaptic enhancement in fascia dentata: cooperativity among coactive afferents. *Brain Res* 157:277-293.
- McNaughton BL (1980) Evidence for two physiologically distinct perforant pathways to the fascia dentata. *Brain Res* 199:1-19.
- McNaughton BL, Barnes CA, and Andersen P (1981) Synaptic efficacy and EPSP summation in granule cells of rat fascia dentata studied in vitro. *J Neurophysiol* 46:952-966.
- McNaughton BL, Barnes CA, and O'Keefe J (1983a) The contributions of position, direction, and velocity to single unit activity in the hippocampus of freely-moving rats. *Exp Brain Res* 52:41-49.
- McNaughton BL, O'Keefe J, and Barnes CA (1983b) The stereotrode: a new technique for simultaneous isolation of several single units in the central nervous system from multiple unit records. *J Neurosci Methods* 8:391-397.
- McNaughton BL, and Morris RGM (1987) Hippocampal Synaptic Enhancement and Information-Storage within a Distributed Memory System. *Trends in Neurosciences* 10:408-415.
- McNaughton BL, Chen LL, and Markus EJ (1991) "Dead Reckoning," Landmark Learning, and the Sense of Direction: A Neurophysiological and Computational Hypothesis. *Journal of Cognitive Neuroscience* 3:190-202.

- McNaughton BL, Barnes CA, Gerrard JL, Gothard K, Jung MW, Knierim JJ, Kudrimoti H, Qin Y, Skaggs WE, Suster M, and Weaver KL (1996) Deciphering the hippocampal polyglot: the hippocampus as a path integration system. *J Exp Biol* 199:173-185.
- McNaughton BL (1998) The neurophysiology of reminiscence. *Neurobiol Learn Mem* 70:252-267.
- McNaughton BL, Battaglia FP, Jensen O, Moser EI, and Moser MB (2006) Path integration and the neural basis of the 'cognitive map'. *Nat Rev Neurosci* 7:663-678.
- Mehta MR, Barnes CA, and McNaughton BL (1997) Experience-dependent, asymmetric expansion of hippocampal place fields. *Proc Natl Acad Sci U S A* 94:8918-8921.
- Metropolis N, Rosenbluth AW, Rosenbluth MN, and Teller AH (1953) Equation of State Calculations by Fast Computing Machines. *Journal of chemical physics* 21:1087-1092.
- Mizumori SJ, McNaughton BL, and Barnes CA (1989) A comparison of supramammillary and medial septal influences on hippocampal field potentials and single-unit activity. *J Neurophysiol* 61:15-31.
- Mizumori SJ, Barnes CA, and McNaughton BL (1990) Behavioral correlates of theta-on and theta-off cells recorded from hippocampal formation of mature young and aged rats. *Exp Brain Res* 80:365-373.
- Mizuseki K, Royer S, Diba K, and Buzsaki G (2012) Activity dynamics and behavioral correlates of CA3 and CA1 hippocampal pyramidal neurons. *Hippocampus* 22:1659-1680.
- Mizuseki K, and Buzsaki G (2013) Preconfigured, skewed distribution of firing rates in the hippocampus and entorhinal cortex. *Cell Rep* 4:1010-1021.
- Mölle M, Yeshenko O, Marshall L, Sara SJ, and Born J (2006) Hippocampal sharp wave-ripples linked to slow oscillations in rat slow-wave sleep. *J Neurophysiol* 96:62-70.
- Monaco JD, and Abbott LF (2011) Modular realignment of entorhinal grid cell activity as a basis for hippocampal remapping. *J Neurosci* 31:9414-9425.
- Monaco JD, Rao G, Roth ED, and Knierim JJ (2014) Attentive scanning behavior drives one-trial potentiation of hippocampal place fields. *Nat Neurosci* 17:725-731.

- Monaghan DT, and Cotman CW (1985) Distribution of N-methyl-D-aspartate-sensitive L-[3H]glutamate-binding sites in rat brain. *J Neurosci* 5:2909-2919.
- Mooney CZD, R. (1993) *Bootstrapping: a non-parametrical approach to statistical inference*. Editor: Sage Publications.
- Morris RG, Garrud P, Rawlins JN, and O'Keefe J (1982) Place navigation impaired in rats with hippocampal lesions. *Nature* 297:681-683.
- Müller GE, and Pilzecker A (1900) Experimentelle Beiträge zur Lehre vom Gedächtnis. *Z. Psychol. Ergänzungsband* 1:1-300.
- Muller RU, and Kubie JL (1987) The effects of changes in the environment on the spatial firing of hippocampal complex-spike cells. *J Neurosci* 7:1951-1968.
- Muller RU, Kubie JL, and Ranck JB, Jr. (1987) Spatial firing patterns of hippocampal complex-spike cells in a fixed environment. *J Neurosci* 7:1935-1950.
- Muller RU, Bostock E, Taube JS, and Kubie JL (1994) On the directional firing properties of hippocampal place cells. *J Neurosci* 14:7235-7251.
- Nadasdy Z, Hirase H, Czurko A, Csicsvari J, and Buzsaki G (1999) Replay and time compression of recurring spike sequences in the hippocampus. *J Neurosci* 19:9497-9507.
- Nakashiba T, Buhl DL, McHugh TJ, and Tonegawa S (2009) Hippocampal CA3 output is crucial for ripple-associated reactivation and consolidation of memory. *Neuron* 62:781-787.
- Navratilova Z, Hoang LT, Schwindel CD, Tatsuno M, and McNaughton BL (2012) Experience-dependent firing rate remapping generates directional selectivity in hippocampal place cells. *Front Neural Circuits* 6:6.
- Neunuebel JP, Yoganasimha D, Rao G, and Knierim JJ (2013) Conflicts between local and global spatial frameworks dissociate neural representations of the lateral and medial entorhinal cortex. *J Neurosci* 33:9246-9258.
- Nie Y, and Tatsuno M (2012) Information-geometric measures for estimation of connection weight under correlated inputs. *Neural Comput* 24:3213-3245.

- Nitz D, and McNaughton BL (2004) Differential modulation of CA1 and dentate gyrus interneurons during exploration of novel environments. *J Neurophysiol* 91:863-872.
- O'Keefe J, and Dostrovsky J (1971) The hippocampus as a spatial map. Preliminary evidence from unit activity in the freely-moving rat. *Brain Res* 34:171-175.
- O'Keefe J, and Conway DH (1978) Hippocampal place units in the freely moving rat: why they fire where they fire. *Exp Brain Res* 31:573-590.
- O'Keefe J, and Speakman A (1987) Single unit activity in the rat hippocampus during a spatial memory task. *Exp Brain Res* 68:1-27.
- O'Keefe J, and Recce ML (1993) Phase relationship between hippocampal place units and the EEG theta rhythm. *Hippocampus* 3:317-330.
- O'Neill J, Senior TJ, Allen K, Huxter JR, and Csicsvari J (2008) Reactivation of experience-dependent cell assembly patterns in the hippocampus. *Nat Neurosci* 11:209-215.
- O'Keefe J, and Nadel L (1978) *The Hippocampus as a Cognitive Map*. Editor: Oxford University Press.
- Ostojic S, Brunel N, and Hakim V (2009) How connectivity, background activity, and synaptic properties shape the cross-correlation between spike trains. *J Neurosci* 29:10234-10253.
- Park E, Dvorak D, and Fenton AA (2011) Ensemble place codes in hippocampus: CA1, CA3, and dentate gyrus place cells have multiple place fields in large environments. *Plos One* 6:e22349.
- Pennartz CM, Lee E, Verheul J, Lipa P, Barnes CA, and McNaughton BL (2004) The ventral striatum in off-line processing: ensemble reactivation during sleep and modulation by hippocampal ripples. *J Neurosci* 24:6446-6456.
- Perkel DH, Gerstein GL, and Moore GP (1967a) Neuronal spike trains and stochastic point processes. I. The single spike train. *Biophys J* 7:391-418.
- Perkel DH, Gerstein GL, and Moore GP (1967b) Neuronal spike trains and stochastic point processes. II. Simultaneous spike trains. *Biophys J* 7:419-440.
- Petsche H, Stumpf C, and Gogolak G (1962) [The significance of the rabbit's septum as a relay station between the midbrain and the hippocampus. I. The control of

hippocampus arousal activity by the septum cells]. *Electroencephalogr Clin Neurophysiol* 14:202-211.

Peyrache A, Khamassi M, Benchenane K, Wiener SI, and Battaglia FP (2009) Replay of rule-learning related neural patterns in the prefrontal cortex during sleep. *Nat Neurosci* 12:919-926.

Qin YL, McNaughton BL, Skaggs WE, and Barnes CA (1997) Memory reprocessing in corticocortical and hippocampocortical neuronal ensembles. *Philos Trans R Soc Lond B Biol Sci* 352:1525-1533.

Quirk GJ, Muller RU, and Kubie JL (1990) The firing of hippocampal place cells in the dark depends on the rat's recent experience. *J Neurosci* 10:2008-2017.

Redish AD, Elga AN, and Touretzky DS (1996) A coupled attractor model of the rodent head direction system. *Network: Computation in Neural Systems* 7:671-685.

Redish AD, McNaughton BL, and Barnes CA (2000) Place cell firing shows an inertia-like process. *Neurocomputing* 32-33:235-241.

Renno-Costa C, Lisman JE, and Verschure PFMJ (2010) The Mechanism of Rate Remapping in the Dentate Gyrus. *Neuron* 68:1051-1058.

Renno-Costa C, Lisman JE, and Verschure PF (2014) A signature of attractor dynamics in the CA3 region of the hippocampus. *PLoS Comput Biol* 10:e1003641.

Reyes A, and Sakmann B (1999) Developmental switch in the short-term modification of unitary EPSPs evoked in layer 2/3 and layer 5 pyramidal neurons of rat neocortex. *J Neurosci* 19:3827-3835.

Ribot TA (1882) *Diseases of memory. An essay in the positive psychology.* . Kegan Paul, Trench & Co, London

Rolls ET, Stringer SM, and Trappenberg TP (2002) A unified model of spatial and episodic memory. *Proc Biol Sci* 269:1087-1093.

Samsonovich A, and McNaughton BL (1997) Path integration and cognitive mapping in a continuous attractor neural network model. *J Neurosci* 17:5900-5920.

Sargolini F, Fyhn M, Hafting T, McNaughton BL, Witter MP, Moser MB, and Moser EI (2006) Conjunctive representation of position, direction, and velocity in entorhinal cortex. *Science* 312:758-762.

- Schlingloff D, Kali S, Freund TF, Hajos N, and Gulyas AI (2014) Mechanisms of sharp wave initiation and ripple generation. *J Neurosci* 34:11385-11398.
- Scoville WB, and Milner B (1957) Loss of recent memory after bilateral hippocampal lesions. *J Neurol Neurosurg Psychiatry* 20:11-21.
- Sharp PE, Kubie JL, and Muller RU (1990) Firing properties of hippocampal neurons in a visually symmetrical environment: contributions of multiple sensory cues and mnemonic processes. *J Neurosci* 10:3093-3105.
- Sharp PE (1991) Computer simulation of hippocampal place cells. *Psychobiology* 19:103-115.
- Sherry DF, and Schacter DL (1987) The evolution of multiple memory systems. *Psychological Review* 94:439-454.
- Shimazaki H, Amari S, Brown EN, and Grun S (2012) State-space analysis of time-varying higher-order spike correlation for multiple neural spike train data. *PLoS Comput Biol* 8:e1002385.
- Si B, and Treves A (2009) The role of competitive learning in the generation of DG fields from EC inputs. *Cogn Neurodyn* 3:177-187.
- Sik A, Tamamaki N, and Freund TF (1993) Complete axon arborization of a single CA3 pyramidal cell in the rat hippocampus, and its relationship with postsynaptic parvalbumin-containing interneurons. *Eur J Neurosci* 5:1719-1728.
- Singer AC, and Frank LM (2009) Rewarded outcomes enhance reactivation of experience in the hippocampus. *Neuron* 64:910-921.
- Skaggs WE, and McNaughton BL (1996) Replay of neuronal firing sequences in rat hippocampus during sleep following spatial experience. *Science* 271:1870-1873.
- Skaggs WE, McNaughton BL, Wilson MA, and Barnes CA (1996) Theta phase precession in hippocampal neuronal populations and the compression of temporal sequences. *Hippocampus* 6:149-172.
- Skaggs WE, and McNaughton BL (1998) Spatial firing properties of hippocampal CA1 populations in an environment containing two visually identical regions. *J Neurosci* 18:8455-8466.

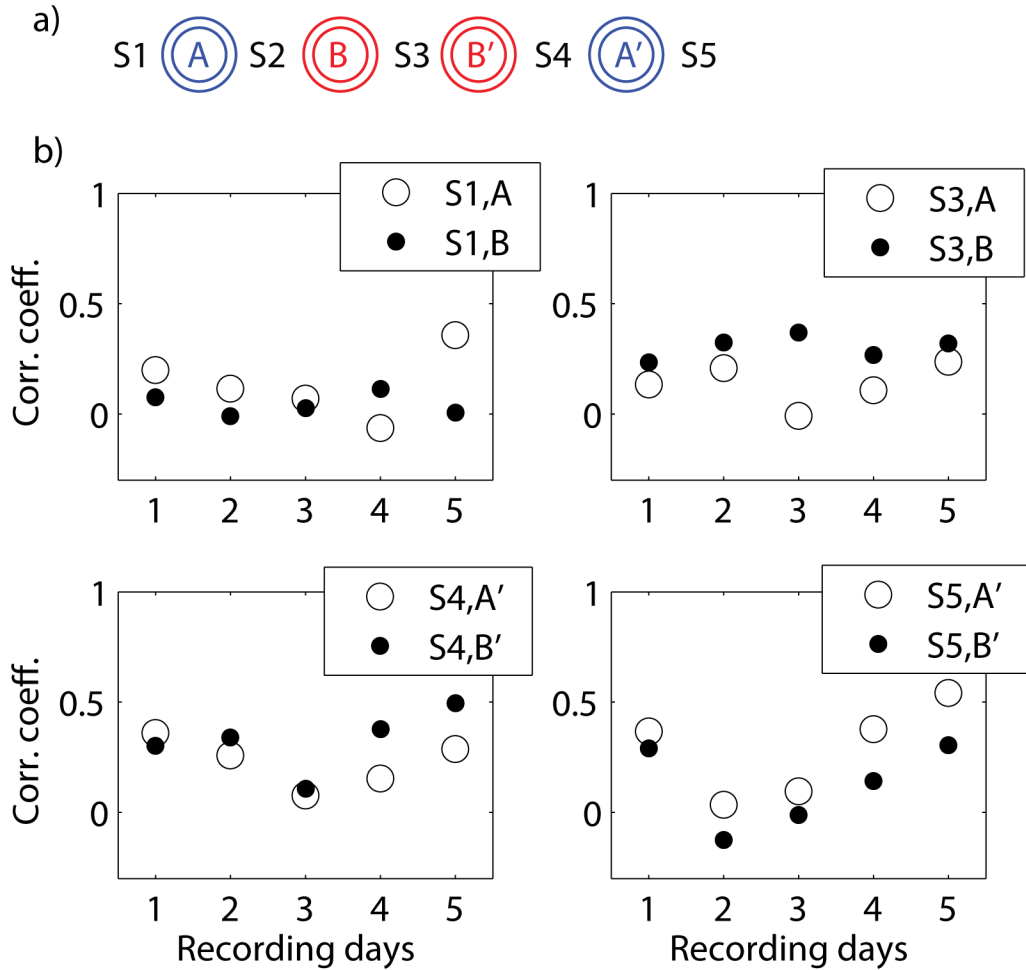
- Solstad T, Moser EI, and Einevoll GT (2006) From grid cells to place cells: a mathematical model. *Hippocampus* 16:1026-1031.
- Solstad T, Yousif HN, and Sejnowski TJ (2014) Place Cell Rate Remapping by CA3 Recurrent Collaterals. *PLoS Comput Biol* 10:e1003648.
- Song S, Sjöström PJ, Reigl M, Nelson S, and Chklovskii DB (2005) Highly nonrandom features of synaptic connectivity in local cortical circuits. *PLoS Biol* 3:e68.
- Spruston N, and Johnston D (1992) Perforated patch-clamp analysis of the passive membrane properties of three classes of hippocampal neurons. *J Neurophysiol* 67:508-529.
- Squire LR (2004) Memory systems of the brain: a brief history and current perspective. *Neurobiol Learn Mem* 82:171-177.
- Stanis JJ, Dees JA, Gerrard JL, Lipa P, VanRhoads SR, McNaughton BL, and et al. (2004) Reactivation of hippocampal neural ensemble patterns is NMDA receptor-dependent. *SfN Abstracts* 329.20
- Stensola H, Stensola T, Solstad T, Froland K, Moser MB, and Moser EI (2012) The entorhinal grid map is discretized. *Nature* 492:72-78.
- Sutherland RJ, O'Brien J, and Lehmann H (2008) Absence of systems consolidation of fear memories after dorsal, ventral, or complete hippocampal damage. *Hippocampus* 18:710-718.
- Sutherland RJ, Sparks FT, and Lehmann H (2010) Hippocampus and retrograde amnesia in the rat model: a modest proposal for the situation of systems consolidation. *Neuropsychologia* 48:2357-2369.
- Swadlow HA (2003) Fast-spike interneurons and feedforward inhibition in awake sensory neocortex. *Cereb Cortex* 13:25-32.
- Swanson LE (1983) The hippocampus and the concept of the limbic system. In W. Seifert (Ed.), *Neurobiology of the hippocampus*. New York: Academic. 3-17.
- Swanson LW, and Kohler C (1986) Anatomical evidence for direct projections from the entorhinal area to the entire cortical mantle in the rat. *J Neurosci* 6:3010-3023.
- Tatsuno M, and Okada M (2004) Investigation of possible neural architectures underlying information-geometric measures. *Neural Comput* 16:737-765.

- Tatsuno M, Lipa P, and McNaughton BL (2006) Methodological considerations on the use of template matching to study long-lasting memory trace replay. *J Neurosci* 26:10727-10742.
- Tatsuno M, Fellous JM, and Amari S (2009) Information-geometric measures as robust estimators of connection strengths and external inputs. *Neural Comput* 21:2309-2335.
- Taube JS, Muller RU, and Ranck JB, Jr. (1990) Head-direction cells recorded from the postsubiculum in freely moving rats. II. Effects of environmental manipulations. *J Neurosci* 10:436-447.
- Teyler TJ, and DiScenna P (1986) The hippocampal memory indexing theory. *Behav Neurosci* 100:147-154.
- Teyler TJ, and Rudy JW (2007) The hippocampal indexing theory and episodic memory: updating the index. *Hippocampus* 17:1158-1169.
- Thomson AM, and Deuchars J (1997) Synaptic interactions in neocortical local circuits: dual intracellular recordings in vitro. *Cereb Cortex* 7:510-522.
- Thomson AM, West DC, Wang Y, and Bannister AP (2002) Synaptic connections and small circuits involving excitatory and inhibitory neurons in layers 2-5 of adult rat and cat neocortex: triple intracellular recordings and biocytin labelling in vitro. *Cereb Cortex* 12:936-953.
- Trappenberg TP (2010) *Fundamentals of Computational Neuroscience*. Oxford University Press.
- Treves A (1990) Threshold-linear formal neurons in auto-associative nets. *Journal of Physics A: Mathematical and General* 23:2631-2650.
- Treves A, and Rolls ET (1992) Computational constraints suggest the need for two distinct input systems to the hippocampal CA3 network. *Hippocampus* 2:189-199.
- Tse D, Langston RF, Kakeyama M, Bethus I, Spooner PA, Wood ER, Witter MP, and Morris RG (2007) Schemas and memory consolidation. *Science* 316:76-82.
- Tsodyks M (1999) Attractor neural network models of spatial maps in hippocampus. *Hippocampus* 9:481-489.

- Tulving E (1972) Episodic and semantic memory. *Organization of Memory*. London: Academic 381:382-402.
- Tulving E (1985) *Elements of Episodic Memory*. Editor: OUP Oxford.
- Ulanovsky N, and Moss CF (2007) Hippocampal cellular and network activity in freely moving echolocating bats. *Nat Neurosci* 10:224-233.
- van Strien NM, Cappaert NL, and Witter MP (2009) The anatomy of memory: an interactive overview of the parahippocampal-hippocampal network. *Nat Rev Neurosci* 10:272-282.
- Vanderwolf CH (1969) Hippocampal electrical activity and voluntary movement in the rat. *Electroencephalogr Clin Neurophysiol* 26:407-418.
- Vazdarjanova A, and Guzowski JF (2004) Differences in hippocampal neuronal population responses to modifications of an environmental context: evidence for distinct, yet complementary, functions of CA3 and CA1 ensembles. *J Neurosci* 24:6489-6496.
- Wang Y, Markram H, Goodman PH, Berger TK, Ma J, and Goldman-Rakic PS (2006) Heterogeneity in the pyramidal network of the medial prefrontal cortex. *Nat Neurosci* 9:534-542.
- Wierzynski CM, Lubenov EV, Gu M, and Siapas AG (2009) State-dependent spike-timing relationships between hippocampal and prefrontal circuits during sleep. *Neuron* 61:587-596.
- Wills TJ, Lever C, Cacucci F, Burgess N, and O'Keefe J (2005) Attractor dynamics in the hippocampal representation of the local environment. *Science* 308:873-876.
- Wilson MA, and McNaughton BL (1993) Dynamics of the hippocampal ensemble code for space. *Science* 261:1055-1058.
- Wilson MA, and McNaughton BL (1994) Reactivation of hippocampal ensemble memories during sleep. *Science* 265:676-679.
- Witter MP, Wouterlood FG, Naber PA, and Van Haeften T (2000) Anatomical organization of the parahippocampal-hippocampal network. *Ann N Y Acad Sci* 911:1-24.

- Wittner L, Henze DA, Zaborszky L, and Buzsaki G (2007) Three-dimensional reconstruction of the axon arbor of a CA3 pyramidal cell recorded and filled in vivo. *Brain Struct Funct* 212:75-83.
- Wood ER, Dudchenko PA, Robitsek RJ, and Eichenbaum H (2000) Hippocampal neurons encode information about different types of memory episodes occurring in the same location. *Neuron* 27:623-633.
- Ylinen A, Bragin A, Nadasdy Z, Jando G, Szabo I, Sik A, and Buzsaki G (1995) Sharp wave-associated high-frequency oscillation (200 Hz) in the intact hippocampus: network and intracellular mechanisms. *J Neurosci* 15:30-46.
- Zhang K (1996) Representation of spatial orientation by the intrinsic dynamics of the head-direction cell ensemble: a theory. *J Neurosci* 16:2112-2126.
- Zhao M, Batista A, Cunningham JP, Chestek C, Rivera-Alvidrez Z, Kalmar R, Ryu S, Shenoy K, and Iyengar S (2012) An L(1)-regularized logistic model for detecting short-term neuronal interactions. *J Comput Neurosci* 32:479-497.

Appendix



Recording sequence and mean firing rate correlations between maze and sleep sessions

a) The sequence of sleep and behavioral sessions during recording. A and A' are sessions in the same running direction and B and B' are sessions in the same running direction, opposite to A. b)

The mean firing rates of all cells for sessions A, A', B and B' as well as for sleep sessions 1, 3, 4 and 5 of all animals were pooled and log transformed. Sleep sessions 1 and 5 were truncated to the last and first 20 minutes, respectively, to include a comparable amount of data as in the other comparisons. The log transformed mean firing rates during ripple events in S1 with A and B, S3 with A and B, S4 with A' and B' as well as S5 with A' and B' are shown. Open circles denote comparisons with running sessions A or A' and closed circles denote comparisons with running sessions B or B'. S1 shows weak correlations with either behavioral session (Wilcoxon rank sum

test, one-tailed, $p=0.15$), which is likely due to the fact that the animal has not been on the track yet. On day 5, however, the correlation between S1 and A may reflect 24-hour retention. There is a significant tendency for the mean firing rates in S3 (Wilcoxon rank sum test, one-tailed, $p=0.008$) and a weaker tendency for S4 and S5 to be more similar to the previous than to the following run session (Wilcoxon rank sum test, one-tailed, $p=0.11$ in both cases).